1970

The Collective Excitations in Ytterbium-172 and Lutetium-172.

Dilip Sen
Louisiana State University and Agricultural & Mechanical College

THE COLLECTIVE EXCITATIONS IN ^{172}Yb AND ^{172}Lu

A Dissertation

Submitted to the Graduate Faculty of the
Louisiana State University and
Agricultural and Mechanical College
in partial fulfillment of the
requirements for the degree of
Doctor of Philosophy

in

The Department of Physics and Astronomy

by

Dilip Sen
M.Sc. Calcutta University, 1955
August 1970

ACKNOWLEDGMENTS

It has been a great privilege to have the opportunity to work under the able guidance of Dr. E. F. Zganjar. In each and every phase of the present work, I received invaluable guidance, encouragement and assistance from Dr. Zganjar which made the present research possible. His pleasant personality has pervaded through my entire academic and extra-academic career to make my stay at L.S.U. enjoyable. I am greatly indebted also to Dr. G. E. Keller who, besides being a great friend, has been responsible to a large extent for my initiation into the experiments. My special thanks are due to Mr. Whitney Blanchard for providing very helpful assistance in working with the PECAC spectrometer. I am also thankful to Mr. Michael Svoren and Mr. Kamal P. Bou-Hamad for their very friendly help in different phases of the present work. It has been a great pleasure to work in the Nuclear Spectroscopy group and the author is thankful to the whole group for providing a pleasant atmosphere.

Mr. Mark Walton is thanked for his invaluable help with the computer programs used in data analysis. Thanks are also extended to Miss Peggy Landry who typed the whole thesis and did a fine job in that.

The author is grateful to the Department of Physics and Astronomy for providing financial assistance in the form of teaching and research assistantships during the entire period Fall 1965 - Fall 1970. Financial assistance in the form of a Fullbright travel grant by the Institute of International Education is also sincerely appreciated. The author would also like to acknowledge the financial assistance provided by the Dr. Charles E. Coates Memorial Fund (L.S.U.) in meeting partially the expenses incurred in the preparation of this thesis.

A final note of thanks go to my wife Swati, my daughter Roon and the other members of my family for providing encouragement throughout my graduate career.

TABLE OF CONTENTS

LIST OF TABLES

LIST OF FIGURES

ABSTRACT

The collective excitations in ^{172}Yb (even-even) and in ^{172}Lu have been experimentally investigated and the results compared with the predictions of microscopic and macroscopic theories. To this end, the γ-ray spectra accompanying the electron capture decays of ^{172}Hf→^{172}Lu→^{172}Yb were separately studied using Ge(Li) and Si(Li) detectors. The measured γ-ray intensities were used, in conjunction with the available conversion electron data, to compute internal conversion coefficients. Multipolarities were determined for most of the transitions in both ^{172}Yb and ^{172}Lu.

For ^{172}Yb, a level scheme containing 28 levels has been proposed in which 97 of the 128 transitions observed were placed. Log ft values, reduced transition probability ratios and inertial parameters were computed and used to identify rotational bands at 1172 keV (K=3), 1466 keV (K=2), 1609 keV (K=2), 1662 keV (K=3), 2073 keV (K=4) and 2174 keV (K=3). These bands and the ground state band contain 23 of the proposed levels. The five remaining levels at 1640, 1706, 2181, 2213 and 2343 keV were classified only according to spin-parity possibilities. The reduced B(E2) transition probability ratios were

computed for interband and intraband transitions and compared with theoretical predictions. The collective or two quasi-particle nature of the two $K=2^+$ states observed has been investigated through the determination of the B(E2) ratios. The $K=2^+$ states observed at 1466, and 1609 keV, compare remarkably well with the energies of 1.4 and 1.7 MeV predicted by microscopic theories. However, both of the states show collective behavior to a large extent. The coupling of each of the two K=2 bands to the ground state band was computed on the basis of the perturbative band mixing theories.

In the study of the electron capture decay of ^{172}Hf to levels of ^{172}Lu, sixteen transitions were observed. For the investigation of the levels in odd-odd ^{172}Lu, delayed coincidence measurements have also been performed in order to uniquely determine the cascade relationships of the 24, 44, 67, 70, 81, 114 and 125 keV transitions. The gate pulses arising from 24 keV γ-rays were obtained using a NaI(Tl) x-ray detector and the corresponding coincidence spectra were recorded using a Ge(Li) detector. A level scheme consisting of 10 levels has been proposed for ^{172}Lu, in which twelve of the sixteen transitions observed were placed. Log ft values for electron capture to these states have been computed and utilized along with the

expected Nilsson states for the last odd proton and odd neutron in order to specify the particle configurations for seven of the ten proposed levels.

CHAPTER I

INTRODUCTION

This thesis presents studies of collective excitations in ^{172}Yb(even-even) and ^{172}Lu(odd-odd). Both of these nuclei presumably have non-spherical shapes, and their low energy excitations (<2 MeV) generally show systematic trends interpretable as rotational and vibrational excitations superimposed on intrinsic states of nucleonic motion in a non-spherical potential. The original theory of Bohr[1] and Bohr and Mottelson[2] has evolved into the Unified Model,[3,4,5] which has given a spectacularly good description of the low energy states of nuclei in the deformed region. In recent years a great deal of sophistication has been achieved by taking into account the higher order corrections due to departures from adiabaticity .[5,6,7]

A completely different approach based primarily on Hartree-Fock methods has been quite successful in providing a many-body treatment of the basic features of the Unified Model.[8-10,20] These, however, are still confined to the explanation of the basic aspects, such as the existance of a non-spherical shape, the moment of inertia and so forth. In contrast to the Copenhagen approach, the "microscopic" approach has been confined mostly to matters of principle and techniques of

ab initio calculations. During the course of these investigations it was strongly felt that the existing literature (based on "microscopic" methods) is not always fully furnished with detailed computations, tables and graphs so that comparison with experimental data becomes very difficult. Quantitative comparisons of experimental data with the presently available sophisticated theories (both phenomenological and microscopic) is as important as the development of the theories themselves. This has been the strongest motivation for the present study.

Recent advances in high resolution semi-conductor devices and highly improved associated electronic circuitry[11-15] has opened up vast possibilities in nuclear spectroscopy. Precise measurements of energies and intensities of transitions between nuclear states is now possible and, consequently, the finer details of nuclear energy-level spectra can be obtained. In this thesis a successful attempt has been made to propose level schemes for the afore-mentioned nuclei, commensurate with the theoretical guide-lines.

With precisely determined energies for the levels comprising a band, one can get a good determination of the corresponding inertial parameter, which is one of the few parameters well computed from a microscopic approach.

The electromagnetic transition probabilities for transitions between the levels of the same band, or between those of different bands, is a quantity very sensitive to the quantum characteristics of the levels concerned. The couplings between the ground state rotational band and the beta and gamma bands need further experimental study to ascertain the merits of band-mixing theories.[7,16,17] Further, the characterization of beta and gamma vibrations as purely surface vibrations is of limited validity and a different approach involving a superposition of quasi-particle states has been proposed.[18,19] The B(E2) ratios are very sensitive to the number of states and the nature of their superposition. Precise measurements of gamma intensities are absolutely necessary for the clarification of these questions.

In regard to the intrinsic structure, the basic truth of the Nilsson orbitals are borne out in the spectacular prediction of spins and parities of low lying levels. Each particle state gives rise to a rotational band whose members each have the same particle configuration. The spin-parity of the band head is just that of the Nilsson orbital. Nilsson's picture has gained momentum from recent Hartree-Fock calculations,[20] which show possible non-spherical average potentials for the ground state configuration.

The applicability of the Nilsson picture to odd nuclei has been spelled out by Mottelsson and Nilsson.[4] However, the corresponding application of the model to odd-odd and even-even nuclei has been limited. Further, an investigation of the contribution of the Coriolis force (R.P.C.) in displacing or mixing the rotational bands is very interesting and important.[21]

The above are a few of the motivating factors behind the present investigation, further details of which are being presented in this thesis in the following manner:

Chapter II contains an attempt to develop a description of the theories of nuclear energy-level spectra for deformed nuclei with special reference to the Copenhagen approach.

The experimental set-up and experimental methods are described in chapter III.

Two subsequent chapters (IV & V) describe the actual experimental investigations of the individual isotopes with relevant comparison to theoretical predictions.

In the final chapter a summary of the conclusions resulting from the present investigation are discussed.

CHAPTER II

THEORIES OF COLLECTIVE NUCLEAR EXCITATIONS

1. Introduction

A nucleus is a bound quantum system of Fermions held together by strong short-range forces and as a consequence every nuclear property is effectively a collective one. However, even the nature of the two-nucleon interaction is not too well known. The difficulties involved in the actual many-body problem of the nucleus with effective interactions are obvious.[22] Alternatively we can try to study the general characteristics of experimentally determined low-energy excitations in nuclei, and look for idealized systems, such as a drop of liquid or an amount of gas exhibiting similar physical properties. This approach has resulted in various nuclear models. We shall, in the following, discuss mainly the "Unified Model" since we feel it satisfies best our projected requirements; namely 1) simplicity, 2) reality, that is applicability to experimental findings and 3) conceptual relationships to the physics involved. Hence, historical order will not always be followed.

One of the earliest collective effects recognized (though not named so) is the fact that nucleons in a

nucleus behave to a certain extent as particles moving independently in a common average central potential (Shell model).[23,24] There are two mechanisms justifying the existance of such an average potential: 1) the scattering of nucleons is hindered by the Pauli principle, which limits the final states available to those above the Fermi level[25] and 2) the Moszkowski-Scott effect[26] to take care of the repulsive core.*

With the inclusion of strong spin-orbit coupling the Shell model correctly predicts the "Magic Numbers" for shell closures, ground state spins of most odd nuclei, islands of isomerism and to a lesser extent the magnetic moments. The general picture of nucleons moving in an average potential and interacting weakly through a residual interaction can qualitatively explain the low lying energy spectra of nuclei near closed shells. However, for quantitative calculations configuration mixing must be included.

A many-body system like a nucleus obviously will have excited states corresponding to the excitation of the many-body system in which many particles participate in a coherent manner. Such a mode is well

---

*These authors use a separation of the nuclear potential into a short range part v_s and a long range part. The strength of v_s and its range d is so adjusted that the wave-functions for this potential and that for the actual one including repulsive core have the same logarithmic derivative at d.

known in the many electron problem, where one gets a coherent plasma mode of oscillation. Thus for nuclei with relatively few particles outside of closed shells, the equilibrium shape is almost spherical and the collective modes correspond to vibrations, especially of the quadrupole type. A variety of such vibrational modes have been observed in nuclei distinguished through the angular momentum (I), parity and isospin of the associated phonons. The most important nuclear vibrations classified in this manner are 1) the giant dipole oscillation ($I = 1^-$, $T = 1$), 2) quadrupole vibration (2^+, $T = 0$) and 3) octupole vibration (3^-, $T = 0$). As we move away from closed shells, the particles added (or subtracted) produce a net pull on the closed shell core[27] and the frequency of shape oscillations about the spherical equilibrium falls considerably so that low energy vibrational excitations are possible. Moving further away from closed shells, the net pull is such that the nucleus acquires a permanent deformation (fig. 1). A system with a non-spherical shape has degrees of freedom corresponding to rotation of the whole nucleus about some axis in space. The existence of such rotational nuclear states is one of the most prominent and well verified features of low energy spectra in the regions $A=24$, $150 \leq A \leq 190$ and $A \geq 220$. In fig. 2 we have tried to summarize the general characteristics of nuclear

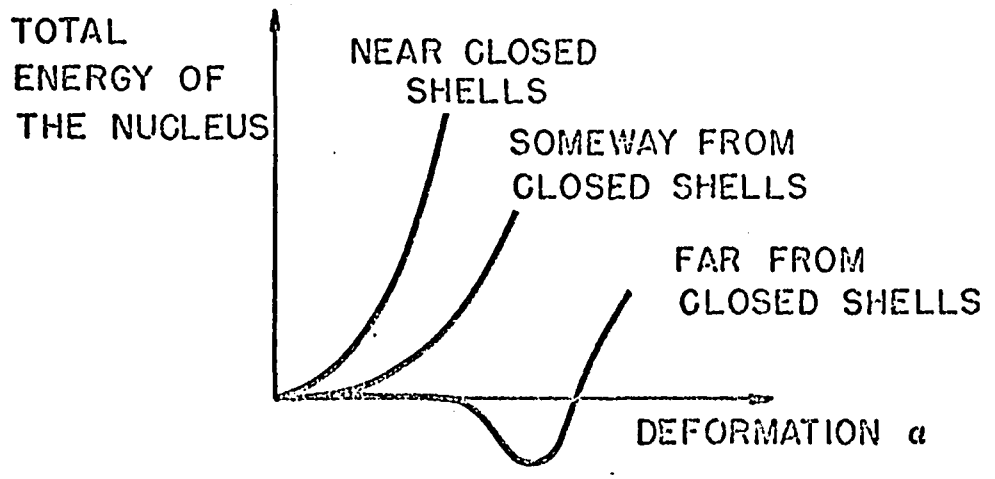

Fig. 1. Nuclear potential energy plotted as a function of deformation.

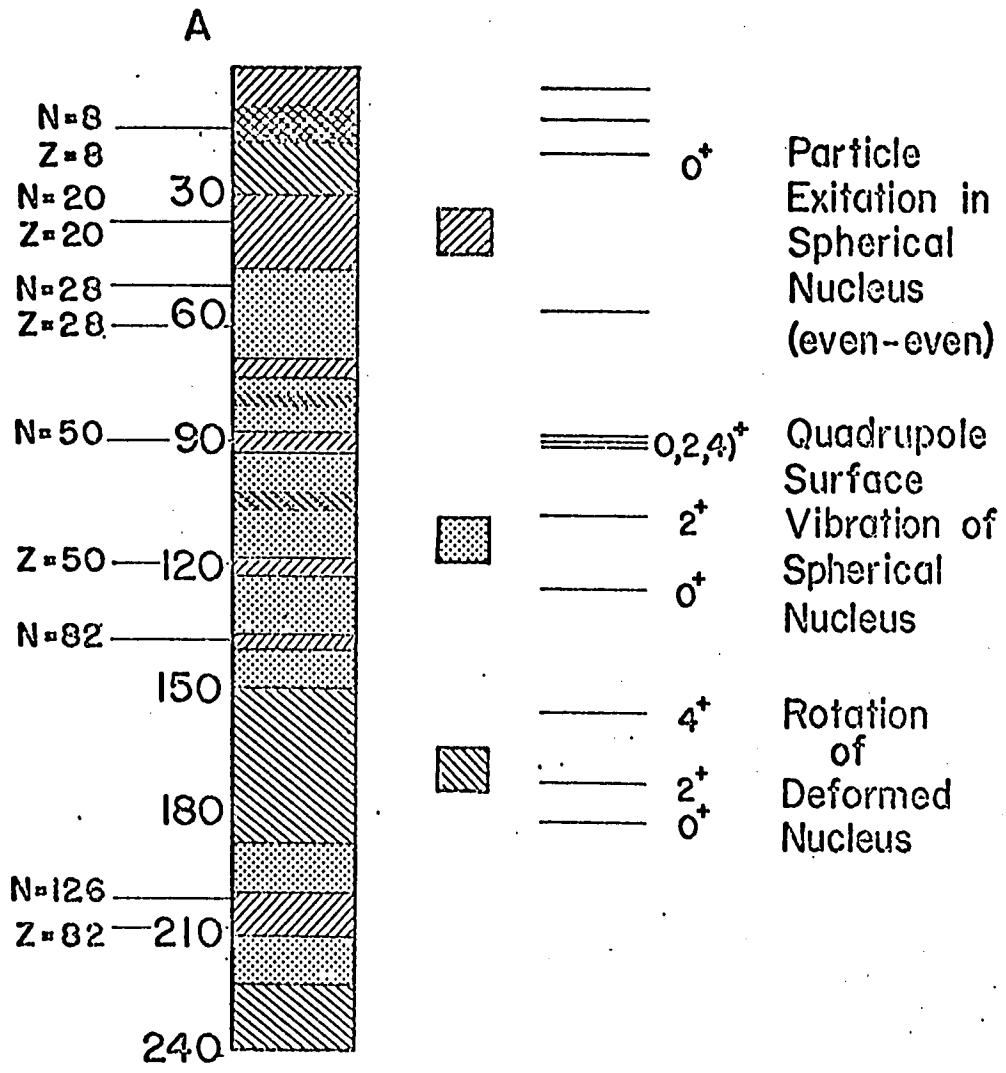

Fig. 2. General nature of the low lying excitations in nuclei in the mass range $10 \leq A \leq 240$.

excitations over the mass number range $10 \leq A \leq 240$.

The following additional facts point to the failure of the single particle approach and the existence of strong cooperative effects in these nuclei.

1) Nuclei in the above-mentioned mass range have electric quadrupole moments exceeding the value predicted on the basis of independent particle motions in an average potential. 2) The E2 transitions for nuclei far from closed shells are about 100 times enhanced over the single particle E2 transition strength. 3) The existence of the so-called energy-gap in even-even nuclei is also not explainable in terms of independent particle motions. Bohr[1] and Bohr and Mottelsson[2] recognized the collective nature of nuclear motion (though more in the line of the liquid drop model) and formulated the theories of nuclear collective rotations and vibrations which have been vital to the understanding of nuclear energy-level spectra.

The unification of the two approaches was made shortly thereafter through the work of Nilsson[3] and Nilsson and Mottelson[4] and is referred to as the Unified Model. In the Unified Model, the average potential is non-spherical, consequently, variations in shape and orientation of the potential gives rise to vibrations and rotations. The two important assumptions are that the potential is symmetric and that the individual motion

of the nucleons in the non-spherical potential is not affected by the slow changes of the potential shape or orientation (abiabaticity). Thus, the wave function of the system may be written as

$$\Psi = \Phi(\text{Euler Angles})\chi(\text{intrinsic coordinates}) \quad (2.1)$$

Furthermore, attempts have been made to account for departures from abiabaticity by considering the asymetry of nuclear shape,[28-30] the coupling of intrinsic and rotational motion[31] or the rotation-vibration coupling.[32,33] A general theory of this coupling has also been formulated by expanding the nuclear Hamiltonian in a power series of the total angular momentum.[7]

The feasibility of the canonical separation of the many body problem to intrinsic and collective motion has been well investigated.[34,35] Recently Villars has formulated[36] such a separation based on an explicit introduction of collective (angular and angular momentum) variables and of a set of intrinsic variables which remain in one-to-one correspondence with particle coordinates by a contact transformation.

In the attempts to understand the collective excitations on a more fundamental basis the predominant question concerns the equilibrium shape of the nucleus.

As Baranger[20] noted, most nuclei are expected to be deformed and the proper question is to find why so many of them are still spherical. Hartree-Fock calculations with simple forces show that practically all nuclei are not only deformed but can have a variety of axially symmetric or assymetric shapes. Even in atomic physics it has been known that starting with a rotationally invariant Hamiltonian, a Hartree-Fock calculation can give non-rotationally invariant shapes.

In the last decade considerable progress has been made towards the unified approach with special recognition of the 1) short range (pairing) correlations and 2) the long range correlations between nucleonic motions and the competition between the two.[21,22,37-39]

2. The Unified Model

2.1 Residual Forces and Coupling Schemes

Let us first try to look at a systematic method for treating the correlations in intrinsic nucleonic motions arising from the residual interactions between the nucleons, that is, the part which is not producing the average spherical shell model potential. The potential field produced by nucleons interacting through a two particle interaction,neglecting exchange,may be written as[10]

$$u(\vec{r}) = \int d^3r' V(\vec{r}-\vec{r}')\rho(\vec{r}') \tag{2.2}$$

in which case, we can write

$$V(\vec{r}_{ij}) = \sum_{\lambda} f_\lambda(r_i,r_j)P_\lambda(\cos\theta_{ij})$$

$$= \sum_{\lambda\mu} f_\lambda(r_i,r_j)\frac{4\pi}{2\lambda+1} Y^*_{\lambda\mu}(\theta_i)Y_{\lambda\mu}(\theta_j) \tag{2.3}$$

Then

$$u(\vec{r}) = \sum_{\lambda\mu} u_{\lambda\mu}(\vec{r}) = \sum_{\lambda\mu} Y_{\lambda\mu}(\theta)\frac{4\pi}{2\lambda+1} \int d^3r' f_\lambda(r,r')$$

$$Y^*_{\lambda\mu}(\theta')\rho(\vec{r}') \tag{2.4}$$

Thus we see

$\lambda = 0$, gives rise to the spherical field

$\lambda = 1$, gives rise to a displacement of the center of mass

$\lambda = 2$, gives rise to a quadrupole deformation.

A similar expansion for a δ-function force gives

$$\delta(r_{ij}) = \sum_{\lambda}\delta(r_i-r_j)\frac{2\lambda+1}{2\pi r^2} P_\lambda(\cos\theta_{ij}) \tag{2.5}$$

with emphasis on higher order multipoles. Thus, in our two-body interaction, we can lump all the

multipoles higher than two into a single short-range force, and represent the effective field as a sum

$$V = V_O + V_Q + V_{PAIR} \tag{2.6}$$

This approach was initiated in the work of Elliot[40] and also separately by Mottelson.[37]

Aligned coupling

We know that in a closed shell nucleus the coupling of particle orbitals gives rise to a spherically symmetric shape. An extra-core particle will produce a polarization of the spherical core (Rainwater effect). If we add one more particle, it will try to orient its orbit to that of the first one in such a way as to effectively utilize the residual long-range part of the interaction (fig. 3a). In this way, for a number of extra-core particles we can express the wave function (satisfying Pauli principle) as

$$\psi = A\phi^j_j(1)\,\phi^j_{-j}(2)\,\phi^j_{j-1}(3)\,\phi^j_{-j+1}(4)\,\cdots$$

(oblate shape) (2.7a)

or as

$$\psi = A\phi^j_{1/2}(1)\,\phi^j_{-1/2}(2)\,\phi^j_{3/2}(3)\,\phi^j_{-3/2}(4)\,\cdots$$

(prolate shape) (2.7b)

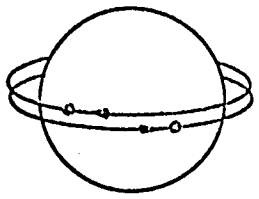

Fig. 3a

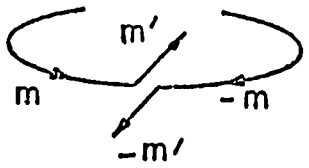

Fig. 3b

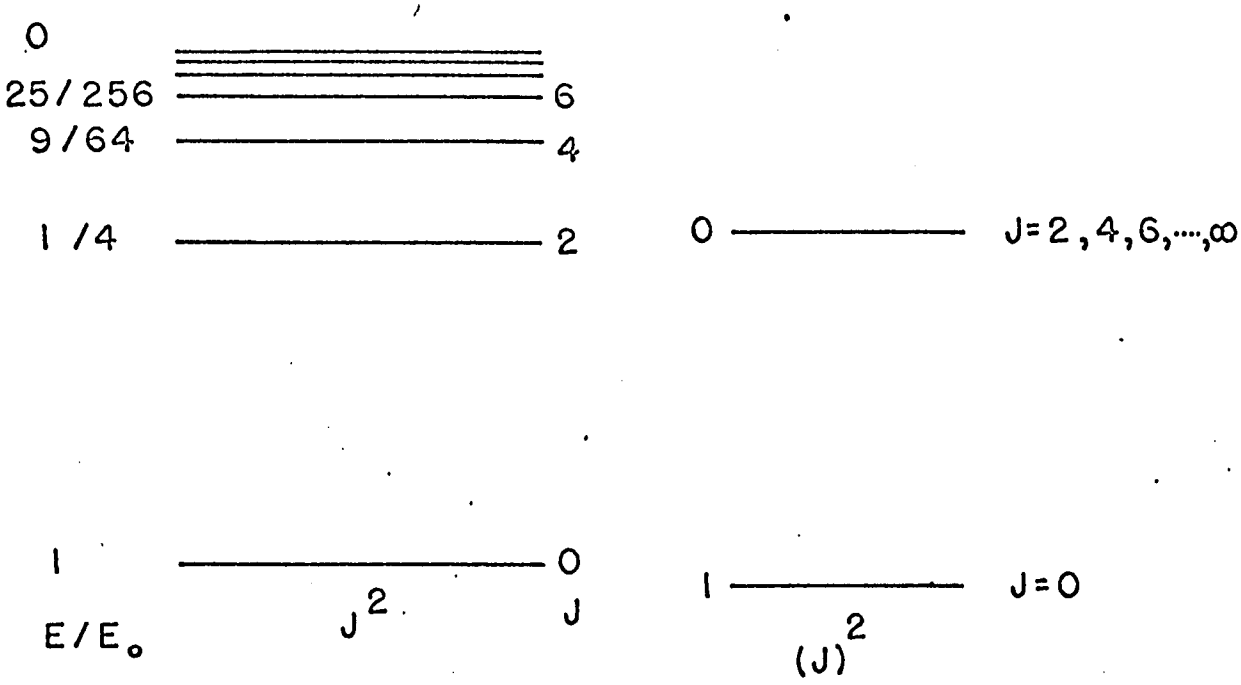

Fig. 3c

Fig. 3a. Classical orbits of two particles outside of an even-even core.

Fig. 3b. The trajectories of two extra-core particles under a short range interaction.

Fig. 3c. The two particle energy spectrum in the J=0 configuration for a δ-function interaction (shown left) and for the pairing interaction (shown right).

From measurements of quadrupole moments we find that towards the beginning of a j-shell a nucleus is prolate and towards the end oblate. Although j ceases to be a good quantum number, m is still good and the above coupling scheme remains valid. Thus, the quadrupole field tries to intermingle the different unperturbed j-shells, allowing for even better alignment, as is prominently observed in rare-earths. The above coupling scheme, however, does not necessarily imply axially symmetric or reflection-symmetric shapes.

Pair-coupling

Now let us turn on the short-range part of the residual force. Classically the two particles moving along time-reversed orbits come close to each other twice in every orbit and under a strong short-range interaction get scattered into new but still time-reversed orbits (fig. 3b). Thus the overall effect is to spacially spread the orbits in a spherically symmetric way.

Further, the energy-spectrum of two particles in a (j^2) configuration under a pure short-range interaction appears as shown in Fig. 3c, which indicates that the J=0 state is the most strongly bound. The pairwise coupling of nucleons in a nucleus, has been recognized in Racah's seniority coupling scheme.[41] In such a scheme, the ground state of an even mass nucleus may

be written as

$$\Psi_o^{(n)} = A[\phi_o(1,2)\phi_o(3,4)---] \qquad (2.8a)$$

and for odd mass as

$$\Psi_{jm}^{(n)} = A[\phi_{jm}(1)\phi_o(2,3)\phi_o(4,5)---] \qquad (2.8b)$$

where $\phi_o(1,2)$ is the J=0 state formed by coupling nucleon 1 and nucleon 2 and so forth. Recently, a schematic force $\hat{G}$ (the pairing force) defined by

$$<(j)^2J|\hat{G}|(j')^2J'> = \delta(J=J'=0)G\ \Omega \qquad (2.9)$$

has been extensively used.[10] The corresponding two particle spectrum is also shown in fig. 3c . The applicability of the pairing force in nuclear structure calculations was put forward by Bohr, Mottelson and Pines[42] following the BCS formalism in superconductivity. If we consider two fermions of opposite spins moving over an unperturbed "Fermi sea" and turn on any attractive interaction between the two, however weak, they always form a bound state. Thus, the unperturbed Fermi sea is unstable against the formation of Cooper pairs . The development of this approach (quasi-particle picture) with regard to the excited states of nuclei

will be discussed more in a later section. However, we would like to point out here that the short-range correlation has much importance regarding the following experimental facts:

1) All even-even nuclei have ground state spin zero and even parity.
2) The low-lying spectra of even-even nuclei have an "energy-gap" corresponding to the energy required to break up a J=0 pair, below which only collective states appear.
3) The separation energy of the odd nucleon in an odd-even nucleus is always less than that for a nucleon from the neighboring even-even nucleus.

2.2 Nilsson States

The second important term in the multipole expansion (eqn. 2.4) of the two nucleon interaction is the quadrupole term which gives rise to the deformation of the average potential. Thus, in the Unified Model, the intrinsic states (Nilsson states) are those of a nucleon moving in the average deformed potential. This problem has been treated by a number of authors, both for axially symmetric[3,43-45] and asymetric[46,47] potential shapes. In the following we take the approach of Nilsson, Nilsson and Mottelson and Lamm [3,4,45] since these axially symmetric potentials have been widely applied with a great deal of success.

In the spherically symmetric oscillator potential the one particle wave functions are characterized by

N = oscillator quantum number

j = total angular momentum

ℓ = orbital angular momentum.

Each j state has (2j+1) fold degeneracy. For a definite m value, we can write

$$\phi_{N\ell jm}(\vec{r}) = R_{N\ell}(r)\,\Theta_{j\ell m}(\theta,\phi) \tag{2.10}$$

These wave functions form a complete set and can be used as a basis for the expansion of other wave functions.

The Nilsson Hamiltonian is

$$H = H_o + C\vec{\ell}\cdot\vec{s} + D\vec{\ell}^2 \tag{2.11}$$

where

$$H_o = -\frac{\hbar^2}{2M}\nabla^2+\frac{M}{2}(\omega_x^2x^2+\omega_y^2y^2+\omega_z^2z^2) \tag{2.12}$$

and x,y,z are the coordinates of the nucleon in a coordinate system fixed at the nucleus. The $\vec{\ell}^2$ term is added to depress the high angular momentum states. Nilsson assumes axial symmetry so that

$$\omega_x^2 = \omega_y^2 = (1 + \tfrac{2}{3}\delta)\omega_o^2 \tag{2.13a}$$

$$\omega_z^2 = (1 - \tfrac{4}{3}\delta)\omega_o^2 \tag{2.13b}$$

where

$$\omega_x\omega_y\omega_z = \overset{o}{\omega}_o^3 = (1 - \tfrac{4}{3}\delta^2 - \tfrac{16}{17}\delta^3)^{\frac{1}{2}}\omega_o^3 \tag{2.13c}$$

(constant volume condition)

and $\overset{o}{\omega}_o = \omega_o(\delta=0)$. By absorbing factors $[\frac{M\omega_o}{\hbar}]^{\frac{1}{2}}$ in x,y,z we can write

$$H_o = \overset{o}{H}_o + H_\delta \tag{2.14a}$$

$$\overset{o}{H}_o = \frac{1}{2}\hbar\omega_o[-\nabla^2+r^2] \tag{2.14b}$$

$$H_\delta = -\delta\hbar\omega_o \frac{4}{3}\sqrt{\frac{\pi}{5}}\, r^2\, Y_{20} \tag{2.14c}$$

The total Hamiltonian then becomes

$$H = H_o + C\vec{\ell}\cdot\vec{S} + D\vec{\ell}^2 \tag{2.15}$$

assuming that the last two terms do not violate the constant volume condition. The deformed wave functions are expanded in terms of the spherical wave functions

$\phi_{N\ell jm}$.

The projections of j on the symmetry axis (the z axis), denoted by Ω, is a constant of the motion. Each state is two fold degenerate ($\pm\Omega$). The (2j+1) fold degenerate spherical state is split into (2j+1)/2 doubly degenerate deformed states. The ordering of the states is illustrated in fig. 4 which is an example of an $h_{11/2}$ state - the highest state with the largest value for a prolate deformation.

In the case of very large deformation where $H_\delta >> C\vec{\ell}\cdot\vec{s} + D\vec{\ell}^2$, the deformed wave functions are characterized by the asymptotic quantum numbers $[N,n_z,\Lambda]\Omega,\pi$ where

N = total oscillator quantum number

n_z = oscillator quanta along the symmetry z axis

Λ = projection of ℓ along z axis

Ω = projection of j along z axis

and π is the parity of the state. The projection of the particle spin along the z axis is usually denoted by Σ, so that $\Omega = \Lambda + \Sigma$.

Figures 5 and 6, show the energy level diagrams in our region of interest ($50 < Z < 82$ and $82 < N < 126$). The energy in oscillator units ($\hbar\omega_o^o$) is plotted against the eccentricity coordinate ε defined below. In Lamm's Hamiltonian the $D\vec{\ell}^2$ term is modified to $D[\vec{\ell}^2-\langle\vec{\ell}^2\rangle_{shell}]$

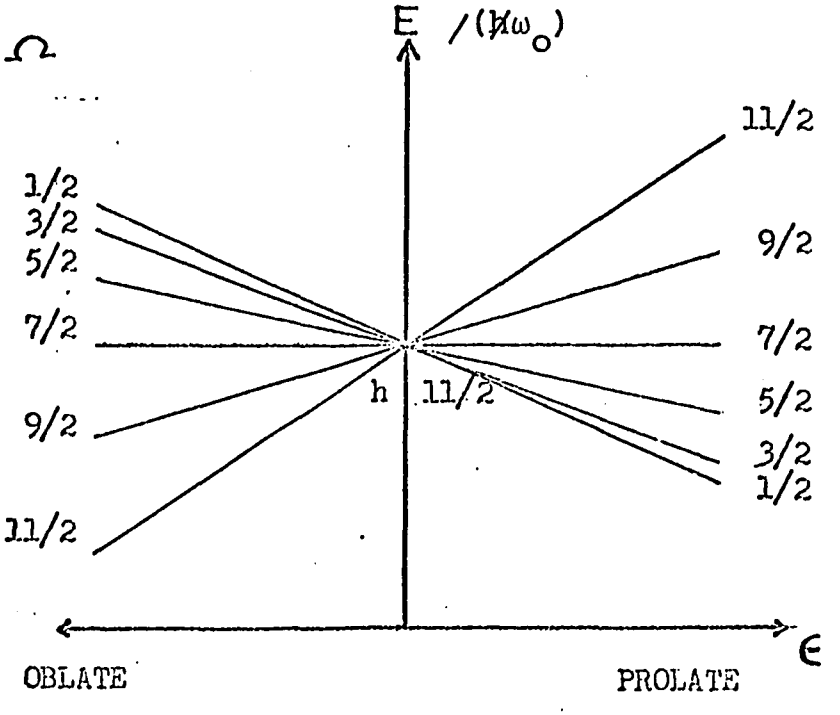

Fig. 4. A schematic representation of the splitting of degenerate spherically symmetric oscillator states under deformation of the nuclear potential.

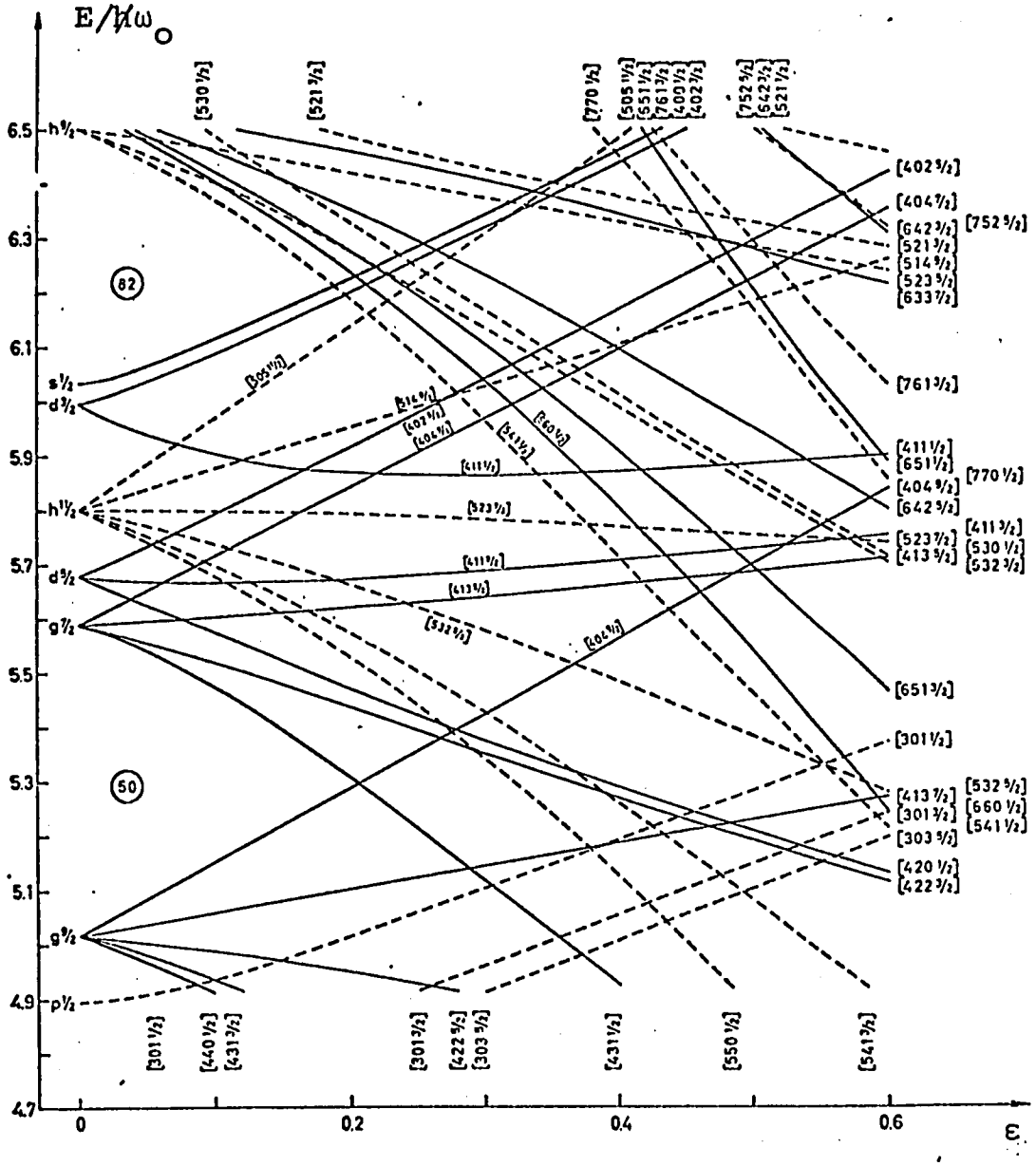

Fig. 5. Nilsson diagram for odd protons 50 < Z < 82.

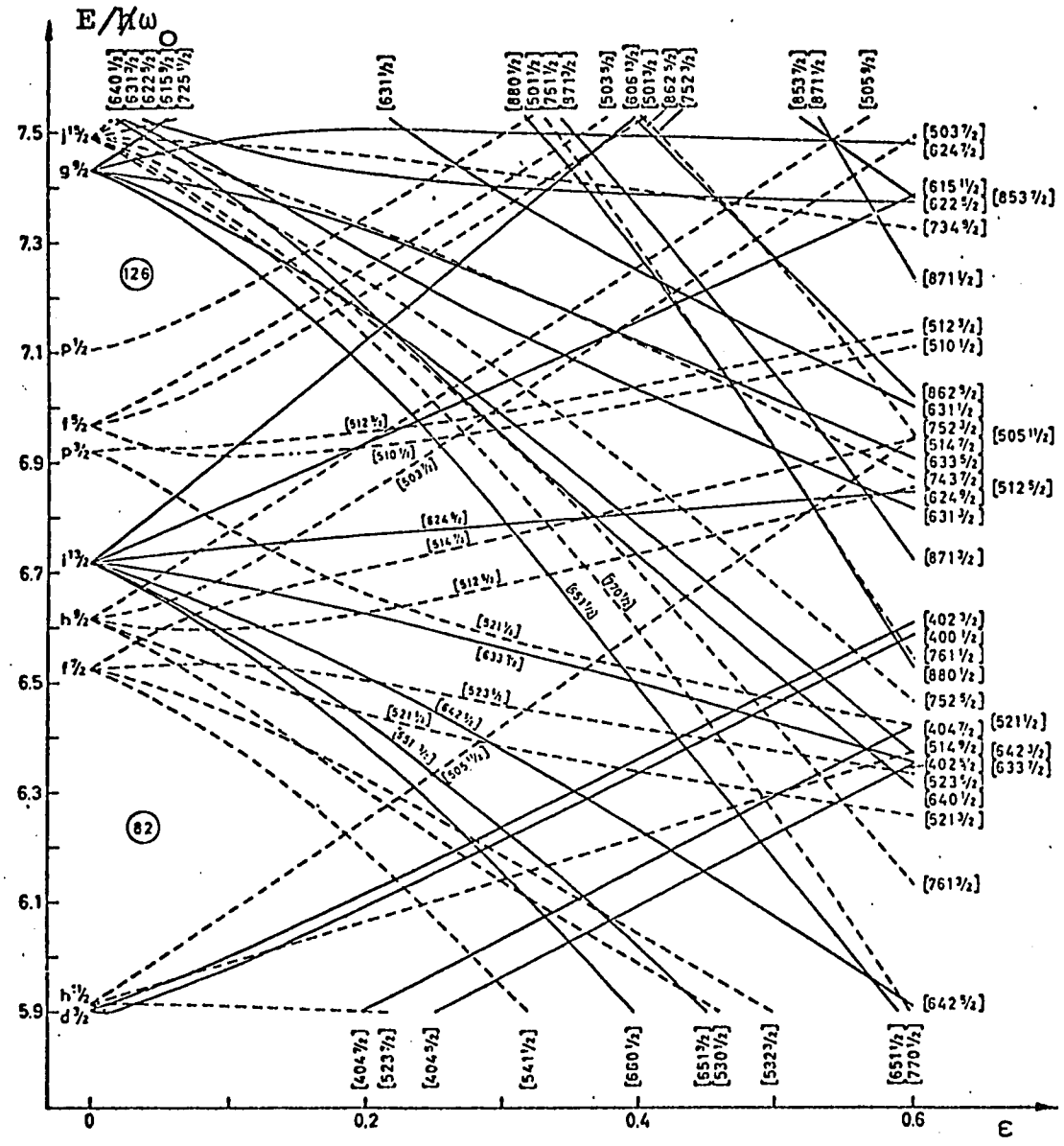

Fig. 6. Nilsson diagram for odd neutrons 82 < N < 126.

in order to keep the distance between the center of gravity points of different N shells constant. The oscillator strengths for the rare-earth region are

$$\hbar\omega_{on} = 44.8\ A^{-1/3}\ \text{MeV}$$
$$\hbar\omega_{op} = 39.8\ A^{-1/3}\ \text{MeV} \qquad (2.16)$$

Further, the deformation parameter ε is related to that of Nilsson,[3] namely δ, by

$$\varepsilon = \delta + \frac{1}{6}\delta^2 + 0(\delta^3) \qquad (2.17)$$

where

$$\delta = 0.95\ \beta$$

and β is the deformation parameter used by Bohr and Mottelson.[2] The value of β can be computed from the static quadrupole moment and the strength of E2 transitions.[48] As an estimate, ε would be about 0.29 for ^{172}Lu.

Each Nilsson state can accomodate two nucleons with projections $\pm\Omega$ along the symmetry axis. The ground state configuration is attained by placing successively two nucleons in each Nilsson state in order

of increasing energy. The ground state of an even-even system always has $K = \Sigma_i \Omega_i = 0$, where K is the projection of the total spin on the symmetry axis. An odd mass system always has $K = \Omega_i$, where i is the last odd nucleon. For an odd-odd system the usual values are $K = \Omega_1 \pm \Omega_2$, where 1 and 2 refer to the last two odd particles (a neutron and a proton). The possible particle or quasi-particle excitations will be discussed individually as we study the even-even and odd-odd nuclei in later chapters.

2.3 The Collective[1] Hamiltonian

We now present the main features of rotational and vibrational states in deformed nuclei. These excitations are explained in terms of the dynamics of a deformable nuclear surface coupled to the motion of individual nucleons. The deformed nuclear surface is represented by

$$R(\theta',\phi') = R_o[1+\Sigma_{\lambda\mu} \alpha_{\lambda\mu} Y^{\lambda}_{\mu} (\theta',\phi')] \qquad (2.18a)$$

$$= R_o[1+\Sigma_{\lambda} \alpha^{*}_{\lambda} \cdot Y^{\lambda}] \qquad (2.18b)$$

measured in spherical polar coordinates fixed in space (the laboratory). R_o is the radius for no deformation, and $Y^{\lambda}_{\mu} (\theta',\phi')$ are the spherical harmonics.

Since $R = R(\theta', \phi')$ describes a real surface, $\alpha_{\lambda\mu} = (-1)^{\mu}\alpha^{*}_{\lambda,-\mu}$ and we can express the deformation as the scaler product of spherical tensors. The general nature of the surface is illustrated in fig. 7 for $\lambda = 1$ to 4. The quantities $\alpha_{\lambda\mu}$ are functions of time and can serve as the collective coordinates. The Hamiltonian (zeroeth order) for the surface motion is

$$H_S = \frac{1}{2}\sum_{\lambda} B_{\lambda}|\dot{\alpha}_{\lambda\mu}|^2 + \frac{1}{2}\sum_{\lambda} C_{\lambda}|\alpha_{\lambda\mu}|^2 \qquad (2.19)$$

where the quantities B_{λ} (mass parameter) and C_{λ} (surface tension) depend on the detailed properties of nuclear matter.

The total nuclear Hamiltonian is

$$H = H_s + H_p + H_{int} \qquad (2.20)$$

where H_p is the single particle Hamiltonian, H_s is that associated with the motions of the surface and H_{int} represents interaction terms such as that between rotation and vibration or between the particle motions and those of the surface.

Experimental data on deformed nuclei show the dominance of a quadripole deformed shape ($\lambda = 2$), although evidence also exists for octopole ($\lambda = 3$) deformations. Henceforth, we shall consider only $\lambda = 2$.

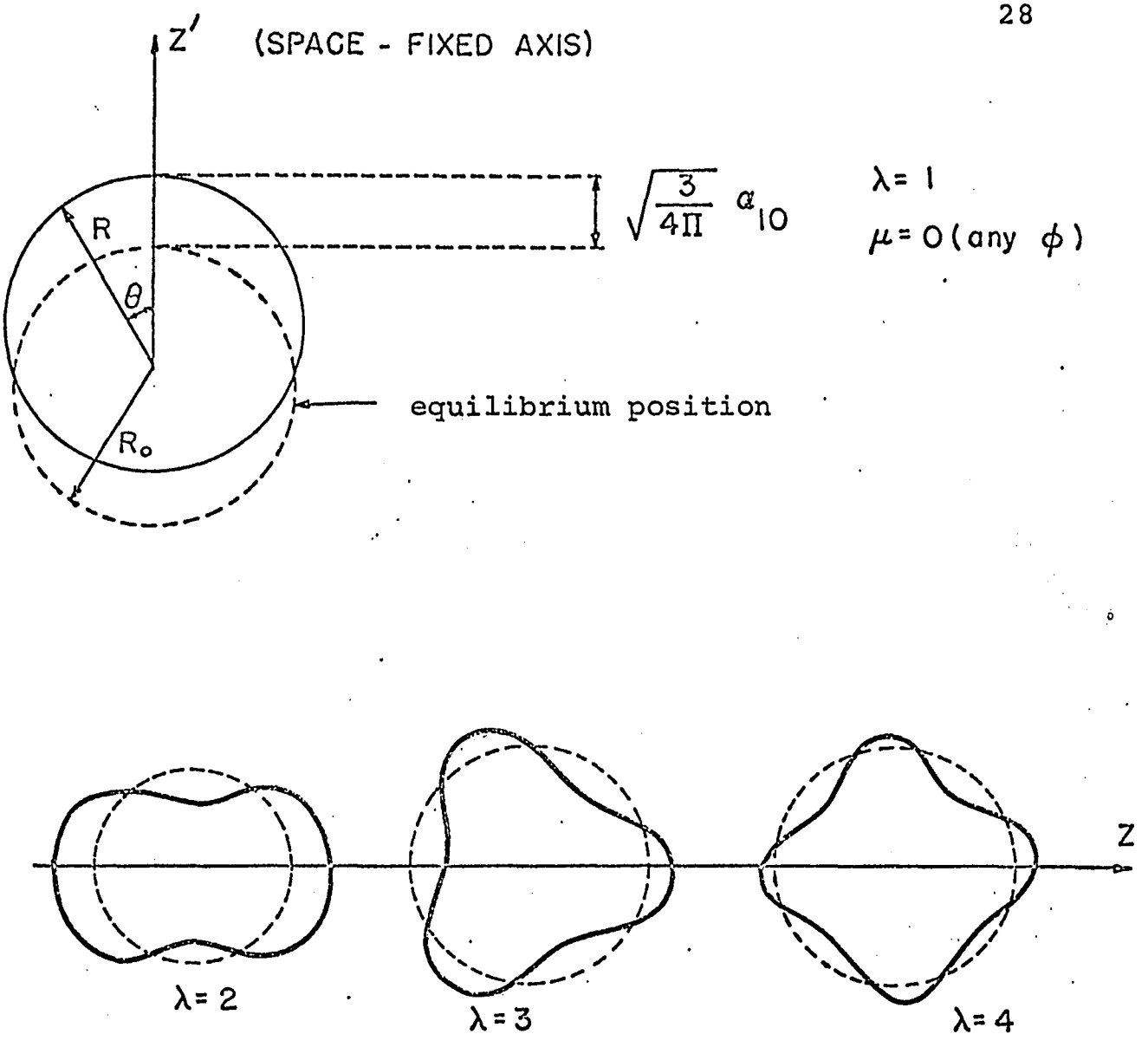

Fig. 7. A schematic representation of the deformed nuclear surface for λ = 1 to 4.

It is convenient to use a coordinate system fixed in the nucleus and its axes (x,y,z) coinciding with the principal axes of the ellipsoid (nucleus). The deformation coefficients a_ν in the body fixed system are related to the α_μ's in eqn. 2.18 by

$$a_\nu = \sum_{\mu=-2}^{2} \alpha_\mu D^2_{\mu\nu}(\theta_i) \quad , \; i = 1,2,3 \tag{2.21}$$

where the three Euler angles θ_1, θ_2 and θ_3 specify the orientation of the body fixed system with respect to the space fixed system. The $D^2_{\mu\nu}$'s are transformation functions for spherical tensors of rank two under rotation in space and are defined as[49]

$$D^2_{\mu\nu}(\theta_i) = e^{-i\mu\theta_1} \langle 2\mu | e^{-i\theta_2 I_y} | 2\nu \rangle e^{-i\nu\theta_3} \tag{2.22}$$

Alternatively, Bohr[1] used the parameters β and γ (fig. 8) defined as

$$\begin{aligned} a_o &= \beta \cos \gamma \\ a_1 &= a_{-1} = 0 \\ \text{and} \quad a_2 &= a_{-2} = \frac{1}{\sqrt{2}} \beta \sin \gamma \end{aligned} \tag{2.23}$$

Thus, the nuclear deformation is characterised by the representative point N on the surface with the

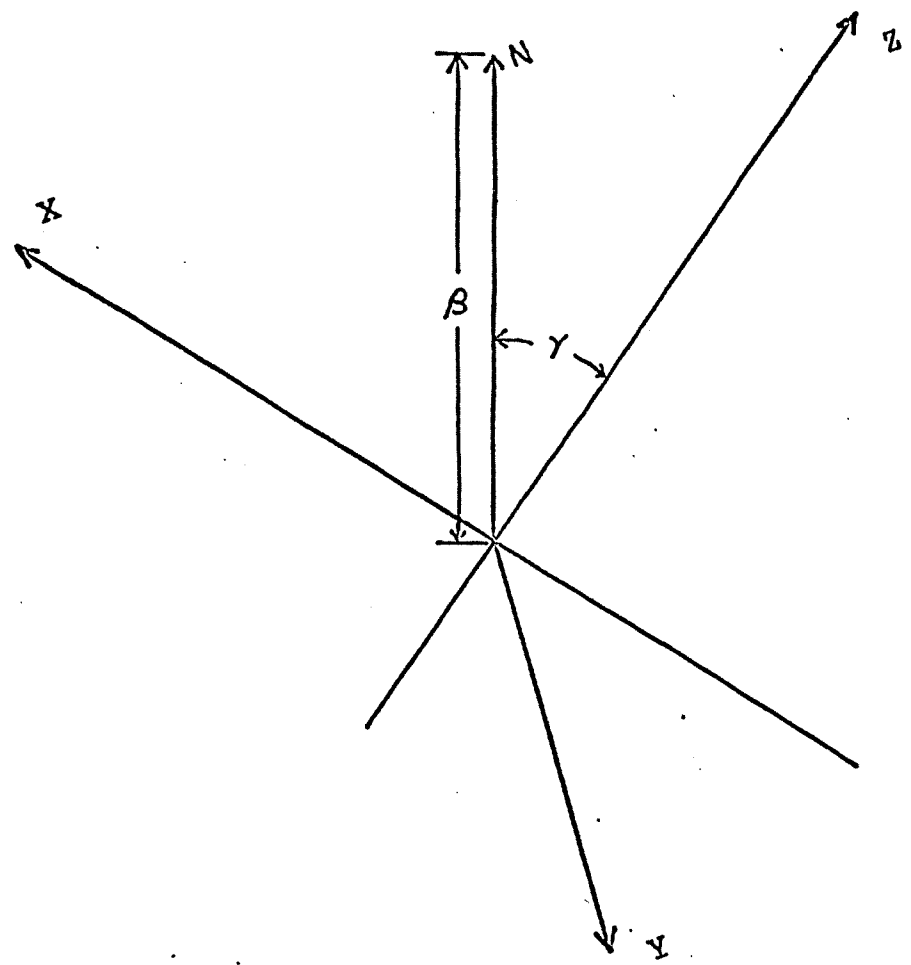

Fig. 8. A diagram illustrating the definitions of the parameters β and γ.

deformation parameter β as the radius vector and the shape parameter γ as the polar angle. If N lies on any one of the three axes (x,y,z) the nucleus will have rotational symmetry. When the ellipsoid has a symmetry axis only two values of γ are possible, $\gamma = 0$ and $\gamma = \pi/3$, corresponding to a prolate or an oblate case. In both cases the symmetry axis coincides with the 3-axis. The values of γ of interest lie in the interval $0 \leq \gamma \leq \pi/3$. Other values of $\gamma = n\pi/3$, n = integer ≥ 1, give axially symmetric ellipsoids with the x or y axis as the symmetry axis.

By expressing $\dot{\alpha}_\mu$ of the kinetic energy term (eqn. 2.19) in terms of (β, γ and θ_i) Bohr[1] obtains the following expression for the collective Hamiltonian

$$H_{coll} = -\frac{\hbar^2}{2B}\left\{\frac{1}{\beta^4}\frac{\partial}{\partial\beta}\beta^4\frac{\partial}{\partial\beta} + \frac{1}{\beta^2}\frac{1}{\sin 3\gamma}\frac{\partial}{\partial\gamma}\sin 3\gamma\frac{\partial}{\partial\gamma}\right\}$$

$$+ \sum_{k=1}^{3}\frac{I_k^2}{2\mathcal{I}_k} + \frac{1}{2}C\beta^2 \qquad (2.24)$$

where B and C are assumed constants which must be calculated from more specific models or determined from experiment. However, one can use quadrupole tensor representations for $B_{\lambda\mu}$ and $C_{\lambda\mu}$, as does Marshalek.[50] The first term is the vibrational kinetic energy and the second the rotational kinetic energy where

I_k = cartesian components of the total nuclear

angular momentum along the axes of the ellipsoid;

$\mathcal{J}_k$ = components of moment of inertia along the axes of the ellipsoid.

$$= 4B\beta^2 \sin^2(\gamma - k\,\frac{2\pi}{3}) \tag{2.25}$$

The rotational energy has the form of the kinetic energy of a top (generally assymetric).

For nuclei having equilibrium deformed shapes, we can make an effective separation of the particle motion and the collective motion under the strong-coupling approximation of Bohr, and write

$$\Psi_{total} = \phi_{part}(\beta\gamma;\vec{r}_i)\psi_{coll}(\beta\gamma\theta_i) \tag{2.26a}$$

where

$$H_{part}\,\phi_n(\beta\gamma;\vec{r}_i) = W_n(\beta,\gamma)\phi_n(\beta\gamma;\vec{r}_i) \tag{2.26b}$$

The shape-dependent energy eigenvalue W_n for the particle Hamiltonian acts like a potential energy term for the collective motions. For the nuclei under investigation here, the effective nuclear field is strongly deformed and describable by a $W(\beta,\gamma)$ with a fairly steep minimum at the values β_e and γ_e at equilibrium deformation (fig. 9). If these minima are steep, then for each

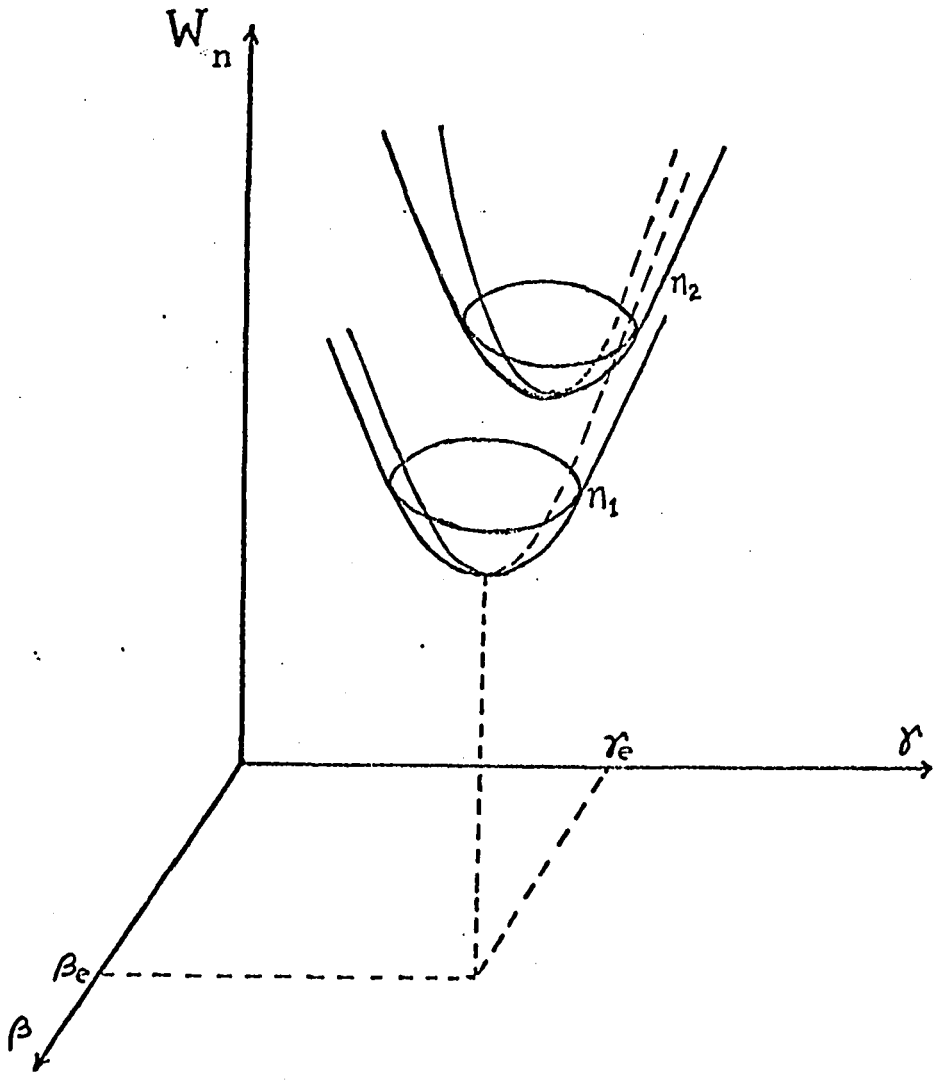

Fig. 9. The intrinsic state energy $W_n(\beta,\gamma)$ plotted against the deformation parameters β and γ.

state of particle excitation, all terms in the Hamiltonian can be expanded about the equilibrium values of β and γ (in the large majority of nuclei $\gamma_e = 0$). Then we have

$$H\psi_{coll} = \{[-\frac{\hbar^2}{2B}(\frac{\partial^2}{\partial\beta^2} + \frac{1}{\beta_e^2}\frac{\partial^2}{\partial\gamma^2} + V(\beta-\beta_e,\gamma-\gamma_e)] + \sum_{k=1}^{3}\frac{I_k^2}{2\mathcal{I}_k(\beta_e,\gamma_e)} + [(\frac{\partial}{\partial\beta}T_{rot})_{\beta_e,\gamma_e}(\beta-\beta_e) + (\frac{\partial}{\partial\gamma}T_{rot})_{\beta_e,\gamma_e}(\gamma-\gamma_e) + \cdots]\}\psi_{coll} \quad (2.27)$$

where

$$H_{coll}\psi_{coll} = [H_{vib}+H_{rot}+H_{rot-vib}]\psi_{coll} = E\psi_{coll} \quad (2.27a)$$

Thus, the collective motion separates into mainly rotational and vibrational parts with a small rotation-vibration interaction term which may be treated by perturbation methods. The zeroeth order wave-function may be written as

$$\Psi_{nucleus} = Af(\beta,\gamma)\Phi_{rot}\chi(\vec{r}_i) \quad (2.28)$$

where $\chi(\vec{r}_i)$ are the single-particle Nilsson states, $f(\beta,\gamma)$ is the vibrational state associated with the

variables β and γ and Φ_{rot} is the rotational wave-function and A is a normalization constant.

2.4 Vibrational States

The characterization of vibrational states is made difficult since the vibrational energies (~ several hundred keV to 2 MeV) are often comparable to intrinsic excitations. However, their existence has been proved experimentally. For vibrations about a spherical equilibrium shape, the Hamiltonian H_s, to first order, reduces to that of a harmonic oscillator. The harmonic oscillations (phonons) are characterized by the quantum numbers λ (the magnitude of the angular momentum) and μ (its projection on the space-fixed axis). These quantum numbers correspond to the appropriate multipole of the deformed nuclear surface. The parity of the phonon is $(-1)^{\lambda}$.

For harmonic vibrations about an equilibrium quadrupole shape, both the equilibrium deformation and the amplitudes of oscillations must be small. Furthermore, in contrast to the spherical case, both the parameters, B_λ and C_λ, and therefore the frequency, depend on $|\nu|$ as well as on λ. For axially symmetric nuclei (with which we are concerned) ν is the projection of λ on the nuclear symmetry axis.

Referring back to H_{vib} in eqn. (2.27a), if

$V(\beta-\beta_e,\gamma-\gamma_e)$ is replaced by $\frac{1}{2} C_\beta(\beta-\beta_e)^2 + \frac{1}{2} C_\gamma(\gamma-\gamma_e)^2$ with corresponding approximations in T_{vib}, then we find that

$$E_{vib} = \hbar\omega_\beta(n_\beta+\tfrac{1}{2}) + \hbar\omega_\beta\ (n_\gamma+1) \qquad (2.29)$$

which corresponds to one dimensional oscillator for β-vibrations and two dimensional oscillator for γ-vibrations. It can be shown that the solutions for the β-vibration involve functions of a_o and the product a_2a_{-2}. Hence, these types of vibrational excitations project zero angular momentum on the symmetry axis (z-axis) and preserve axial symmetry. For γ-vibrations the wavefunction is proportional to γ or to sin γ ($\gamma<<1$) and is thus proportional to a_2 or a_{-2}. Hence the first γ-vibrational excitation has a projection ν on the symmetry axis (z) of two units of angular momentum. This is not a constant of motion strictly since in γ-vibrations axial symmetry is not strictly preserved. As we shall explain in the next section, we expect to see a K=2 rotational band with the first γ-vibrational state as the band head. A corresponding K=0, rotational band is expected to occur with the first β-vibrational state as the band head. However, since more energy is needed to set the nucleus into vibrations than to rotate the ellipsoidal potential, a rotational band based purely on the ground state (K=0) is expected to appear first.

For a discussion of the vibrational states taking

into account anharmonic terms, the reader is referred to the article by Alaga.[51]

2.5 Rotational States

In the original form of T_{rot}, namely

$$T_{rot} = \sum_{k=1}^{3} \frac{I_k^2}{2\mathcal{J}_k(\beta,\gamma)} \tag{2.30}$$

where $\mathcal{J}_k = 4B\beta^2 \sin^2(\gamma - \frac{2\pi k}{3})$, we get rotational bands like that of a top only under certain assumptions specified below.

Following Bohr and Mottelson we assume that one can define a stable moment of inertia function $\mathcal{J}_k(\beta_e,\gamma_e)$ [at the equilibrium deformation] which is constant, and that the nucleus has axial symmetry. Thus, the nucleus behaves like a symmetric top whose rotation is followed adiabatically by the individual nucleon motions within the nucleus. Now we are dealing with a specific picture of the nucleus. The total angular momentum $\vec{I}$ of the nucleus is

$$\vec{I} = \vec{R} + \vec{j} \tag{2.31}$$

where $\vec{R}$ = angular momentum associated with surface motion

$\vec{j}$ = angular momentum associated with particle motion.

The following representation is used (see fig. 10): The total angular momentum is $\vec{I}$ and its projections on the z' (space-fixed) and z (body-fixed) axes are denoted M and K respectively. Though the particle angular momentum $\vec{j}$ is not a good quantum number, its projection, Ω, on the nuclear symmetry axis (assumed here same as the z-axis) is a constant of the motion. Thus, for the axially symmetric case $\Omega = K$. For the even-even nucleus, in its intrinsic ground state all the nucleons pair off so that total spin is zero and, therefore, $\vec{I} = \vec{R}$ and $K = \Omega = 0$ (axial symmetry implies $\vec{R}$ is normal to the z-axis). The odd-mass number case is treated as an odd particle plus an even-even core, and for the odd-odd case, we have two odd particles plus an even-even core.

Assuming axial symmetry, $\mathcal{I}_x = \mathcal{I}_y = \mathcal{I}$, the rotational Hamiltonian becomes ($R_3 = 0$)

$$H = \frac{\hbar^2}{2\mathcal{I}} [\vec{I}^2 - I_3^2] + \frac{\hbar^2 j_3^2}{2\mathcal{I}_3} - \frac{\hbar^2}{2\mathcal{I}} (I_+ j_- + I_- j_+) + \frac{\hbar^2}{2\mathcal{I}} \vec{j}^2 \qquad (2.32)$$

The third term represents the rotation-particle coupling (RPC) due to the coriolis interaction and the last term only affects the intrinsic part of the motion.

The nucleus is assumed to have axial symmetry ($\gamma_e = 0$) and to be symmetric under reflection (r) in a plane

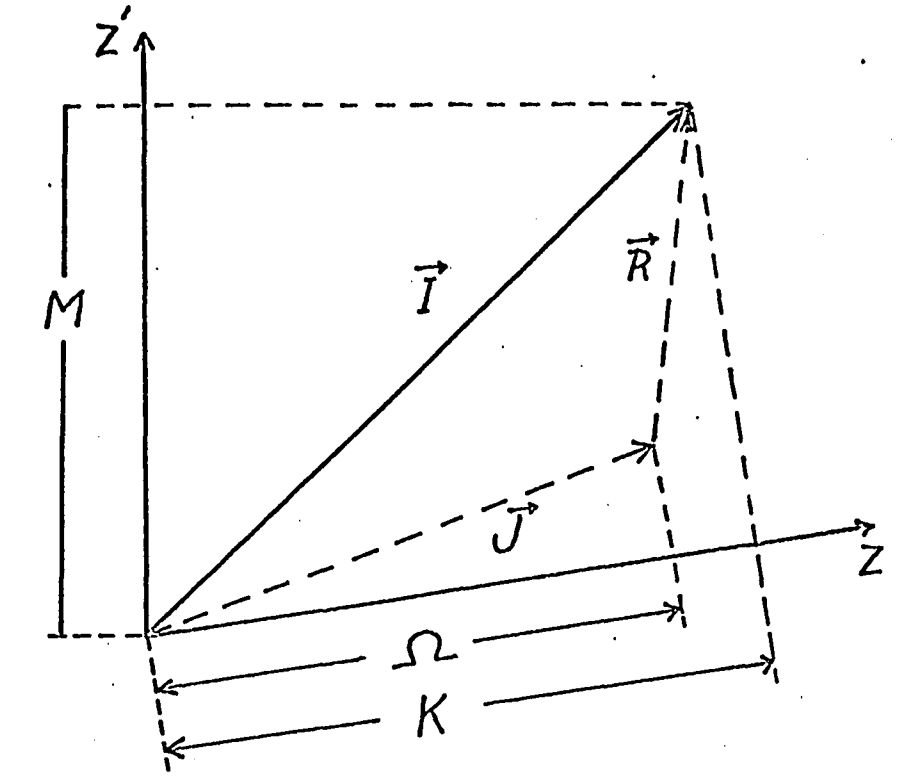

(a)

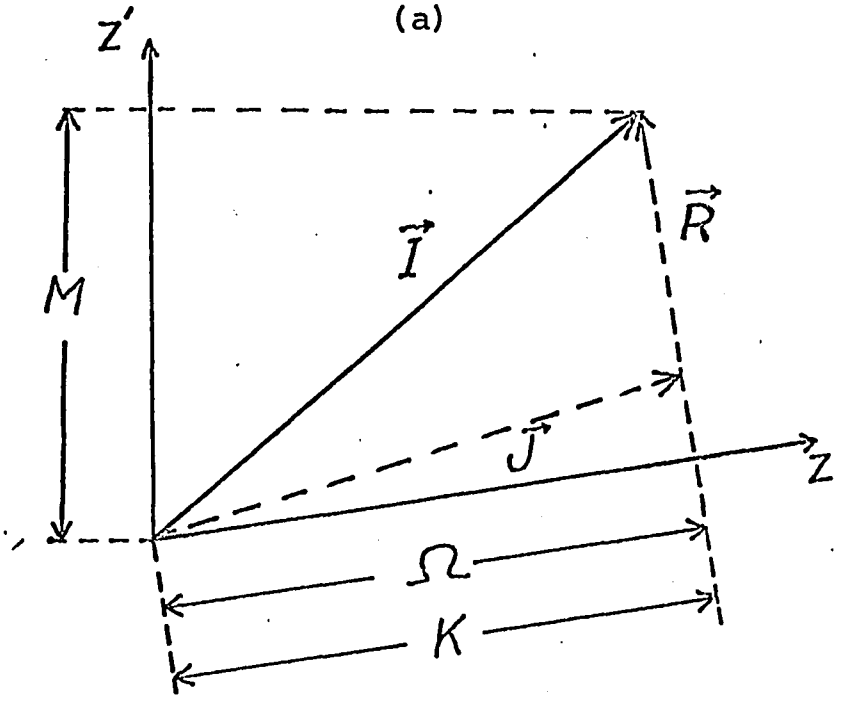

(b)

Fig. 10. A schematic illustration of the coupling scheme for angular momenta in axially-symmetric nuceli. In (a) z is not the symmetry axis and Ω is not a good quantum number and in (b) z is the symmetry axis and Ω is a good quantum number.

perpendicular to the symmetry axis. Taking into consideration the symmetries of the nucleus the adiabatic wave-function may be written as

$$|\tau IMK> = \frac{2I+1}{8\pi^2}\frac{1}{\sqrt{2}}\{D^I_{MK}(\theta_i)\chi_K + (-1)^{I+K} D^I_{M,-K}\chi^\tau_{-K}\} \quad (2.33)$$

where χ^τ_K is the intrinsic wave-function with τ the intrinsic quantum numbers other than K. The $D^I_{MK}(\theta_i)$ are the transformation functions defined in eqn. 2.22. The allowed spin-values are I = K, K+1, K+2,---.

For the K=0 case, since $\chi^\tau_{K=0}$ and $\chi^\tau_{-K=0}$ are degenerate, two possibilities arise.

$$\chi^\tau_0 = r\chi^\tau_{-0} \quad \text{where } r = \pm 1 \quad (2.34)$$

and

$$I = 0, 2, 4\text{---} \quad \text{for } r = +1$$

$$= 1, 3, 5\text{---} \quad \text{for } r = -1$$

For even-even nuclei, particles are coupled pairwise in time reversed orbits where r = +1. Consequently K = 0 bands contain only even spins. In an odd-odd nucleus with $\Omega_n = \Omega_p$, both the r = +1 even I band and the r = -1, odd I band occur slightly displaced from each other.

The energy of a rotational level of spin I is given (to zeroeth order) by

$$E_I = E_0 + \frac{\hbar^2}{2\mathcal{J}} [I(I+1)-K^2] \qquad (2.35)$$

where E_0 is the energy eigen-value of the intrinsic state. For the rotational bands based on the one phonon β or γ-vibrational state E_0 is the corresponding vibrational energy. Since I=K, K+1, K+2,--- for the different levels of the same rotational band (except K=0) the energy spacing is given by

$$\Delta E_I = A[I(I+1)-K(K+1)] \qquad (2.36)$$

where K is the angular momentum of the band-head and $A = \hbar^2/2\mathcal{J}$.

The coupling of rotational angular momenta and that of the β, or γ-vibration is shown in fig. 11a and 11b. Figure 12 is a schematic representation of the ground state rotational band along with the rotational bands based on β and γ-vibrational states. For comparison, the vibrational levels of a spherical nucleus are also shown.

The coriolis term (see eqn. 2.32) couples (to lowest order) different rotational bands with $\Delta K = \pm 1$. For K = 1/2 it also has diagonal matrix elements as it

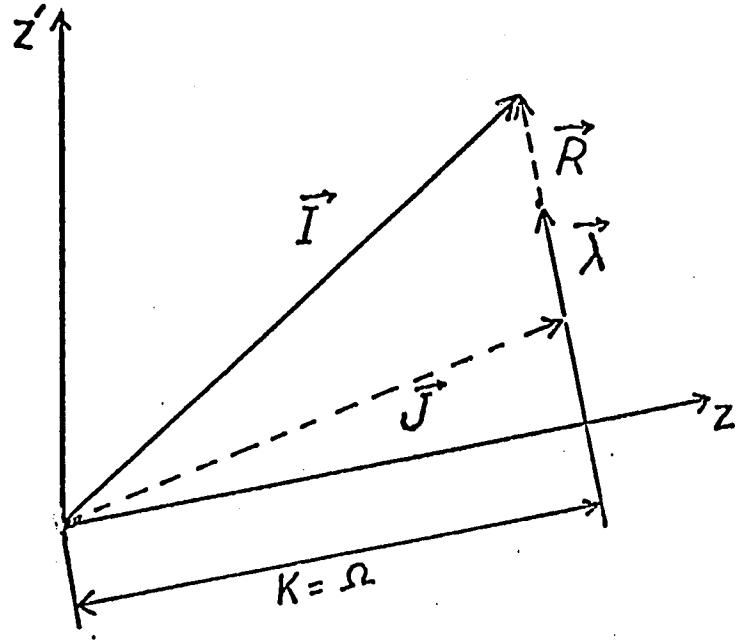

(a) BETA VIBRATION

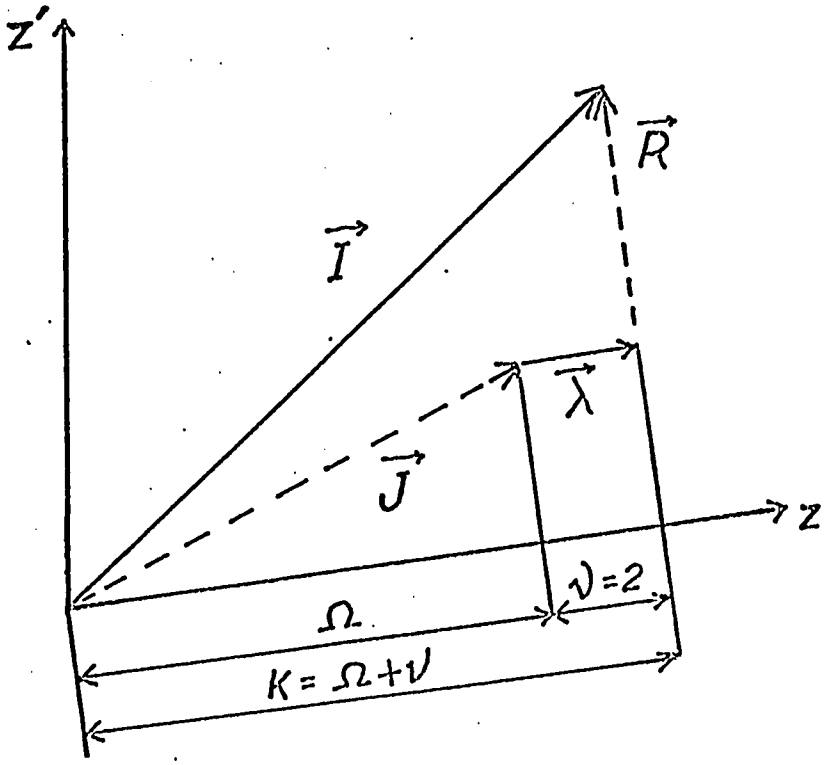

(b) GAMMA VIBRATION

Fig. 11. A schematic representation of the coupling of angular momenta in β and γ bands.

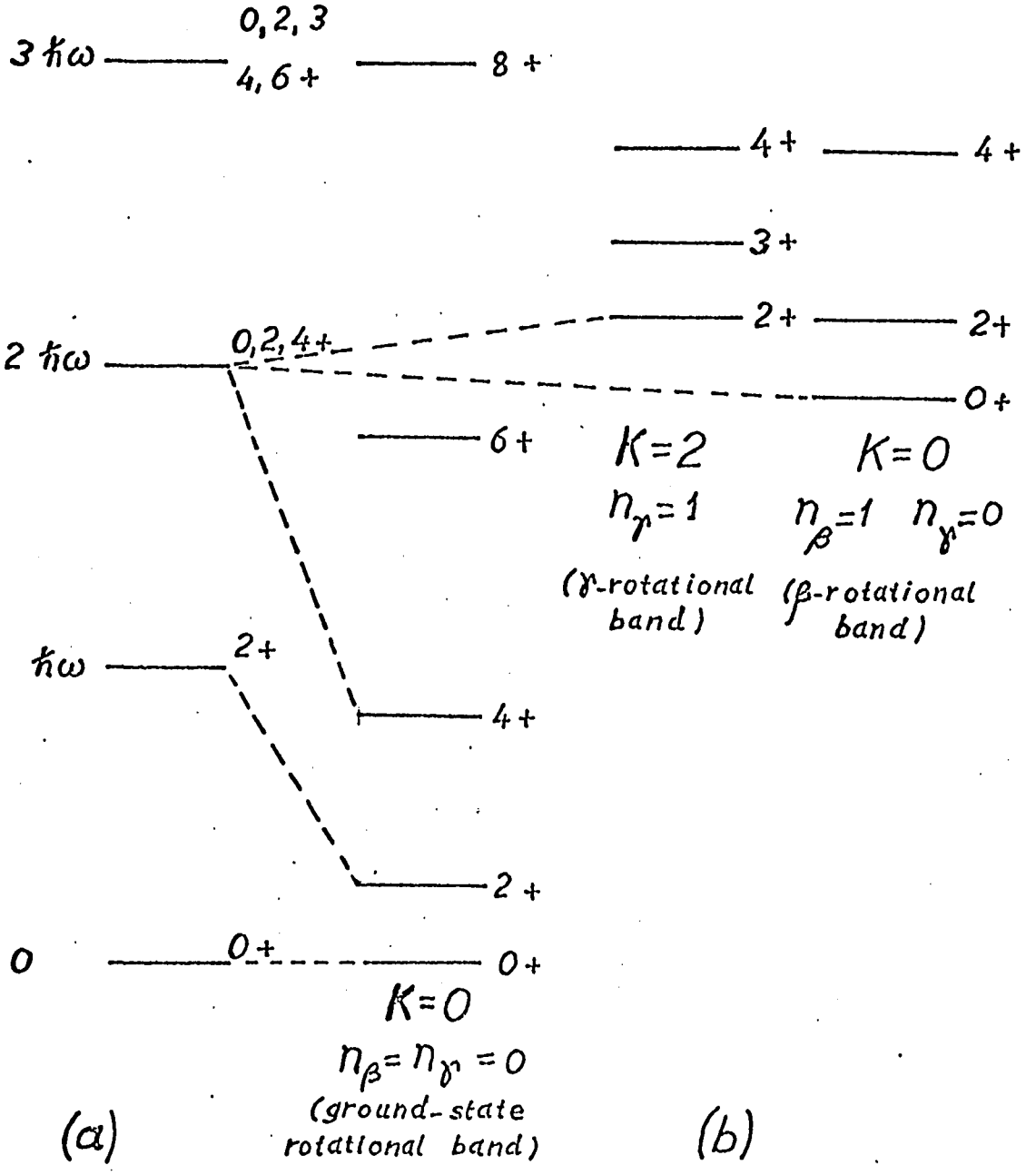

Fig. 12. (a) The nature of the vibrational states in spherical nuclei and (b) the nature of rotational bands in deformed nuclei. Dotted lines indicate the correspondence between the states in spherical and deformed nuclei.

may couple the two parts of the total wave-function with $K = \frac{1}{2}$ and $K = -\frac{1}{2}$. Thus, for odd-nuclei pictured as a single nucleon moving around the $I = K = 0$ even-even core, the $K = \frac{1}{2}$ rotational bands deviate from the usual $I(I+1)$ spacing. In this case

$$E_{rot} = \frac{\hbar^2}{2}\{I(I+1)+\delta_{K-\frac{1}{2}}\ a(-)^{I+\frac{1}{2}}(I+\tfrac{1}{2})\} \qquad (2.37)$$

where $a = -\langle K = \frac{1}{2}|j+|K = -\frac{1}{2}\rangle$ is the measure of the decoupling of the intrinsic motion from the collective rotation.

The higher order effects of the coupling may be expressed in a more general form (as discussed in detail in ref. 7) and then the rotational energy (eqn. 2.36) is modified to the form

$$E_I = E_o+A[I(I+1)-K(K+1)]+B[I(I+1)-K(K+1)]^2 \qquad (2.38)$$

where departures from adiabaticity are included in the B-term.

The higher order effects arising from the coupling of states differing in K by two units play an important role in the coupling of the γ-vibrational band to the ground state rotational band. This band-mixing effect shows up dominantly in the reduced transition probability ratios and has been studied in

the present work and will be discussed further.

The values of the inertial parameters A and B (in the region of interest A ~ 14 keV and B ~ -6 e.v) can be obtained by fitting the experimentally obtained level energies of the rotational band to eqn. 2.38. The value of $A(=\hbar^2/2\mathcal{J})$ reflects very much on the dynamics of the situation. Experimentally determined values of the moment of inertia $\mathcal{J}$ lie between theoretical estimates based on a rigid rotor and that for irrotational flow (liquid drop). Microscopic theories[53,54] seem to give a rather good account of the values of $\mathcal{J}$ in the region of highly deformed nuclei. Attempts have been made recently, to describe the spacing of rotational bands by introducing a variable moment of inertia.[52]

2.6 Deexcitation Processes

A nucleus in radioactive transmutation usually decays into an excited state of the daughter nucleus. This state subsequently de-excites to the ground state predominantly by either γ-emission or by internal conversion.

The transition probability per unit time for the emission of the γ-ray from a randomly oriented nuclear state I to a state I' is[55]

$$T(L,I\to I') = \frac{1}{2I+1} \sum_{M,M'} T(L,M\to M')$$

$$= \frac{8\pi(L+1)}{L[(2L+1)!!]^2} \frac{1}{\hbar} \left[\frac{E}{\hbar c}\right]^{(2L+1)} |\langle f|T^{\sigma}_{LM}|i\rangle|^2 \qquad (2.39)$$

where the T^{σ}_{LM} (multipole moments) are irreducible tensor operators of rank L, corresponding to the expansion of the nuclear electromagnetic field in angular momentum representation. They can be separated into electric and magnetic multipole operators which are of opposite parity, namely

$$\frac{\pi_i}{\pi_f} = \begin{cases} (-1)^L \text{ for electric multipole L} \\ (-1)^{L-1} \text{ for magnetic multipole L} \end{cases} \qquad (2.40)$$

Because of their spherical tensor nature, one can use the Wigner-Eckart theorem and define a reduced transition probability

$$B(L,I_iM_i\to I_fM_f] = \langle I_iLM_iM|I_fM_f\rangle^2 \times$$

$$|\langle I_f \| T_L \| I_i\rangle|^2 \qquad (2.41)$$

where the first factor is just a Clebsch-Gordan coefficient. The second factor is the reduced matrix element and is independent of M_i, M_f and M. Furthermore, in such a γ-transition from a state

$|E_i I_i \pi_i> \rightarrow |E_f I_f \pi_f>$, the following conservation rules apply:

$$E_f - E_i = E_\gamma \qquad \text{(conservation of energy)}$$

$$|I_i - I_f| \leq L \leq I_i + I_f \qquad \text{(conservation of angular momentum)} \tag{2.42}$$

$$\frac{\pi_i}{\pi_f} = \pi_\gamma \qquad \text{(conservation of parity)}$$

By making the appropriate transformation (of the multipole moment operators) to the body-fixed coordinate axes, we can evaluate the matrix element $<I_f M_f K_f| \sum_\nu D^L_{\mu\nu}(\theta_i) M(L,\nu) |I_i M_i K_i>$. The reduced transition probability can then be written[7]

$$B(L) = |<I_i L K_i K_f - K_i | I_f K_f><K_f | M(L, K_f - K_i) | K_i>$$

$$+ (-1)^{I_i + K_i} <I_i, L, (-K_i K_f + K_i | I_f K_f>$$

$$\times \; <K_f | M(L, K_i + K_f | -K_i>|^2 \tag{2.43}$$

In eqn. 2.43 both terms vanish if $L < |K_i - K_f|$ and the second term vanishes for $L < K_i + K_f$.

K-intensity rules: If we now consider the branching ratios ($L<K_f+K_i$) we find

$$\frac{B(L)(I_iK_ij_i\rightarrow I_fK_fj_f)}{B(L)(I_iK_ij_i\rightarrow I_f,K_fj_f)} = \frac{\langle I_iL,K_i,K_f-K_i|I_fK_f\rangle^2}{\langle I_iL,K_i,K_f-K_i|I_f,K_f\rangle^2} \times \left\{\frac{\text{matrix element}}{\text{matrix element}}\right\}^2 \qquad (2.44)$$

From the assumption of adiabaticity the intrinsic matrix elements are equal and hence cancel.

If $L<K_f-K_i$, the Clebsch-Gordan coefficient in the matrix element vanishes and hence we have the K-selection rule, in deformed nuclei,[56] where the degree of K-forbiddenness is defined by $\nu^* = \Delta K-L$. The above equation also applies to beta transitions if the reduced transition probabilities B(L) are replaced by $(ft)^{-1}$. For the K-selection rules in β-decay we can defines a hindrance factor

$$F_\beta = (ft)_{obs}/\overline{ft} \qquad (2.45)$$

where $\overline{ft}$ represents a rough average of ft values for transitions with similar $\Delta I,\Delta\pi$ in the same nuclear region.

The large strength of the E2 transitions

connecting levels of the ground state rotational band is rather well explained in the Bohr-Mottelson picture as collective transitions connecting states of the same intrinsic character. Furthermore, the enhancement of E2 transitions over M1 transitions between levels of the β and γ-vibrational bands and those of the ground state rotational band is also understandable because of the quadrupole nature of the deformation. However, the experimentally determined branching ratios deviate from the predicted values. These deviations are due to the K-mixing or band-mixing effect, that is, the coupling between the ground state rotational band and the β and γ bands. Bohr and Mottelson have proposed a generalized intensity rule based on an expansion of the Coriolis term which can be written as[57]

$$B(L)(I_i K \to I_f K+\Delta K) = \text{const.} \langle I_i K+\Delta K-L, LL | I_f K+\Delta K\rangle^2 \times \frac{(I_i-K)!\,(I_i+K+\Delta K-L)!}{(I_i+K)!\,(I_i-K-\Delta K+L)!} \qquad (2.46)$$

The other competative process of deexcitation is internal conversion. In this,the transition energy is transferred directly to an electron in the atomic orbital which is then ejected with an energy

$$E_e = (E_i - E_f) - E_b \ , \qquad (2.47)$$

where E_b is the electron orbital binding energy. Since internal conversion and γ-decay compete, the branching ratio provides a measure of the relative probability in a given transition, and so the conversion coefficient is defined as

$$\alpha_i = \frac{\text{ith shell conversion probability}}{\gamma\text{-emission probability}} = \frac{N_i}{N_\gamma} \qquad (2.48)$$

where N_i and N_γ are the number of conversion electrons from the ith shell and photons respectively observed per unit time. The conversion coefficients as well as the ratios of conversion coefficients (sub-shell ratios) depend strongly upon the transition multipolarity. The internal conversion coefficient for transitions of pure multipolarity have been calculated.[58-60] Thus, a comparison of the experimental and theoretical values of conversion coefficients can supply important information on the multipolarity of nuclear transitions.

3. Non-Adiabatic Effects and Band Mixing

We have already indicated that to explain quantitatively the experimentally observed spacing of levels in the rotational bands and also the observed

B(E2) branching ratios we need to take into account higher order effects (couplings). These couplings give rise to departures from adiabaticity. In this section we shall try to summarize some of the important developments in this direction although we don't intend that the list will be complete.

Within the Bohr-Mottelson frame-work, the Hamiltonian is written as[17]

$$H = H_{int}+H_{rot}+h_o(\vec{I}^2-I_3^2)+h_2I_-^2+h_{-2}I_+^2 \qquad (2.49)$$

where only the mixing of the ground state band with the β- and γ-bands have been considered. The intrinsic operators $h_{\pm 2}$ change K by 2 units while h_o leaves K unchanged. Also $I_{\pm} = I_1 \pm iI_2$.

The perturbed wave function may written as

$$|IMO\rangle_g' = |IMO\rangle_g-\varepsilon_o I(I+1)|IMO_\beta\rangle-\varepsilon_2 f_2(I)|IM2_\gamma\rangle$$

$$|IMO\rangle_\beta' = |IMO\rangle_\beta+\varepsilon_o I(I+1)|IMO\rangle_g$$

$$|IMO\rangle_\gamma' = |IM2\rangle_\gamma+\varepsilon_2\{\frac{1+(-1)^I}{2}\}f_2(I)|IMO\rangle_g \qquad (2.50)$$

where

$$f_2(I) = \{2(I-1)I(I+1)(I+2)\}^{1/2}$$

$$\varepsilon_o = \langle O_\beta | h_o | O_g \rangle / \hbar\omega_\beta \qquad (2.51)$$

$$\varepsilon_o = \langle 2_\gamma | h_2 | O_g \rangle / \hbar\omega_\gamma$$

The energies of the ground state rotational band become

$$E(I) = [\frac{\hbar^2}{2} + 4\varepsilon_2{}^2\hbar\omega_\gamma]I(I+1)$$

$$- [\varepsilon_o{}^2\hbar\omega_\beta + 2\varepsilon_2{}^2\hbar\omega_\gamma]I^2(I+1)^2 \qquad (2.52)$$

The mixing of the γ and ground state band also produces a slight change in the effective moment of inertia.

The interband branching ratios assume a simple form if the intrinsic quadrupole moments of the ground and excited bands are identical. In that case the B(E2) branching ratios are just the Alaga[56] ratios multiplied by the factors

$$\left[\frac{1+z_o\{I_f(I_f+1)-I_i(I_i+1)\}}{1+z_o\{I_f'(I_f'+1)-I_i(I_i+1)\}}\right]^2 \text{ for } \beta\text{-band} \qquad (2.53a)$$

$$\left[\frac{1+z_2 f_2(I_i I_f)}{1+z_2 f_2(I_i I_{f'})}\right]^2 \quad \text{for } \gamma\text{-band} \qquad (2.53b)$$

where

$$f_2(I_i I_f) =$$

$$\frac{[f_2(I_f)C(I_i 2 I_f;20) - f_2(I_i)C(I_i 2 I_f;00)\{1+(-1)^{I_f}\}/2}{\sqrt{12}\ C(I_i 2 I_f;2-2)} \qquad (2.53c)$$

The z_K are defined by

$$z_o = -\varepsilon_o \langle O_g | M'(E2) | O_g \rangle / \langle O_\beta | M'(E2) | O_g \rangle \qquad (2.54a)$$

$$z_2 = -\sqrt{24}\ \varepsilon_2 \langle O_g | M'(E2) | O_g \rangle / \langle 2_\gamma | M'(E2) | O_g \rangle \qquad (2.54b)$$

Evidently a small mixing amplitude ε_K may produce z_K values that give rise to large correction factors for the interband branching ratios. The values of z_2 have been calculated (see Chap. IV) to check if a consistent set of z_2 parameters is obtainable for the branching ratios in ^{172}Lu decay.

Within the framework of the Bohr-Mottelson picture, further calculations have been done by relaxing some of the restrictions. These non-adiabatic calculations have developed mainly in two directions. One, developed primarily by Faessler,[32] is designed to take into account the rotation-vibration interaction. The results of calculations based upon this approach

compare reasonably well with experimental results for even-even nuclei. The other approach, developed primarily by Davydov,[28-30,65] takes into account departures from axial symmetry. We don't intend to describe these models, though the comparison with our experimental findings will be mentioned in relevent sections of Chaps. IV and V.

Since the improvements in the agreement with the experimental results, accruing from non-adiabatic corrections are not sufficiently general, the need to solve exactly Bohr's collective Hamiltonian has been felt. This solution has been carried out by Kumar and Baranger[61] as a part of their program, which also includes a determination of the parameters of the collective Hamiltonian on the basis of the pairing plus quadrupole model. A further attempt to get a numerical solution to Bohr's Hamiltonian has been recently done by diagonalization with the basic set of states corresponding to the quadrupole vibrations around a spherical equilibrium.[62]

We have presented above the salient aspects of the Unified Model relevent to the present work. For further details the reader is referred to references (6, 7, 10, 21, 37 and 38).

4. Quasi-Particle Theories

In this section we present some of the salient features of the microscopic theories[18,10,19,22,39,68] of nuclear excitations based on an effective pairing plus quadrupole interaction (over and above an average potential). The Hamiltonian is then

$$H = H_o + H_{pair} + H_Q \tag{2.55}$$

where H_o = Nilsson Hamiltonian

$$H_{pair} = -G \sum_{kk'} a^+_{k+} a^+_{k-} a_{k'-} a_{k'+} \tag{2.56}$$

and

$$H_Q = -\frac{1}{2}\chi \Sigma Q^*_\mu \sum_{ks} \sum_{k's'} \langle k|q_\mu|k'\rangle \, a^+_{ks} a_{k's'} \tag{2.57}$$

The operators a_{ks} and a^+_{ks} are the annihilation and creation operators for nucleons in the state (k,s), where k stands for all of the single particle quantum number and $s = \pm$ specifies the time reversed conjugate states. G is the strength of the pairing interaction and χ that of the quadrupole one. The terms Q_μ are defined as

$$Q_\mu = \sum_{ks} \sum_{ks'} \langle k|q_\mu|k'\rangle \langle a^+_{ks} a_{k's'}\rangle \tag{2.57}$$

where

$$\langle k|q_\mu|k'\rangle = c_o\int d^3r\phi_k^* r^2 Y_{2\mu}\phi_{k'} \quad , \quad \mu = \pm 2, \pm 1, 0 \qquad (2.58)$$

are the matrix elements of the single particle operators q_μ.

We first confine ourselves to the pairing correlation. The pairing energy is, on the average,

$$\delta = 11.2 \text{ Mev } A^{-\frac{1}{2}} \quad . \qquad (2.59)$$

This is obtained from the discontinuity in the binding energy in neighboring even-even and even-odd nuclei. Bohr, Mottelson and Pines[42] suggested the applicability of the BCS method to explain the existence of the so called energy-gap in the internal excitation states (exclusive of vibrational and rotational states) in deformed even-even nuclei. The assumptions are

1) The pairing potential is of the form $G\delta(\vec{x})$, so that the potential is constant in momentum space.
2) The pair correlations are expected only near the Fermi level.

Considering an even number of protons or neutrons the pair correlated ground state may be written as

$$\Psi = A_o \exp\left(\sum_k \phi_k a^+_{k+} a^+_{k-}\right) \Omega_o \tag{2.60}$$

where Ω_o = nucleon vacuum. The ϕ_k are the amplitudes for the single particle states k. This can also be written as (on expanding)

$$\Psi = A_o \prod_k (1+\phi_k a^+_{k+} a^+_{k-}) \Omega_o \tag{2.61}$$

because the higher order terms vanish. The normalized state vector becomes

$$\Psi = \prod_k (1+|\phi_k|^2)^{-1/2} (1+\phi_k a^+_{k+} a^+_{k-}) \Omega_o \tag{2.62}$$

For the occupation number n_{ks} of the state (k,s) and the particle number N,

$$n_{ks} = a^+_{ks} a_{ks} \quad , \quad N = \sum_{ks} n_{ks} \tag{2.63}$$

we have

$$\begin{aligned} \langle n_{ks} \rangle &= |\phi_k|^2 (1+|\phi_k|^2)^{-1} \\ \langle N \rangle &= 2\sum_k |\phi_k|^2 (1+|\phi_k|^2)^{-1} \end{aligned} \tag{2.64}$$

The above state vector does not conserve N.

The state vector can also be written as

$$\Psi_o^{BCS} = \prod_k (U_k + V_k a_{k+}^+ a_{k-}^+) \Omega_o \tag{2.65}$$

where

$$U_k = (1+|\phi_k|^2)^{-1/2}$$

$$V_k = \phi_k (1+|\phi_k|^2)^{-1/2} \tag{2.66}$$

so that

$$|U_k|^2 + |V_k|^2 = 1$$

and (2.67)

$$2 \sum_k V_k^2 = N$$

Thus, V_k^2 is the probability that the state (k,s) is occupied by a pair and U_k^2 is the probability that it is empty. The pairing correlation effectively smears out the Fermi surface as shown in fig. (13a). Since there is no relation between the pair occupancy of a state (k,s) and that of another state (k's'). Ψ_o^{BCS} has components corresponding to states with different number of particles. Variational calculations, using a modified Hamiltonian,

$$\tilde{H} = H - \lambda N, \tag{2.68}$$

in which U_k and V_k are varied to give the lowest energy lead to

$$V_k^2 = \frac{1}{2}[1-(\varepsilon_k-\lambda)/E_k] \tag{2.69a}$$

$$E_k = \sqrt{(\varepsilon_k-\lambda)^2+\Delta^2} \tag{2.69b}$$

where ε_k is the single particle energy in state k. The parameters λ and Δ are determined using the above equations along with the conditions

$$\Delta = G \sum_k U_k V_k$$
$$2 \sum V_k^2 = N \tag{2.70}$$

The parameter Δ gives a measure of the diffuseness of the Fermi surface and λ denotes the chemical potential which is equal to the Fermi energy when Δ is zero.

Bogoliubov[66] and Valatin[67] introduced an equivalent representation of the system, so that the interacting neutrons or protons are replaced by a system of independent entities called quasi-particles for

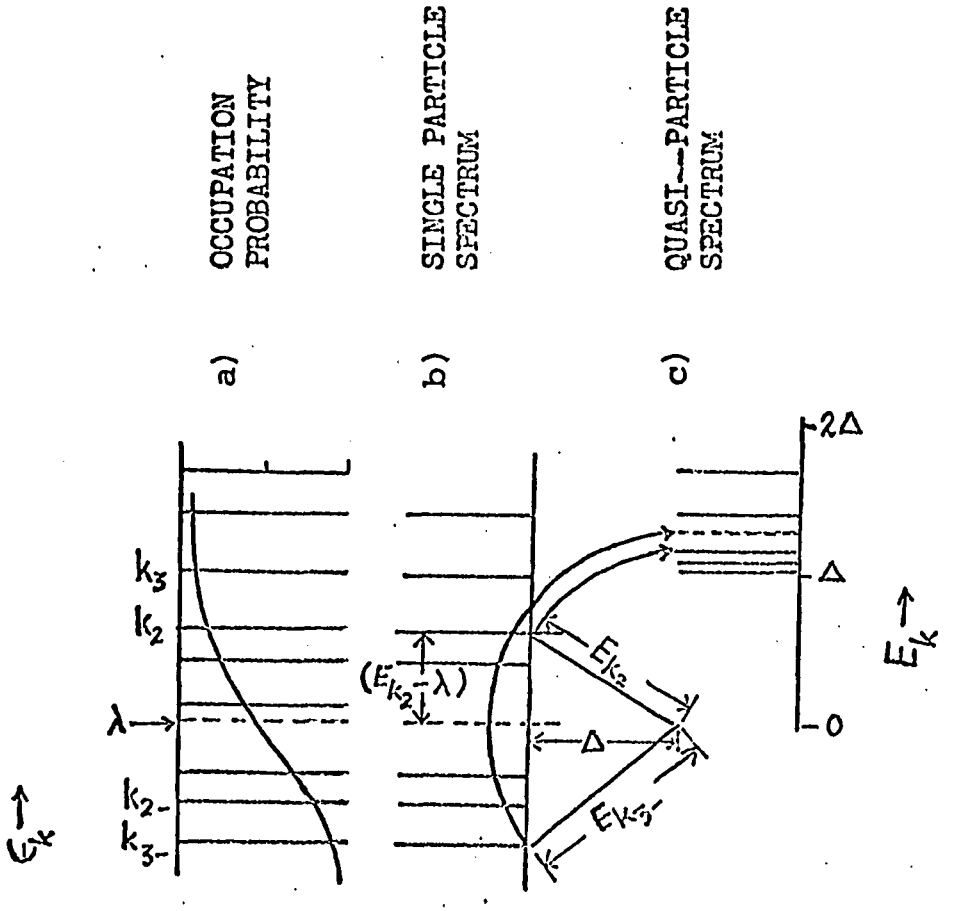

Fig. 13. The pair correlated distribution function and the single quasi-particle spectrum.

which the vacuum state is the Ψ_o^{BCS} defined above. All excitations are then expressed, relative to this ground state, in terms of quasi-particle operators

$$\alpha_{k+}^{+} = U_k a_{k+}^{+} - V_k a_{k-}$$

$$\beta_{k-}^{+} = U_k a_{k-}^{+} + V_k a_{k+} \qquad (2.71)$$

The quasi-particle vacuum Φ_o, as defined by the conditions

$$\alpha_{k+}\Phi_o = 0$$

$$\beta_{k-}\Phi_o = 0 \quad , \qquad (2.72)$$

is seen to be the same as Ψ_o^{BCS}. Thus, in the above definition, α_{k+}^{+} is an operator which acts to create a particle in level k with amplitude U_k corresponding to the probability that k is unoccupied by a pair and to create a hole with amplitude V_k corresponding to the probability that level k is occupied by a pair. The quasi-particle has some properties of a particle and some of a hole. The quasi-particle is a nucleon hole when $\varepsilon_k < \lambda$ and a particle when $\varepsilon_k > \lambda$ only for the case G = 0. The excited states are obtained by operating on Φ_o with the quasi-particle operators.

Thus, for an even-even nucleus, low lying excited states may be obtained by breaking a nucleon pair with the promotion of one particle or by promoting both to a higher state. This is equivalent to the creation of two quasi-particles. An excited two-quasi-particle state of energy $E_k+E_{k'} = \sqrt{(\varepsilon_k-\lambda)^2+\Delta^2} + \sqrt{(\varepsilon_{k'}-\lambda)^2+\Delta^2}$ may, for example, be written as

$$\Phi_{(2)} = \alpha_k^+\beta_{k'}^+\Phi_o$$

Since $E_k+E_{k'}>2\Delta$ always, the energy-gap appears in the intrinsic excitations of even-even nuclei.

For an odd nucleus, the ground state may be represented as

$$\Phi_o^{odd} = \alpha_k^+\Phi_o \tag{2.73}$$

and low lying excited states may be obtained by changing the orbital $k \to k'$ where $\varepsilon_{k'}>\varepsilon_k$, and the excitation energy is

$$\Delta E_{kk'} = \sqrt{(\varepsilon_k-\lambda)^2+\Delta^2} - \sqrt{(\varepsilon_{k'}-\lambda)^2+\Delta^2} \tag{2.74}$$

so that there is no energy-gap. For an odd-odd nucleus, two quasi-particle states may also occur. However, in this case further modifications are required

because of the lack of identity between neutrons and protons. In fig. 13 we present the nature of the pair correlated distribution function and also the nature of the single quasi-particle spectrum.

If the pairing correlations are confined to states near the Fermi surface, the removal of one of these states from the correlated wave function caused by placing a particle into it will reduce the energy gap for states near the Fermi surface. This is the "blocking effect". In addition, calculations have also been done introducing residual interactions between quasi-particles. A lot of progress has been made in these directions through the works of Soloviev,[19] Belayev[68] and Migdal.[69]

The γ-transitions are affected by pairing correlations in the following ways:

1) The pairing correlation considerably slows down electric transitions between single quasi-particle states near the Fermi level, but does not affect significantly the magnetic transitions between corresponding states.

2) For transitions from two quasi-particle states to the ground state opposite conditions apply.

The effects of pairing correlations on β-decay matrix elements[70,71] are determined by the change in the number of protons or neutrons in paired states.

The single particle transition strengths are multiplied by factors involving the occupancy coefficients U_k and V_k. This fact may be utilized as a possible method to evaluate U_k^2 and V_k^2 from experimental log ft values. However, this requires that the single particle β-decay matrix elements be known accurately.

Now we would like to discuss briefly some recent microscopic calculations on collective excitations which are relevent to the present research. A number of investigations have been carried out on the vibrational levels using the method of Sawada.[72] However, we confine ourselves here to the works of Bes,[31] Marshalek[50,17] and Paulichenkov[33].

Marshalek, using a generalization of the Araujo method,[73] has discussed collective vibrations of spheroidal nuclei and has calculated the B coefficient (eqn. 2.38) and the band-mixing parameters z_k. The existence of two $K=2^+$ bands have been proposed by both Soloviev[19] and by Marshalek.[50]

Marshalek contends that the lowest $K=2^+$ band is more likely to be a two-quasi-particle state while the higher $K=2^+$ state is considered to be the γ-band head. However, Soloviev classifies the higher $K=2^+$ state as the two-quasi-particle state.

The E2 transition strengths from the $K=2^+$ states to the ground state band depend very much on the

two quasi-particle or collective (γvibrational) nature of the deexciting state. The transition strength is small if the $K=2^+$ state is a two quasi-particle state. However, according to Soloviev[19] and Belayev[68] a particular vibrational state with K=n may be described as a coherent superposition of all the possible two quasi-particle states with K=n in the neighborhood of the Fermi level. In that case, the $K=2^+$ deexciting states may show either weak or strong collective behavior depending on the number of states and the nature of their superposition. Experimentally, such states may reveal different structures depending on the type of measurement done. For example, a single nucleon transfer measurement is more likely to show the two quasi-particle nature, while any measurement involving radiative process is expected to show more of the collective behavior.

Marshalek has carried out a Hartree-Fock-Bogliuvov calculation of the parameter B. He expresses B as the sum

$$B = B_c + B_\lambda + B_\Delta + B_\beta + B_\gamma \qquad (2.75)$$

The term B_c arises from the effect of the Coriolis force on independent quasi-particle motion (the gap parameters Δ_n, Δ_p and the Lagrange multipliers

λ_n and λ_p held fixed). B_λ introduces the correction from a readjustment of the parameters λ_n and λ_p. B_Δ arises from the change in the pairing correlation due to the Coriolis force (Mottelson-Valatin effect[74]) which acts with opposite sign on particles in time-reversed states and hence has a cancelling effect on their correlation (Coriolis antipairing or CAP). The terms B_β and B_γ arises from the rotation-vibration interaction which produces centrifugal stretching of the deformed field. Based on the numerical values of Marshalek, the dominant contribution to B seems to come from B_c and B_Δ, and not from B_β and B_γ. However, this is in contrast to the contention of the Bohr-Mottelson approach in which the term B is a consequence mainly due to the rotation-vibration interaction. This point seems to need further investigation.

Marshalek[50,17] has calculated the electric quadrupole transition probabilities using time dependent Hartree-Fock-Bogliubov equations. He further obtained the band mixing parameters, z_K. However, Marshalek worked within the adiabatic approximation of slow, but large amplitude vibrations and the energy-gaps Δ_p and Δ_n were used as adjustable parameters to obtain proper numerical values for the B parameter and the z_K coefficients. Bes[31] solved the TDHFB equation

in the nonadiabtic limit using the random-phase approximation (RPA). The Coriolis force is considered up to second order in the calculations of the mixing parameters. Pavlichenkov[33] carried out microscopic calculations (RPA method) including the rotation-vibration interaction. His development is a microscopic counterpart of the Bohr-Mottelson approach to the rotation-vibration interaction. A comparison of the results of these calculations with the results of the present study will be presented in Chap. IV.

CHAPTER III

INSTRUMENTATION, EXPERIMENTAL PROCEDURE AND DATA ANALYSIS

In the present investigation both Lithium drifted Germanium, Ge(Li), and Lithium drifted Silicon, Si(Li) spectrometer systems were used. The components involved were two Ge(Li) detectors and one Si(Li) detector each coupled to low noise charge sensitive preamplifiers and shaping main amplifiers. The pulse analyzers consisted of a 4096 channel single parameter and a 4096 x 4096 dual parameter system. A delayed coincidence experiment was also performed where a thin window NaI(Tl) detector was used to provide gate pulse. Block diagrams of the equipment are presented in figures 14 and 15.

1. Ge(Li) and Si(Li) Detectors

Ge(Li) and Si(Li) detectors are basically (p-i-n) diodes with a reverse bias. Ionizing radiation on entering such a device loses energy in forming electron-hole pairs. These pairs are then collected by an applied electric field and the resulting charge is interpreted as an electronic pulse (see fig. 16). For good spectrometer characteristics it is very important that the detector collect all the charge produced. Possible sources of charge loss are

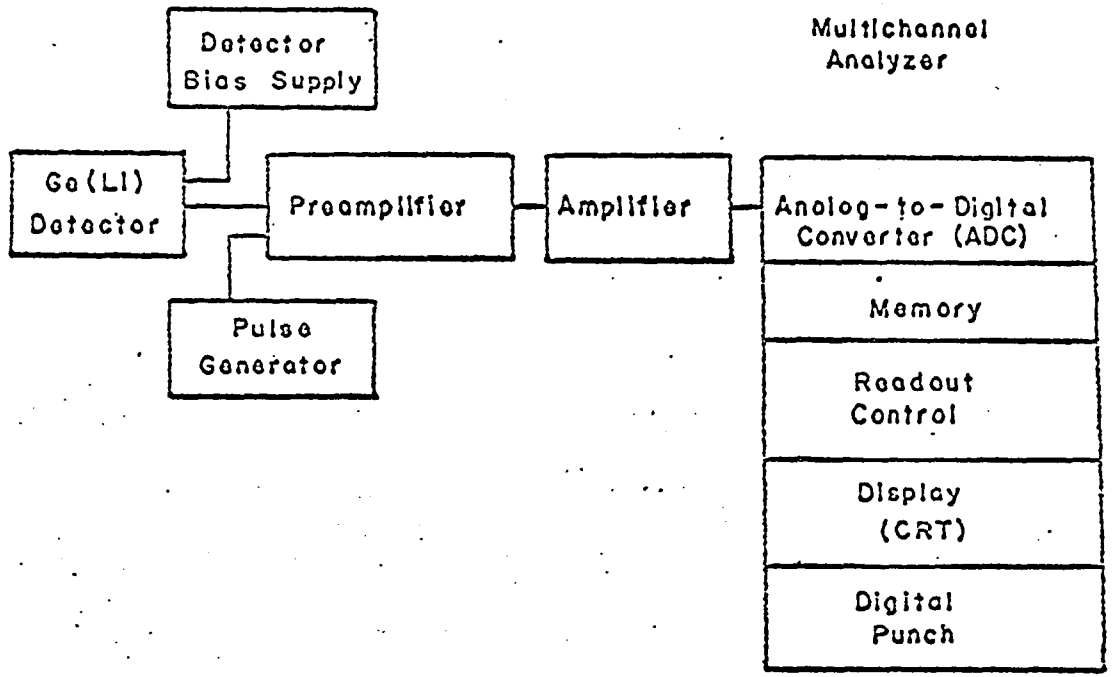

Fig. 14. Block diagram of the single parameter spectrometer system.

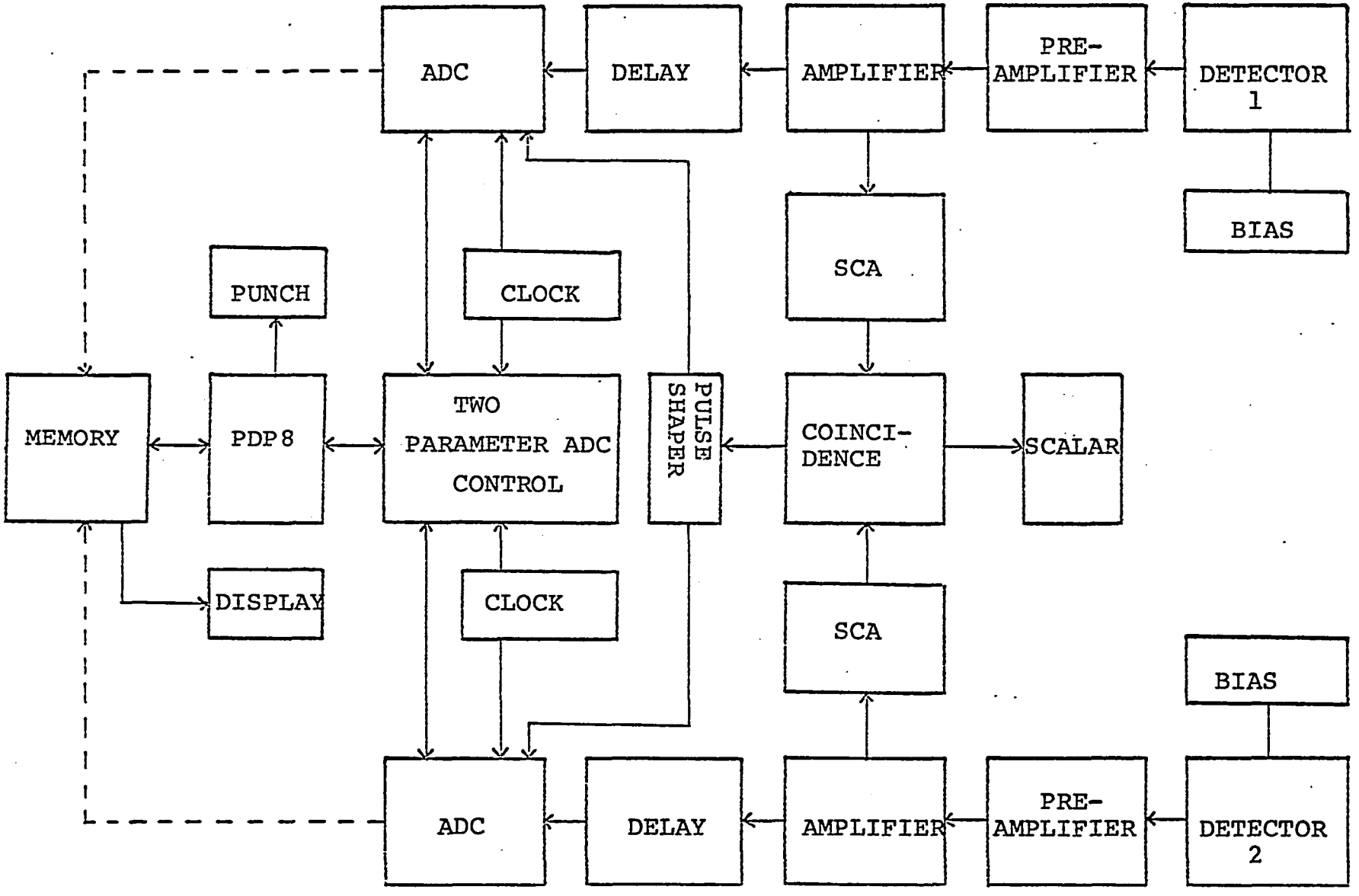

Fig. 15. Block diagram of the two parameter spectrometer system.

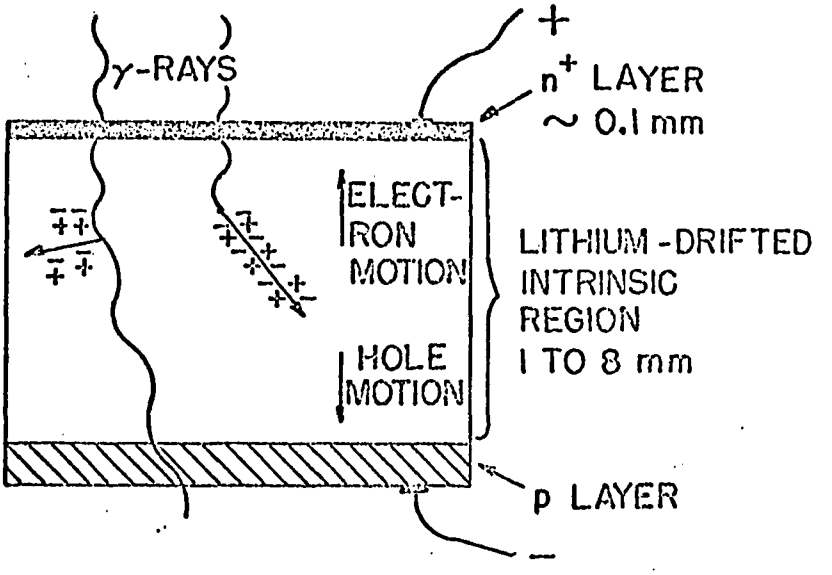

Fig. 16. The detection of ionizing radiation in a semiconductor detector.

"recombination" and "trapping".

The most important characteristic of semiconductor detectors is high energy resolution, which is 20 to 25 times higher than that of a NaI(Tl) scintillator. However, the efficiency of commonly used NaI(Tl) scintillation detectors is usually much higher than semiconductor detectors. Hence, for intensity measurements a Ge(Li) detector of large volume is preferable, and in this regard Ge(Li) detectors of 100 cm^3 are now being fabricated. A device of that size has a full energy peak efficiency as high as that of a 1.5" diameter by 1" thick NaI(Tl) detector. However, for general nuclear spectroscopic work, the higher energy resolution is more important. The poorer detection efficiency can be easily compensated for by using high activity sources and properly designed amplifiers and analyzers, as have been employed in the present investigation.

The factors affecting the energy resolution of semiconductor detectors are

1) Statistical fluctuation in the production and collection of electron-hole pairs.
2) Charge collection efficiency.
3) Detector leakage current noise.
4) Pre-amplifier and amplifier noise.

An expression for the FWHM due to statistical

spread is, to first order,

$$4E = 0.129 \sqrt{(EF)} \text{ (Kev)} \qquad (3.1)$$

where E is the energy absorbed by the detector and F is a semi-emperical factor called the Fano factor. The average energy required to produce an electron-hole pair in Germanium is 2.98 ev/pair at $77^{o}K$.

Low charge collection efficiency arises from defects in the intrinsic region of the detector, which may cause loss of current due to trapping and recombination. This can be partly removed using a higher reversed bias. However, the bias used is limited by the considerations of leakage current and noise. The leakage current depends also on the operating temperature and resistivity of the detector. Thus, the Ge(Li) detector is maintained at liquid nitrogen temperature in order to reduce all these effects. Since the detector also acts like a capacitor, it is important to match its impedence to that of the input stage of the pre-amplifier in order to obtain the best signal to noise ratio. This was accomplished here by using an optimum number of FET's in parallel at the input stage of the pre-amplifier.

Table 1

*Semiconductor Detectors

Detector type	Volume cm^3	Compensated depth cm	Area cm^2	Capacitance Pico Farads	Resolution (keV) FWHM
Ge(Li) planar	2	0.5	4	12	2.5 @ 662 keV
Ge(Li) coaxial	8	0.6 diameter 2.2 height	2.6	45	2.4 @ 662 keV
Si(Li)	0.16	0.2	0.8	10	0.8 @ keV

*Table 1 summerizes the basic properties of the semiconductor detectors used in the present investigation. For the planar Ge(Li) detector the resolution quoted is for an operating bias of 440 volts, with the detector coupled to a room temperature FET preamplifier and 1.6μ sec hsaping time on the main amplifier. For the coaxial Ge(Li) detector, the operating bias was 750 volts and the shaping time used was 2μ sec.

2. Pre-Amplifiers and Amplifiers

The pre-amplifier as the name indicates senses the charge pulse generated in the detector by the ionizing radiation and converts it to a voltage pulse (linearly amplified) suitably prepared to convey it across the cable to the main amplifier. A diagram of a charge sensitive pre-amplifier is shown in fig. 17. The FET pre-amplifiers used in the present investigation satisfy very well the main requirements of 1) low noise, 2) linearity and 3) temperature stability (see table 2).

The main amplifiers used with operational characteristics are presented in table 2. In the main amplifier, pulse shaping as well as amplification is performed. Pulse shaping is done with RC networks having much shorter time constants than that of the pre-amplifier, in order to remove the slow decay tail of the pre-amplifier pulse and thus avoid pulse pile-up. Furthermore, the time constants shown in the table seem to give the best signal to noise ratio.

3. Multichannel Analyzers

The multichannel analyzers used were a Nuclear Data model 161F-181MR (4K channel ADC and 1K memory) and a Nuclear Data model 50/50 system (4K channel ADC with 4K memory). A Digital Equipment Corporation Programmed Data Processor (PDP8/L) is part of the

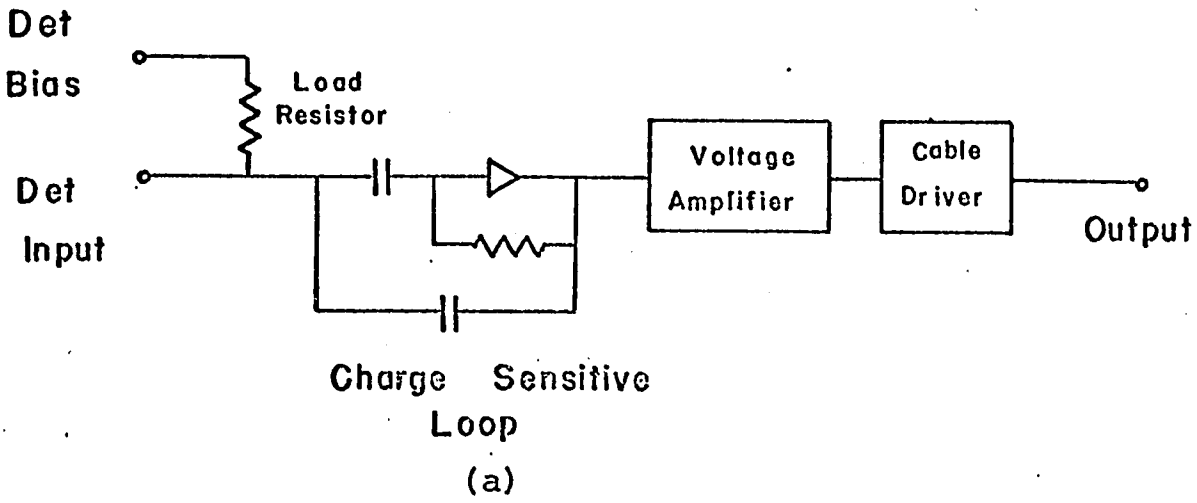

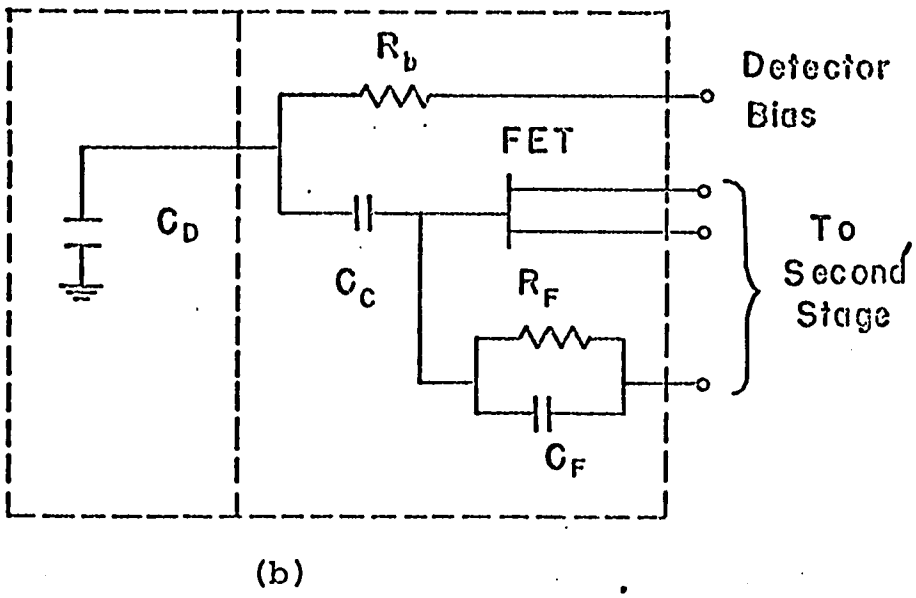

Fig. 17 (a) A block diagram of a charge sensitive preamplifier.
(b) A block diagram of a cooled FET preamplifier. The cooled portions are enclosed in dashed lines.

Table 2

Characteristics of the pre-amplifiers and amplifiers

Detector		Pre-amplifier			Amplifier			
Model	Voltage	Model	FET's at input	Temp.	Model	First diff.	Second diff.	Int.
Ge(Li) 2 cm^3 planar	440	Tennelec TC 130	Two	Room	TC 200	1.6μ sec	1m sec	1.6μ sec
Ge(Li) 8 cm^3 coaxial	750	Ortec 118A	One	Room	Ortec 440	2μ sec	unipolar	2μ sec
Si(Li) 0.16 cm^3 planar	550	Kevex 1000/2000	One	77°K	TC 200	1.6μ sec	1m sec	1.6μ sec

50/50 system. The ADC's are interfaced both to the storage and display unit and to the PDP8/L. Single parameter analysis, two parameter analysis and time-shared single parameter analysis can be performed using panel switches or under computer control. The two parameter storage configuration (matrix) is $2^n x 2^m$, where the sum of n+m must be less than or equal to 12. The system permits continuous monitoring of data during acquisition and computer manipulation. The data may be displayed in any one of five formats; contour (XY), isometric and isometric reverse (three dimensional) and XZ or YZ. The 4K locations in the memory may be digitally selected for diplay in increments as small as 64 channels. Furthermore, analog selection of any segment of the displayed data may be obtained under diaplay intensification. The selected area, digital or analog, may be read out or manipulated as desired without destroying any portion of the data. The data is read out on a paper tape punch system and is converted to computer cards on an IBM-046 tape to card converter. The data cards are then subjected to the analysis described in section 5.

4. Source Production

A source of 5y ^{172}Hf was prepared by (α,2n) and (α,3n) reactions on natural Yb. Six months time was

allowed for the short lived contaminants to decay away. The Hf fraction was then separated from the Yb target† and the experimental studies begun. The only discernable activities at that time were ^{172}Hf, ^{175}Hf, and ^{172}Lu. All γ-ray energy calibrations and 17 of the γ-ray intensity runs were done with the equilibrium sample. Neither ^{172}Hf nor ^{175}Hf contribute to the γ-ray spectrum above about 400 keV and, consequently, the high energy portion of the ^{172}Lu spectrum is most easily obtained from the equilibrium sample. During the 9 month period that followed, seven sources of pure ^{172}Hf and ^{172}Lu were obtained by an ion exchange procedure* described below. These sources were used to obtain precise relative γ-ray intensities and to search for unknown contaminants by correlating the relative intensities with time.

5. Chemical Separation

The separation* of the Hf and Lu fractions was done using an ion exchange column packed with Dowex 1-X8 ion exchange resin in chloride form. The column was washed with concentrated HCl and the Hf-Lu sample was loaded onto the column after HCl gas was passed through

---

†the separation was performed by L.D. McIsaac of the Nuclear Technology Branch of Idaho Nuclear Corporation, Idaho Falls, Idaho.

*the separation procedure was obtained from L.D. McIsaac (see previous footnote).

the HCl solution in which it was contained. This latter procedure insured that the solution was concentrated. The Lu fraction was carried down and out of the column with a wash of concentrated HCl. When no additional activity could be removed, a 6N solution of HCl was used to remove the Hf fraction.

6 . Measurements and Data Analysis

The γ-ray energies and relative intensities were determined from spectra taken with all three of the detectors. The photopeak efficiency calibrations for the Ge(Li) detectors and the non-linearity corrections for the analyzer systems are described in ref. 75. The photopeak efficiency calibration for the Si(Li) detector is described in Chapter V.

For energy calibration purposes, γ-rays of accurately known energy were analyzed simultaneously with the source. The set of energy standards employed in this work is given in ref. 75. The γ-ray spectra were analyzed with a computer routine developed by Helmer et al.[76] which fits a Gaussian to the photopeaks and then makes a fit of the calibration energies to the corresponding photopeak centroids which were previously corrected for the nonlinearity of the system. By using the coefficients of the energy calibration fit, energies of the source lines were computed from the

corresponding peak centroid values also corrected for the non-linearity.

After the energies of the major lines in the spectrum were determined, they then served as standards in the spectra which were run without calibration sources. These latter spectra were used to obtain precise relative γ-ray intensities and also γ-ray energies for the weak lines. The computer routine in this case computes the intensity by dividing the photopeak area by the photopeak efficiency for the corresponding energy. The efficiencies of the Ge(Li) detectors used here have been determined to be accurate to within 5% over the energy range 80 to 2500 keV.

CHAPTER IV

THE DECAY OF ^{172}Lu AND THE ROTATIONAL BANDS OF ^{172}Yb

1. Introduction

The 5y ^{172}Hf electron capture decays to 6.7d ^{172}Lu and, consequently, it is possible to study the isotopes together in secular equilibrium and individually after ion exchange separation. In this chapter we present the investigations on the decay of ^{172}Lu to ^{172}Yb.

The even-even ^{172}Yb nucleus is well removed from shell closure and presumably has a non-spherical shape. A number of investigations of the level structure of ^{172}Yb have been reported: 1) From the electron capture decay of ^{172}Lu which predominantly populates states of ^{172}Yb above 1.8 MeV[77-87]; 2) from the β^- decay of ^{172}Tm which populates states below 1.8 MeV[88,89]; 3) from (d,p), (d,t), and (d,d') reactions[90]; and 4) from Coulomb excitation studies.[91-93]

A thorough investigation has been done on the K=3 band at 1172 keV.[94-98] However, except for the work of Prather[86] and the unpublished work of Roche *et al.*[87], an overall investigation of the band structure of ^{172}Yb, with high resolution Ge(Li) detectors, has not been reported. There is a definite discrepancy regarding the K assignment of the band

comprising the 1609, 1700, 1803, and 1926 keV levels (K=2 or 3), and the K assignment of the band at 2174 keV (K=3 or 4).[86,88,89,97] The abundance of K-forbidden transitions points to the existence of couplings between bands and, consequently, a study of band mixing effects seems very appropriate (see refs. 89, 93 and 97). Furthermore, in the latest work[86] only 78 transitions were placed into the proposed scheme. All these facts point to the necessity of a further study of the level structure of ^{172}Yb; and even more so, because of the recent theoretical developments (see Chapter II). Accurate determination of level characteristics and the nature of their deexcitation can only be obtained with precisely measured gamma energies and intensities. In the work reported here we have been able to provide a better characterization of the level-structure of ^{172}Yb as a result of precise measurement of the γ-ray energies and intensities.

2. Experimental Results

Typical γ-ray spectra obtained in the present investigation are displayed in figs. 18-22. The γ-ray energies and intensities presented in table 3 represent weighted averages of the separate measurements. The quoted energy uncertainty is the largest of

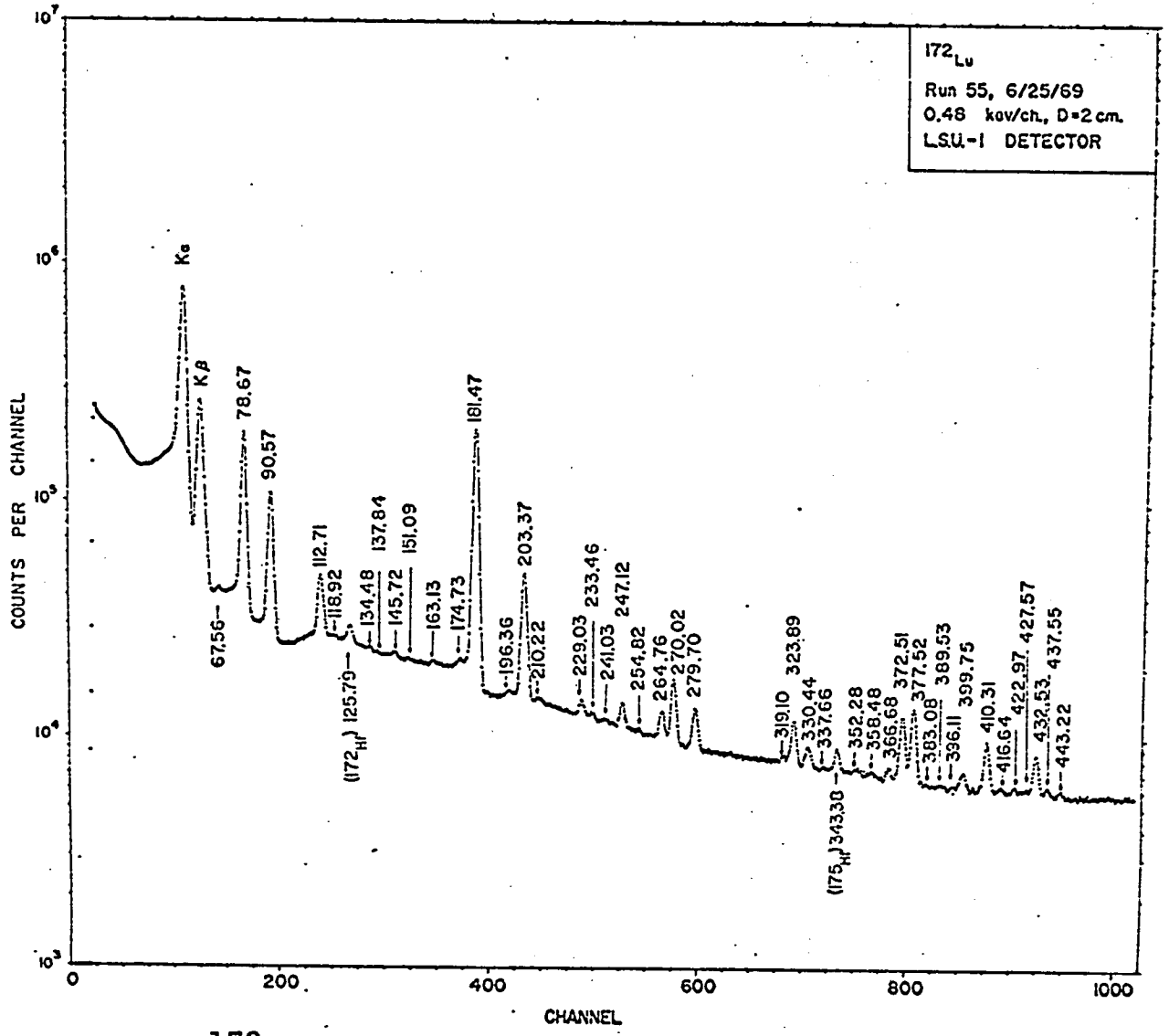

Fig. 18. The ^{172}Lu γ-ray spectrum from 0 → 0.48 MeV.

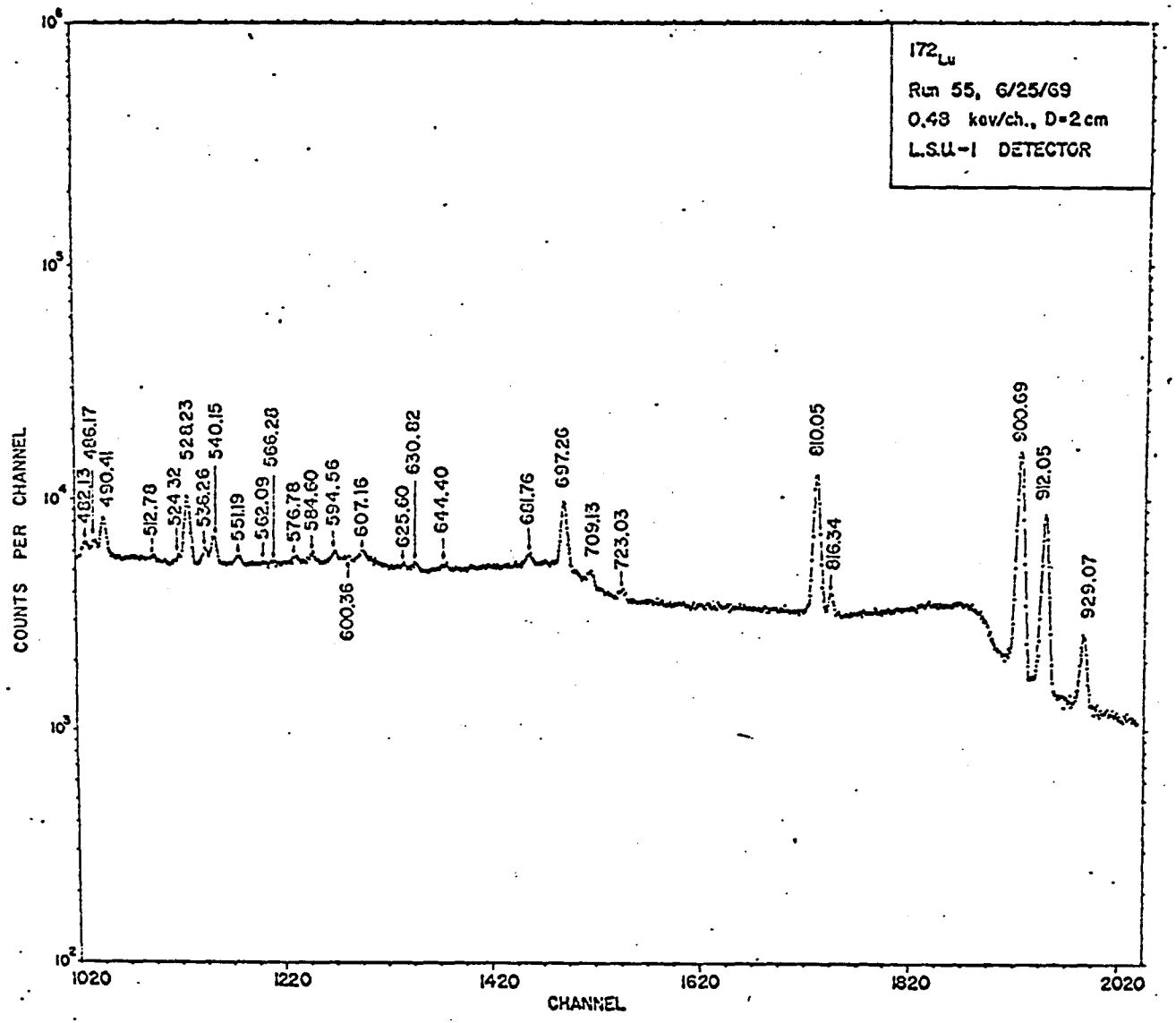

Fig. 19. The ^{172}Lu γ-ray spectrum from 0.48 → 0.95 MeV.

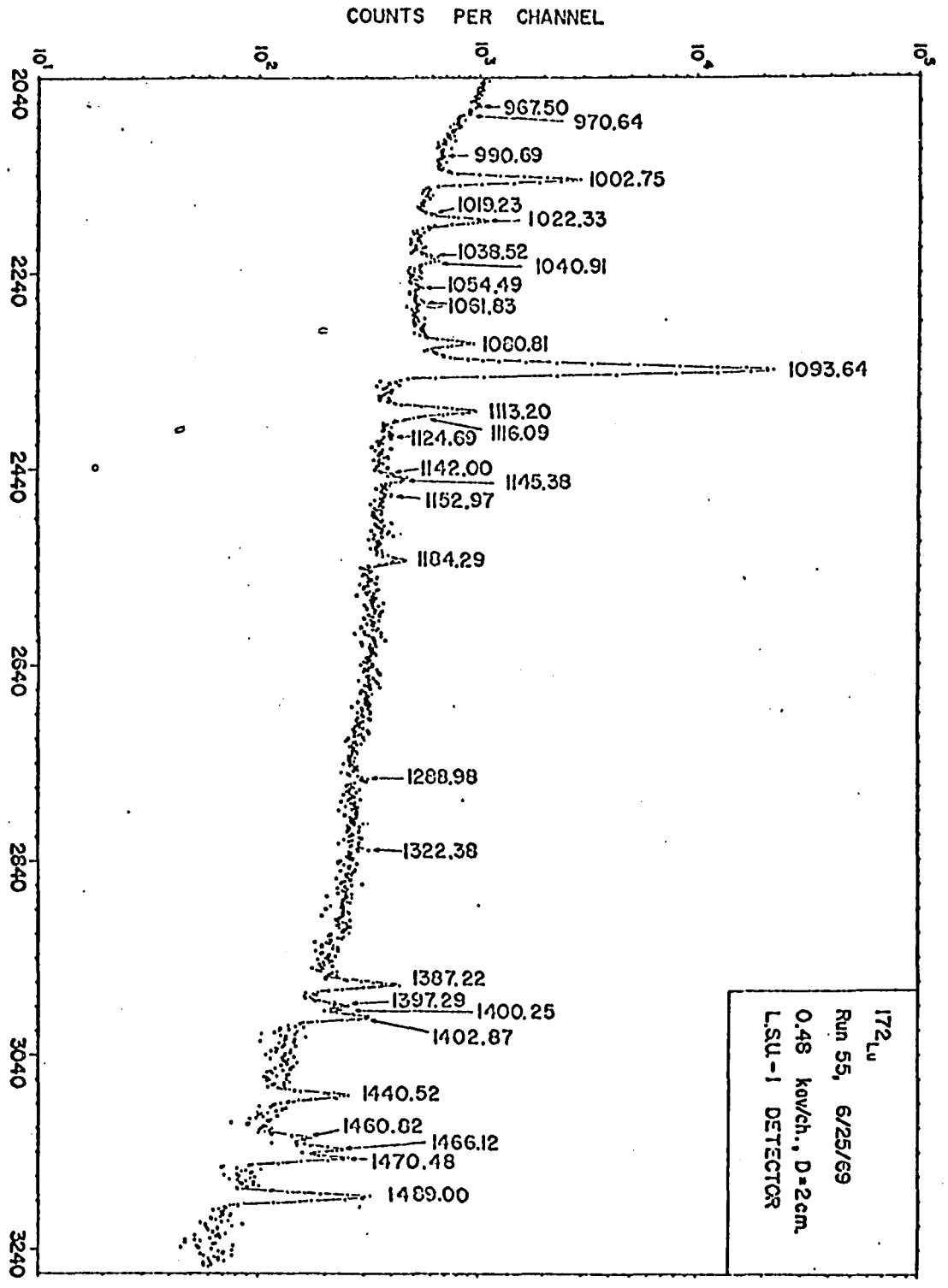

Fig. 20. The ^{172}Lu γ-ray spectrum from 0.95 → 1.5 MeV.

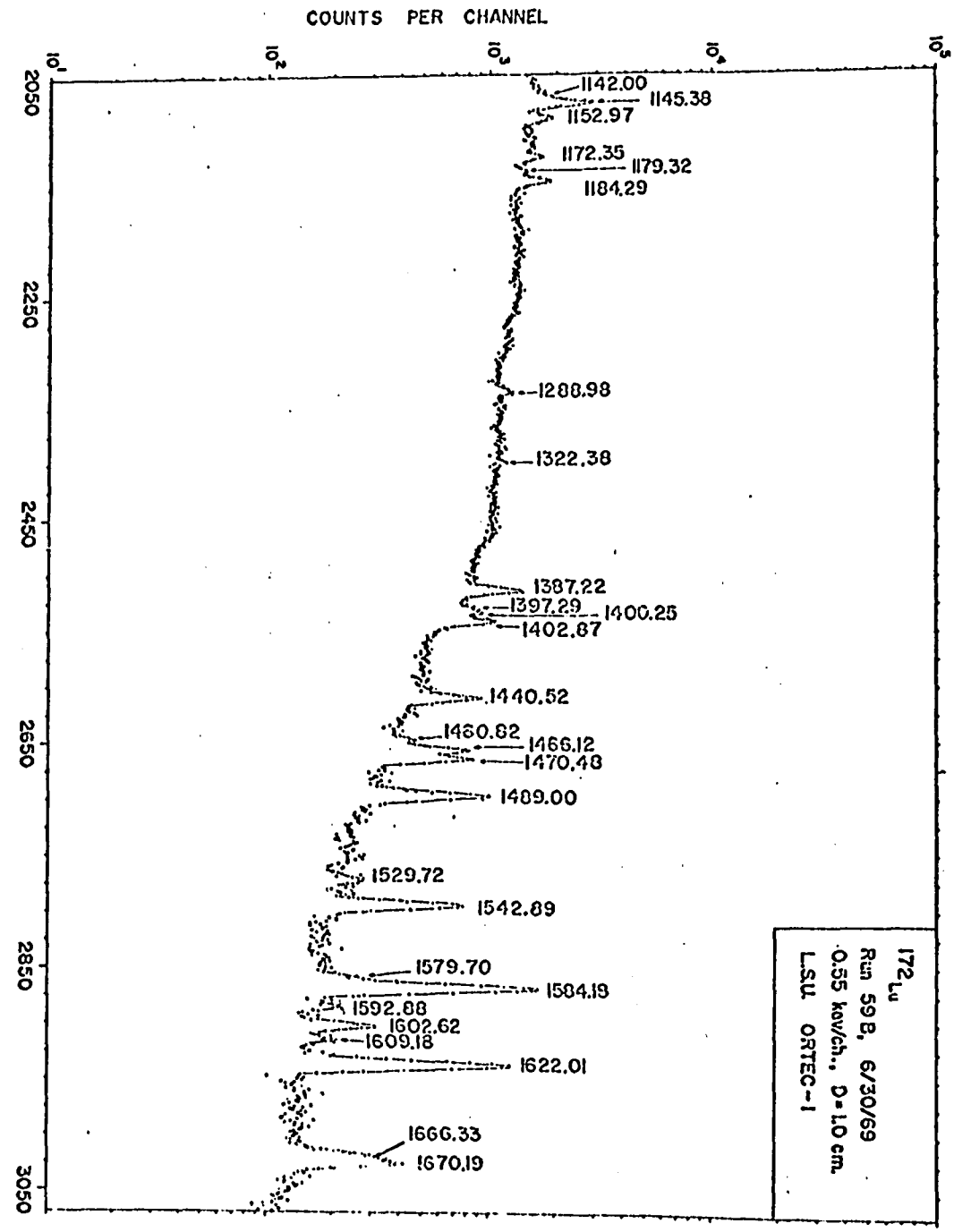

Fig. 21. The ^{172}Lu γ-ray spectrum from 1.13 + 1.69 MeV.

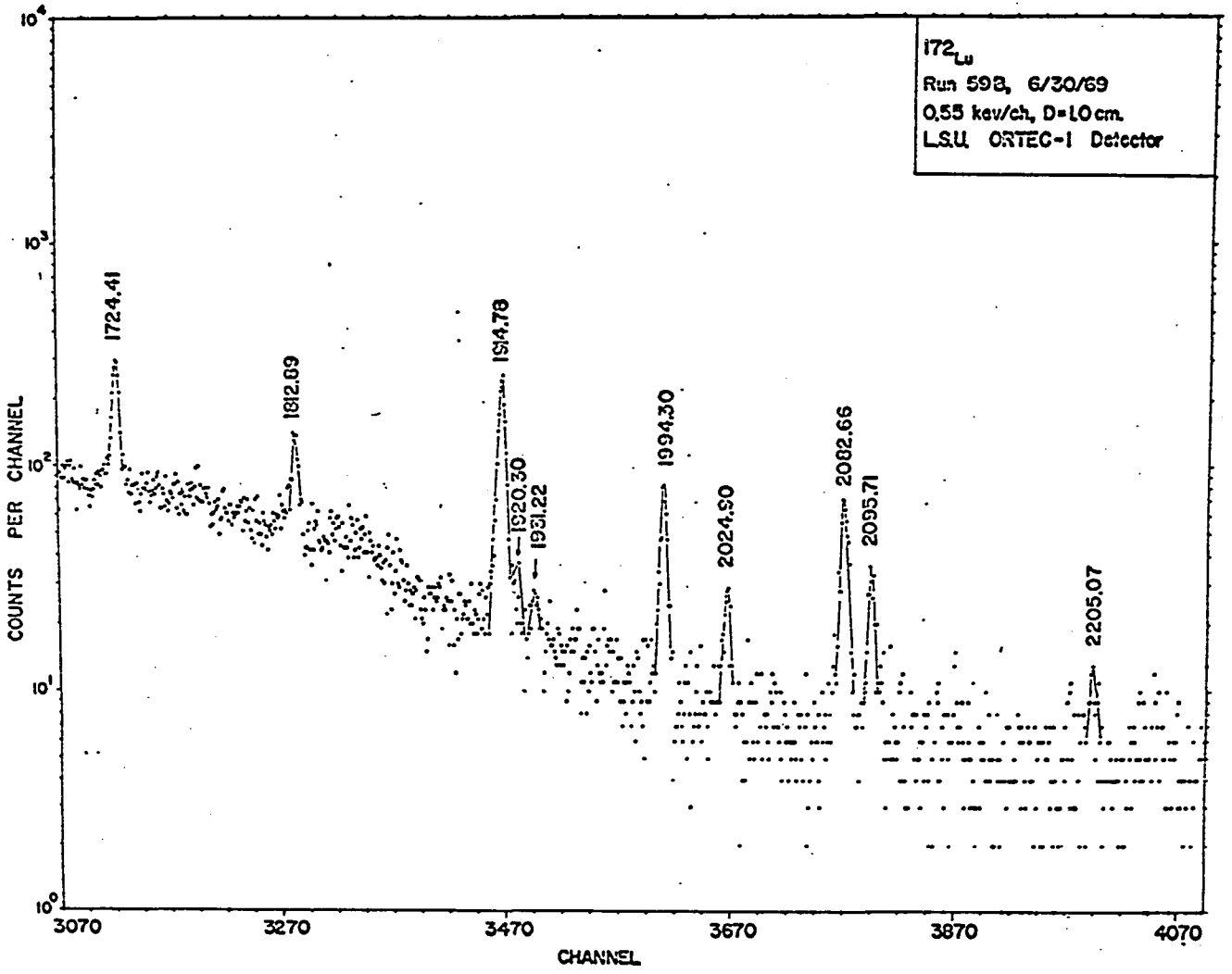

Fig. 22. The ^{172}Lu γ-ray spectrum from 1.69 → 2.25 MeV.

Table 3

The energies and relative intensities of γ-rays from the decay of ^{172}Lu

energy (keV)	intensity[a)]	energy (keV)	intensity[a)]
78.67 ± 0.02	54.85 ± 2.24	247.12 ± 0.04	2.23 + 0.31
90.57 ± 0.02	25.51 ± 1.32	254.82 ± 0.26	0.38 ± 0.06
112.71 ± 0.05	7.35 ± 0.49	264.76 ± 0.03	3.21 ± 0.43
118.92 ± 0.33	0.10 ± 0.02 (np)	270.02 ± 0.04	9.14 ± 0.59
134.48 ± 0.20	0.17 ± 0.02	279.70 ± 0.03	5.53 ± 0.49
137.94 ± 0.23	0.18 ± 0.04 (np)	319.10 ± 0.19	0.76 ± 0.08
142.63 ± 0.07	0.48 ± 0.02	323.89 ± 0.05	6.97 ± 0.28
145.72 ± 0.15	0.36 ± 0.10	330.44 ± 0.08	2.96 ± 0.34
151.09 ± 0.23	0.22 ± 0.08	337.66 ± 0.28	0.30 ± 0.04 (np)
163.13 ± 0.49	0.41 ± 0.13 (np)	347.98 ± 0.35	0.13 ± 0.05 (np)
174.73 ± 0.21	0.60 ± 0.05 (np)	352.28 ± 0.37	1.11 ± 0.35 (np)
181.47 ± 0.02	100.00 ± 5.00	358.48 ± 0.12	0.55 ± 0.06
196.36 ± 0.16	0.47 ± 0.04	366.68 ± 0.17	1.54 ± 0.19
203.37 ± 0.02	24.24 ± 0.99	372.51 ± 0.03	12.83 ± 0.84
210.22 ± 0.09	0.30 ± 0.06	377.52 ± 0.02	15.88 ± 0.48
229.03 ± 0.05	1.58 ± 0.13 (np)	383.08 ± 0.26	0.26 ± 0.09
233.46 ± 0.20	1.65 ± 0.45 (np)	399.75 ± 0.12	2.54 ± 0.15
241.03 ± 0.14	0.33 ± 0.05 (np)	410.31 ± 0.03	9.79 ± 0.34

energy (keV)	intensity[a)]	energy (keV)	intensity[a)]
416.64 ± 0.16	0.38 ± 0.06	594.56 ± 0.10	2.89 ± 0.34
422.97 ± 0.25	0.82 ± 0.11	607.16 ± 0.08	3.25 ± 0.25
427.57 ± 0.15	0.69 ± 0.10	625.60 ± 0.13	1.47 ± 0.18
432.53 ± 0.06	7.70 ± 0.47	630.82 ± 0.13	1.49 ± 0.27
437.55 ± 0.14	1.13 ± 0.10	644.40 ± 0.28	1.18 ± 0.28
443.42 ± 0.11	0.76 ± 0.11	681.76 ± 0.12	3.75 ± 0.29
482.13 ± 0.07	3.48 ± 0.24	697.26 ± 0.04	29.22 + 1.29
486.17 ± 0.09	3.57 ± 0.36	709.13 ± 0.09	3.62 ± 0.21
490.41 ± 0.02	9.68 ± 0.64	723.03 ± 0.12	2.43 ± 0.19
512.78 ± 0.19	0.75 ± 0.12	810.05 ± 0.02	79.67 ± 1.88
524.32 ± 0.23	1.16 ± 0.22	816.34 ± 0.13	5.49 ± 0.33
528.23 ± 0.03	19.56 ± 0.57	836.51 ± 0.27	0.86 ± 0.25 (np)
536.26 ± 0.12	3.43 ± 0.19	862.37 ± 0.45	1.59 ± 0.73 (np)
540.15 ± 0.05	6.52 ± 0.44	900.69 ± 0.05	144.27 ± 3.30
551.19 ± 0.16	2.10 ± 0.12	912.05 ± 0.03	73.97 ± 1.75
562.09 ± 0.33	0.57 ± 0.13 (np)	929.07 ± 0.06	15.75 ± 0.53
566.28 ± 1.6	0.83 ± 0.44	953.01 ± 0.20	2.03 ± 0.33 (np)
576.78 ± 0.14	1.75 ± 0.16	960.38 ± 0.27	0.56 ± 0.17 (np)
584.60 ± 0.23	1.81 ± 0.23	963.66 ± 0.39	0.83 ± 0.17 (np)

energy (keV)	intensity[a)]	energy (keV)	intensity[a)]
967.50 ± 0.18	0.94 ± 0.13	1166.46 ± 0.28	0.72 ± 0.15
970.64 ± 0.29	0.50 ± 0.17	1172.35 ± 0.27	1.26 ± 0.23 (np)
979.67 ± 0.26	0.68 ± 0.11 (np)	1179.32 ± 0.28	0.61 ± 0.16 (np)
990.69 ± 0.23	0.56 ± 0.18 (np)	1184.29 ± 0.09	2.44 + 0.17
1002.75 ± 0.04	26.45 ± 0.62	1288.98 ± 0.21	0.77 ± 0.10
1019.23 ± 0.53	0.87 ± 0.50	1322.38 ± 0.16	0.76 ± 0.12
1022.33 ± 0.08	7.41 ± 0.29	1387.22 ± 0.06	4.05 ± 0.16
1038.52 ± 0.83	1.03 ± 0.50 (np)	1397.29 ± 0.38	1.72 ± 0.24
1040.91 ± 0.30	1.91 ± 0.25	1400.25 ± 0.48	0.98 ± 0.15 (np)
1054.49 ± 0.13	0.43 ± 0.06 (np)	1402.87 ± 0.22	3.09 ± 0.23
1061.83 ± 0.22	0.50 ± 0.11 (np)	1440.52 ± 0.09	3.37 ± 0.24
1080.81 ± 0.04	5.72 ± 0.16	1466.12 ± 0.07	3.34 ± 0.18
1093.64 ± 0.02	319.75 ± 6.66	1470.48 ± 0.06	3.03 ± 0.14
1113.20 ± 0.07	9.46 ± 0.44	1489.00 ± 0.07	5.53 ± 0.22
1116.09 ± 0.34	1.00 ± 0.22	1529.72 ± 0.23	0.69 ± 0.13
1124.69 ± 0.40	0.51 ± 0.07 (np)	1542.89 ± 0.04	4.84 ± 0.27
1141.99 ± 0.69	0.50 ± 0.20 (np)	1572.12 ± 0.13	0.20 ± 0.06 (np)
1145.38 ± 0.19	2.43 ± 0.35 (np)	1579.70 ± 0.23	1.01 ± 0.10
1152.97 ± 0.25	0.97 ± 0.15 (np)	1584.18 ± 0.03	12.78 ± 0.63

energy (keV)	intensity[a)]	energy (keV)	intensity[a)]
1592.88 ± 0.12	0.40 ± 0.09 (np)	1914.78 ± 0.11	2.92 ± 0.14
1602.62 ± 0.17	1.45 ± 0.15	1920.30 ± 0.10	0.49 ± 0.20 (np)
1609.18 ± 0.20	0.52 ± 0.07	1931.22 ± 0.31	0.21 ± 0.04
1622.01 ± 0.06	10.74 ± 0.41	1994.30 ± 0.21	0.81 ± 0.09
1666.33 ± 0.30	0.87 ± 0.35	2024.20 ± 0.65	0.27 ± 0.09
1670.19 ± 0.20	2.80 ± 0.34	2082.66 ± 0.45	1.51 ± 0.30
1724.41 ± 0.15	2.18 ± 0.10	2095.71 ± 0.41	0.54 ± 0.14
1812.89 ± 0.10	0.93 ± 0.06	2205.07 ± 0.43	0.15 ± 0.05 (np)

a) Unplaced γ-rays are marked (np).

1) the uncertainty in the weighted average; 2) the rms deviation of the individual measurements from the average; or 3) the uncertainty for a particular energy given by the precision of the associated calibration lines used. The γ-ray intensities are normalized to 100 units for the 181 keV transition. The K-shell conversion coefficients were computed using the γ-ray intensities of table 3 and the conversion electron intensities of Prather,[86] Kaye,[95] Harmatz,[79] and Dzelepov.[82] The K-conversion coefficients and the assigned multipolarities are shown in table 4. The uncertainties quoted are those obtained considering the uncertainty in both the conversion electron and the γ-ray intensity. Uncertain multipole assignments are placed in parenthesis. Theoretical internal conversion coefficients up to 1600 keV were taken from the tables of Hager and Seltzer;[99] and for the range above 1600 keV from the tables of Sliv and Band.[100] Because of the large uncertainty in the experimental conversion coefficients no attempt was made to compute the mixing ratios in the mixed multipole cases.

3. Decay Scheme

A decay scheme consistent with experimentally determined transition energies, intensities, multipolarities, and the coincidence results of Prather,[86]

Table 4

K-conversion coefficients for transitions in ^{172}Yb

transition energy	$\alpha_K \times 10^{2}$ [d]		multipole assignment	transition energy	$\alpha_K \times 10^{2}$ [d]		multipole assignment
90	156.2 ± 9.1	a)	E2	270	18.01± 1.3		M1
	>82.7	b)		279	8.01± 0.8		E2
112	104.3 ± 7.1	a)	M1 + E2	319	12.6 ± 3.4	b)	M1
	76.1	b)		323	11.4 ± 0.4		M1
134	92.7 ±18.9	a)	M1 + E2	330	4.8 ± 0.3		M1 + E2
	142.7	b)		337	7.1 ± 2.0	b)	M1
145	100 ±16	b)	M1 + E2	358	9.06± 2.4	b)	M1
151	53 ±13	b)	M1 + E2	366	1.51± 0.4	b)	(E2)
163	77.2 ±12	b)	M1	372	5.43± 0.5		M1 + E2
181	22.0 ± 7.1	a)	E2	377	0.96± 0.09		E1
	21.6 ± 2.1	b)		399	6.2 ± 0.4		M1
196	19.08± 1.6		E2	410	4.7 ± 0.2		M1 + E2
203	16.03± 0.7	a)	E2	416	5.6 ± 1.6	b)	M1 + E2
	15.30± 0.7			427	4.59		(M1)
210	56.3 ±14		M1	432	0.88± 0.11		E1
229	30.8 ± 2.0	b)	M1	437	5.04± 0.65		M1
	34.3 ± 3.0			443	1.32± 0.2		E2
247	12.49± 1.8		E2	352	1.67± 0.7	b)	(E2)
264	4.9 ± 1.2	b)	E1				
	4.1 ± 2.0						

transition energy	$\alpha_K \times 10^{2}$ [d]	multipole assignment	transition energy	$\alpha_K \times 10^{3}$ [d]	multipole assignment
482	3.08± 0.4	M1	709	11.07± 5.0	M1 + E2
486	2.94± 0.4	M1	723	4.56± 2.0	(E2)
490	3.34± 0.3	M1	810	10.4 ± 0.25 a)	M1
512	3.17± 0.9	M1 + E2		10.46± 0.4	
524	3.46± 1.7	M1 + E2	816	13.55± 1.0	M1
528	3.02± 0.2	M1	900	8.37± 0.19 a)	M1
536	2.66± 1.0	M1 + E2		8.48± 0.27	
540	3.58± 0.4	M1	912	5.07± 0.13 a)	E2 + M1
551	2.59± 0.7	M1		4.90± 0.17	
576	3.9 ± 1.6	(M1)	929	7.03± 0.29 a)	M1
584	2.48± 0.13	M1		7.50± 0.17	
594	1.46± 0.3	M1 + E2	967	8.42± 0.46	M1 + E2
607	0.63± 0.2	E2	1002	3.81± 0.15 a)	M1 + E2
625	0.72± 0.09 b)	E2		3.99± 0.14	
630	2.47± 0.60	M1	1022	5.48± 0.4	M1
681	1.82± 0.20	M1	1040	6.35± 1.6	M1
697	1.51± 0.07	M1	1080	4.59± 0.30 a)	M1
				4.72± 0.48	
			1093	2.58± 0.06 a)	E2
				2.79± 0.08	

transition energy	$\alpha_K \times 10^3$ [d]	multipole assignment	transition energy	$\alpha_K \times 10^3$ [d]	multipole assignment
1113	4.41± 0.6	M1	1584	0.85± 0.2	E2
1116	10.55± 5.0	(M1)	1602	2.26± 0.53 [c]	M1 + E2
1184	1.51± 0.44	E2	1622	0.93± 0.1	E2
1288	3.77± 0.8	M1 + E2	1666	1.52± 0.8	E2
1322	1.32± 0.4	E2	1670	0.94± 0.22	E2
1387	1.56± 0.14	E2	1724	1.43± 0.25	E2
1397	1.17± 0.3	E2	1812	1.30± 0.35	E2
1400	1.18± 0.5	E2	1914	1.77± 0.17 [c]	M1 + E2
1402	1.68± 0.36	E2	1994	1.43± 0.5 [c]	M1 + E2
1440	1.36± 0.42	E2	2024	2.34± 1.1 [c]	M1 + E2
1466	1.38± 0.42	E2	2082	1.18± 0.27 [c]	M1
1470	1.69± 0.51	E2	2095	1.17± 0.41 [c]	M1 + E2
1542	1.1 ± 0.3	E2			

[a] using the conversion electron data of ref. 95.

[b] using the conversion electron data of ref. 79.

[c] using the conversion electron data of ref. 82.

[d] for the values not referenced the conversion electron data of Prather, ref.86, was used.

and Ottesson and Helmer[88] is presented in fig. 23. It was possible to place 97 γ-rays in the level scheme consisting of 28 levels. The level energies have been assigned mostly on the basis of transitions to the levels of the ground state rotational band. The energies of the transitions incorporated in the scheme are consistent with the level energies to within the specified uncertainty of the transition energies. Four new levels at 1792, 1706, 2181, and 2213 keV are proposed; and their spin-parity possibilities are indicated in fig. 23. With the exception of the 1792 keV state, these same levels have been reported by Roche et al.[87] based on energy-sum considerations.

The level at 1609 keV, though proposed earlier from the decay of ^{172}Tm[88,89] and listed in the report of Roche et al.[87], has not been reported in previous studies on the decay of ^{172}Lu. The placement of the 142, 1609, and 1529 keV transitions as depopulating the 1609 keV level is entirely consistent with the results of the studies on the decay of ^{172}Tm.[88,89] None of these transitions could be consistently placed elsewhere in the level scheme. Furthermore, the B(E2) ratio obtained from the 1609 and 1529 keV transitions is very consistent with theoretical estimates and is discussed in the next section.

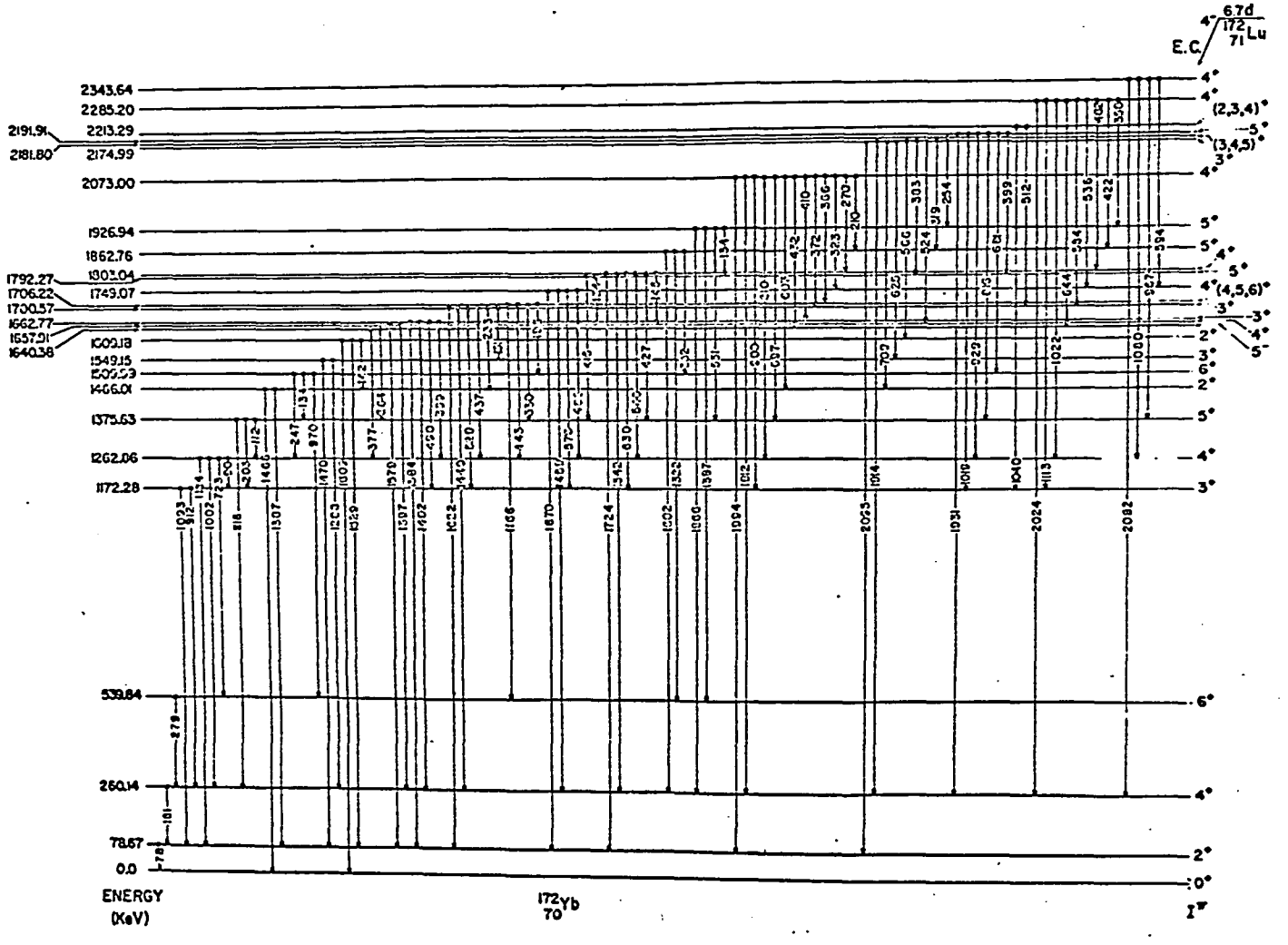

Fig. 23. The proposed level scheme of ^{172}Yb.

Without conversion electron data on the 1609 keV transition, it is not felt legitimate to assign it as an E1 transition as was done in ref. 86.

The 134, 1387, and 399 keV γ-rays seem amenable to placement as transitions in more than one part of the level scheme on the basis of both energy-sum and multipolarity considerations. It is felt that there are more than one γray of close energy involved in these transitions. All alternative positions for these transitions are shown in table 5 which is a summary of the proposed levels in ^{172}Yb and their depopulating transitions arranged, for convenience, according to final rotational band assignments. To compute electron capture branching ratios, the intensity of these multiply placed transitions have been restricted to a single placement as follows: 1) For the 134 keV transition, the total intensity has been placed as depopulating the 1509 keV level on the basis of the coincidence measurements of Prather;[86] 2) ninety-five percent of the intensity of the 1387 keV transition is assumed to depopulate the 1466 keV level on the basis of B(E2) ratios; and 3) for the 399 keV M1 transition, the total intensity has been placed as depopulating the 1662 keV level because the alternative placement between the 2191 and 1792 keV levels is K forbidden.

Theoretical total conversion coefficients (K+L+M) were computed from the tables of Hager and Seltzer[99]

based on the multipolarity assignments in table 4. The contribution from higher shells (N+O+P) was included in the total conversion coefficient of the 78 and 90 keV transitions using the tables of Dragoun.[101] The total intensity of the 78, 1466, and 1609 keV transitions was set equal to 100 units; and the resulting normalized total transition intensities are listed in table 5. This procedure yields total transition intensities per 100 decays since no electron capture to the ground state (ΔI, $\Delta\pi$= 4,yes) is expected.

The percentage of electron capture to each of the proposed levels was computed by taking the difference between the total depopulating intensity and the total populating intensity. The log ft values obtained using the nomographs of ref. 77 are presented in table 6. It must be pointed out that the γ-ray intensity of the 78 keV transition given in table 3 was adjusted downward 3.8% (the uncertainty on it being 4.1%) before computing the total transition intensity given in table 5. This was done so that the electron capture ratios summed to exactly 100 units. This does not mean that there was an error in the relative γ-ray intensities but rather that the total intensity of the 78 keV transition is difficult to determine. For example, the same result could have been achieved by using only 35% of the N+O+P conversion intensity given by Dragoun.[101]

Table 5

Proposed states in ^{172}Yb and their depopulating transitions

K	initial state	Iπ	transition (keV)	total transition intensity/100 decays	final state	Iπ
	78.67	2+	78.67	99.23 ± 4.20	0.0	0+
K=0	260.14	4+	181.47	27.35 ± 1.37	78.67	2+
	539.84	6+	279.70	1.20 ± 0.10	260.14	4+
	1172.28	3+	912.05	14.73 ± 0.35	260.14	4+
			1093.64	63.62 ± 1.33	78.67	2+
	1262.86	4+	90.57	30.07 ± 1.56	1172.28	3+
			723.03	0.49 ± 0.04	539.84	6+
			1002.75	5.26 ± 0.12	260.14	4+
K=3			1184.29	0.49 ± 0.03	78.67	2+
	1375.63	5+	112.71	4.47 ± 0.30	1262.86	4+
			203.37	6.04 ± 0.25	1172.28	3+
			1116.09	0.20 ± 0.04	260.14	4+
	1509.99	6+	134.48	0.08 ± 0.01	1375.63	5+
			247.12	0.50 ± 0.07	1262.86	4+
			970.64	0.10 ± 0.03	539.84	6+

K	initial state	Iπ	transition (keV)	total transition intensity/100 decays	final state	Iπ
	1662.77	3+	399.75	0.54 ± 0.03	1262.86	4+
			490.41	2.00 ± 0.13	1172.28	3+
			1402.87	0.61 ± 0.05	260.14	4+
			1584.18	2.53 ± 0.13	78.67	2+
K=3	1749.07	4+	486.17	0.74 ± 0.08	1262.86	4+
			576.78	0.36 ± 0.03	1172.28	3+
			1489.00	1.10 ± 0.04	260.14	4+
			1670.19	0.55 ± 0.07	78.67	2+
	1862.76	5+	1322.38	0.15 ± 0.03	539.84	6+
			1602.62	0.29 ± 0.03	260.14	4+
	1466.01	2+	1387.22	0.08 ± 0.01	78.67	2+
			1466.12	0.66 ± 0.04	0.0	0+
	1549.15	3+	1288.98	0.15 ± 0.02	260.14	4+
			1470.48	0.60 ± 0.03	78.67	2+
K=2	1657.91	4+	1397.29	0.34 ± 0.05	260.14	4+
			1579.70	0.20 ± 0.02	78.67	2+
	1792.27	5+	134.48	0.08 ± 0.01	1657.91	4+
			416.64	0.08 ± 0.01	1375.63	5+

K	initial state	Iπ	transition (keV)	total transition intensity/100 decays	final state	Iπ
	1609.18	2+	142.63	0.19 ± 0.01	1466.01	2+
			1529.72	0.14 ± 0.03	78.67	2+
			1609.18	0.10 ± 0.01	0.0	0+
	1700.57	3+	151.09	0.09 ± 0.03	1549.15	3+
			437.55	0.24 ± 0.02	1262.86	4+
			528.23	4.01 ± 0.12	1172.28	3+
			1440.52	0.06 ± 0.05	260.14	4+
			1622.01	2.13 ± 0.08	78.67	2+
K=2	1803.04	4+	145.72	0.16 ± 0.04	1657.91	4+
			427.57	0.15 ± 0.02	1375.63	5+
			540.15	1.34 ± 0.09	1262.86	4+
			630.82	0.30 ± 0.06	1172.28	3+
			1542.89	0.96 ± 0.05	260.14	4+
			1724.41	0.43 ± 0.02	78.67	2+
	1926.94	5+	134.48	0.08 ± 0.01	1792.27	5+
			551.19	0.43 ± 0.03	1375.63	5+
			1387.22	0.81 ± 0.01	539.84	6+
			1666.33	0.17 ± 0.07	260.14	4+

K	initial state	Iπ	transition (keV)	total transition intensity/100 decays	final state	Iπ
	2073.00	4+	210.22	0.09 ± 0.02	1862.76	5+
			270.02	2.20 ± 0.14	1803.04	4+
			323.89	1.57 ± 0.06	1749.07	4+
			366.68	0.32 ± 0.04	1706.22	(4,5,6)+
			372.51	2.77 ± 0.18	1700.57	3+
			410.31	2.08 ± 0.07	1662.77	3+
			432.53	1.54 ± 0.09	1640.38	5-
			607.16	0.65 ± 0.05	1466.01	2+
			697.26	5.90 ± 0.26	1375.63	5+
K=4			810.05	15.98 ± 0.38	1262.86	4+
			900.69	28.82 ± 0.66	1172.28	3+
			1812.89	0.18 ± 0.01	260.14	4+
			1994.30	0.16 ± 0.02	78.67	2+
	2191.91	5+	399.75	0.54 ± 0.03	1792.27	5+
			681.76	0.76 ± 0.06	1509.99	6+
			816.34	1.10 ± 0.07	1375.63	5+
			929.07	3.15 ± 0.11	1262.86	4+
			1019.23	0.17 ± 0.10	1172.28	3+
			1931.22	0.04 ± 0.01	260.14	4+
	2174.99	3+	383.08	0.05 ± 0.02	1792.27	5+
			566.28	0.17 ± 0.09	1609.18	2+
K=3			625.60	0.29 ± 0.04	1549.15	3+
			709.13	0.72 ± 0.04	1466.01	2+
			1914.78	0.58 ± 0.03	260.14	4+
			2095.71	0.11 ± 0.03	78.67	2+

K	initial state	Iπ	transition (keV)	total transition intensity/100 decays	final state	Iπ
	2285.20	4+	358.48	0.12 ± 0.01	1926.94	5+
			422.97	0.17 ± 0.02	1862.76	5+
			482.13	0.72 ± 0.05	1803.04	4+
K=3			536.26	0.70 ± 0.04	1749.07	4+
			584.60	0.37 ± 0.05	1700.57	3+
			644.40	0.24 ± 0.06	1640.38	5-
			1022.33	1.48 ± 0.06	1262.86	4+
			1113.20	1.88 ± 0.09	1172.28	3+
			2024.90	0.05 ± 0.02	260.14	4+
	2181.80	(3,4,5)+	254.82	0.09 ± 0.01	1926.94	5+
			319.10	0.17 ± 0.02	1862.76	5+
			524.32	0.24 ± 0.05	1657.91	4+
	2213.29	(2,3,4)+	512.78	0.16 ± 0.02	1700.57	3+
			1040.91	0.38 ± 0.05	1172.28	3+
	2343.64	4+	594.56	0.58 ± 0.07	1749.07	4+
			967.50	0.19 ± 0.04	1375.63	5+
			1080.81	1.14 ± 0.03	1262.86	4+
			2082.66	0.30 ± 0.06	260.14	4+
	1640.38	5-	264.76	0.65 ± 0.09	1375.63	5+
			377.52	3.18 ± 0.10	1262.86	4+
	1706.22	(4,5,6)+	196.36	0.12 ± 0.01	1509.99	6+
			330.44	0.62 ± 0.07	1375.63	5+
			443.42	0.16 ± 0.02	1262.86	4+
			1166.46	0.14 ± 0.03	539.84	6+

Table 6

Electron capture (%) to the proposed levels in ^{172}Yb.

level (keV)	$I\pi$	electron capture (%)	log ft
2343	4+	2.21 ± 0.10	7.30
2285	4+	5.74 ± 0.15	7.08
2213	(2,3,4)+	0.54 ± 0.06	8.24
2191	5+	5.22 ± 0.17	7.31
2181	(3,4,5)+	0.50 ± 0.05	8.34
2174	3+	1.92 ± 0.11	7.76
2073	4+	62.25 ± 0.85	6.44
1926	5+	0.40 ± 0.08	8.84
1862	5+	0.24 ± 0.09	9.14
1803	4+	0.41 ± 0.19	8.89
1792	5+	0.03 ± 0.02	10.13
1749	4+	~0	
1706	(4,5,6)+	0.72 ± 0.09	8.84
1700	3+	3.84 ± 0.25	8.12
1662	3+	3.61 ± 0.20	8.18
1657	4+	0.15 ± 0.08	9.56
1640	5-	2.06 ± 0.17	8.44
1609	2+	0.26 ± 0.09	9.38
1549	3+	0.37 ± 0.06	9.27
1509	6+	~0	
1466	2+	~0	
1375	5+	1.51 ± 0.49	8.78
1262	4+	3.40 ± 1.65	8.51
1172	3+	4.31 ± 2.20	8.48
539	6+	0.32 ± 0.12	9.93
260	4+	~0	
78	2+	~0	

4. Rotational Bands

4.1 Reduced Transition Probabilities and Inertial Parameters

Reduced transition probability ratios were computed from the γ-ray energies and intensities of table 3 in order to determine K quantum number assignments. The results of this analysis are presented in table 7 along with the values to be expected for various choices of K as determined from the Bohr Mottelson model[1,2,5] and using the Clebsch Gordan coefficients tabulated by Yamazaki.[102] The material in table 7 has been grouped, for convenience, according to final rotational band assignments. The theoretical values listed are those which are possible assuming the K of the final state to be correct. In the case of K-forbidden transitions the same reduced transition probability ratios are taken for all values of $K \geq L$. The final rotational band assignments are also graphically displayed in fig. 24 along with the levels for which no K assignment could be made (far right).

The inertial parameters of the proposed rotational bands have been determined by fitting the band head and first two rotational level energies in each band to equation 2.38. These results are presented in table 8.

Table 7

The reduced transition probability ratios for depopulating transitions in ^{172}Yb

band K	initial level energy	Iπ	transition energy, σL		final level Iπ	K	reduced transition probability experimental	theory K=0	K=1	K=2	K=3	K=4
	1172	3+	1093	E2	2+	0	1.74 ± 0.05	0	0.4	2.5		
			912	E2	4+	0	1	0	1	1		
	1262	4+	1184	E2	2+	0	0.040± 0.003	1.1	12.0	0.34		
			1002	E2	4+	0	1	1	1	1		
			723	E2	6+	0	0.47 ± 0.04	1.75	12.2	0.09		
K=3	1375	5+	203	E2	3+	3	0.17 ± 0.01		0.062	0.096	0.26	
			112	(E2)	4+	3	1		1	1	1	
	1509	6+	247	E2	4+	3	0.63 ± 0.11		0.080	0.17	0.57	
			134	(E2)	5+	3	1		1	1	1	
	1662	3+	1584	E2	2+	0	2.25 ± 0.20	0	0.4	2.5		
			1402	E2	4+	0	1	0	1	1		
			490	M1	3+	3	2.06 ± 0.18			0.33	3	
			399	M1	4+	3	1			1	1	
K=3	1749	4+	1670	E2	2+	0	0.29 ± 0.04	1.1	12.0	0.34		
			1489	E2	4+	0	1	1	1	1		
			576	M1	3+	3	0.29 ± 0.04			0.08	0.43	3.9
			486	M1	4+	3	1			1	1	1
	1862	5+	1602	(E2)	4+	0	0.73 ± 0.14	0	0.57	1.75		
			1322	E2	6+	0	1	0	1	1		

band K	initial level energy	Iπ	transition energy, σL		final level Iπ	K	reduced transition probability experimental	theory K=0	K=1	K=2	K=3	K=4
	1466	2+	1466	E2	0+	0	0.63 ± 0.04	0.70	2.78	0.70		
			1387	E2	2+	0	1	1	1	1		
K=2	1549	3+	1470	E2	2+	0	2.04 ± 0.28	0	0.4	2.5		
			1288	E2	4+	0	1	0	1	1		
	1657	4+	1579	(E2)	2+	0	0.32 ± 0.05	1.1	12.0	0.34		
			1397	E2	4+	0	1	1	1	1		
	1609	2+	1609	(E2)	0+	0	0.59 ± 0.14	0.70	2.78	0.70		
			1529	(E2)	2+	0	1	1	1	1		
	1700	3+	1622	E2	2+	0	1.76 ± 0.14	0	0.4	2.5		
			1440	E2	4+	0	1	0	1	1		
			528	M1	3+	3	9.80 ± 0.90			0.33	3	
			437	M1	4+	3	1			1	1	
K=2			233	(M1)	2+	2	2.03 ± 0.92		0.12	0.72	2.86	
			151	(M1)	3+	2	1		1	1		
	1803	4+	1724	E2	2+	0	0.26 ± 0.02	1.1	12.0	0.34		
			1542	E2	4+	0	1	1	1	1		
			630	M1	3+	3	0.14 ± 0.03			0.88	0.43	3.9
			540	M1	4+	3	1			1	1	1
			427	M1	5+	3	0.21 ± 0.03			1.78	0.79	0.12
	1926	5+	1666	E2	4+	0	0.086± 0.03	0	0.57	1.75		
			1387	E2	6+	0	1	0	1	1		

band K	initial level energy	Iπ	transition energy, σL		final level Iπ	K	reduced transition probability experimental	theory K=0	K=1	K=2	K=3	K=4
	2174	3+	2095	M1	2+	0	0.14 ± 0.04	0.75	1.33			
			1914	M1	4+	0	1	1	1			
			709	(E2)	2+	2	1.32 ± 0.18		0.86		0.86	
			625	E2	3+	2	1		1		1	
K=3	2285	4+	1113	M1	3+	3	0.99 ± 0.06			0.08	0.43	3.9
			1022	M1	4+	3	1			1	1	1
			584	M1	3+	2	0.29 ± 0.04		0.19	1.67	1.67	
			482	M1	4+	2	1		1	1	1	
			358	M1	5+	2	0.38 ± 0.05		1.04	2.33	0.20	
			536	E2	4+	3	1.28 ± 0.19		0.53		0.08	
			422	(E2)	5+	3	1		1		1	
	2073	4+	1994	(E2)	2+	0	0.54 ± 0.07	1.1	12.0	0.34		
			1812	E2	4+	0	1	1	1	1		
			900	M1	3+	3	1.32 ± 0.04			0.08	0.43	3.9
			810	M1	4+	3	1			1	1	1
			697	M1	5+	3	0.58 ± 0.03			1.78	0.79	0.12
K=4			410	M1	3+	3	0.69 ± 0.04			0.08	0.43	3.9
			323	M1	4+	3	1			1	1	1
			210	M1	5+	3	0.16 ± 0.03			1.78	0.79	0.12
			372	M1	3+	2	0.53 ± 0.05		0.19	1.67	1.67	
			270	M1	4+	2	1		1	1	1	
	2191	5+	929	M1	4+	3	1.95 ± 0.13			0.14	0.97	2.18
			816	M1	5+	3	1			1	1	1
			681	M1	6+	3	1.17 ± 0.11			1.37	1.37	0.15

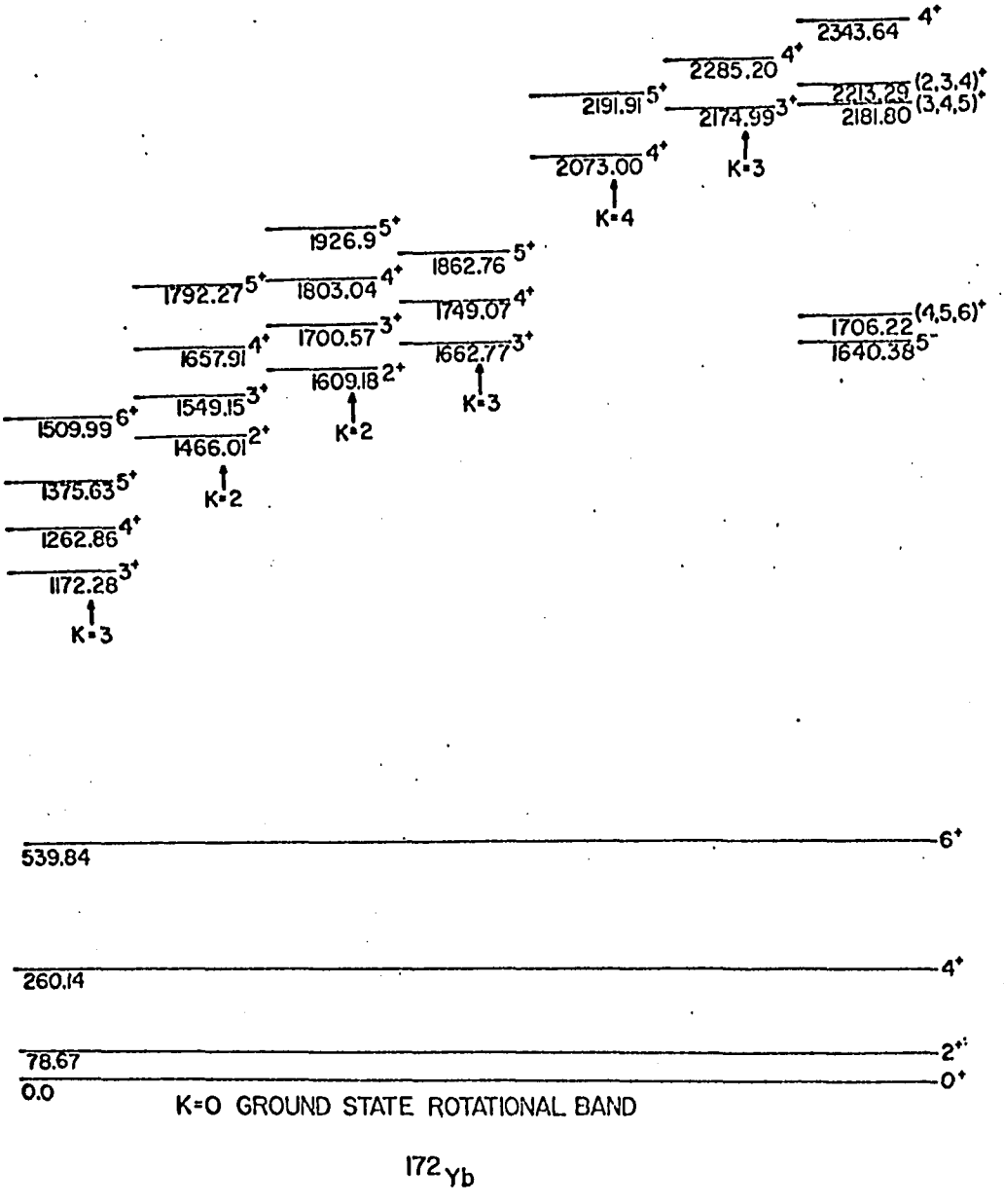

Fig. 24. The proposed band structure of ^{172}Yb.

Table 8

Inertial parameters for the rotational bands in ^{172}Yb

band head energy E_o(keV) [a]	K	A (keV)	B (eV)
0.0	0	13.14	-4.36
1466	2	13.95	-15.4
1609	2	16.03 (13.84) [b]	-173.0
1172	3	11.33	-2.07
1662	3	10.64	+26.43
2174	3	13.77	
2073	4	11.89	

[a] $E_I = E_o + A[I(I+1) - K(K+1)] + B[I(I+1) - K(K+1)]^2$.

[b] using 2^+ and 4^+ members only.

4.2 The K=0 Ground State Band

The 78, 260, and 539 keV levels have the correct energy spacing and spin sequence to comprise the 2^+, 4^+, and 6^+ members of the K=0 ground state rotational band. The spin-parity assignments of these levels have been made previously on the basis of Coulomb excitation experiments.[91-93] The values for the inertial parameters, A=13.14 keV and B=-4.36 eV, are consistent with the values of neighboring even-even nuclei.

4.3 The K=3 Band at 1172 keV

The electron capture decay of ^{172}Lu predominantly populates excited states in ^{172}Yb with energies above 1.8 MeV. The decay then proceeds through the intrinsic state at 1172 keV.[94-98] The 1172, 1262, 1375, and 1509 keV levels comprise the 3^+, 4^+, 5^+, and 6^+ members of a K=3 rotational band. The inertial parameters obtained from a fit of the first three levels to equation 2.38 are: A=11.33 keV and B=-2.07 eV. The predicted energy, 1510.32 keV, of the 6^+ level compares very well with the observed value of 1509.99 keV. The experimental reduced transition probabilities in table 7 are consistent with a value of $K \geq 2$ for the K-forbidden transitions, and in good agreement with K=3 for the remaining cases. The L-subshell ratios of ref. 95 indicate that the 112 keV transition is 30% M1. This is consistent with these results since a 30% reduction in the 112 keV intensity raises the RTP

ratio from 0.17 to 0.23, in even better agreement with the value for K=3. The same situation[95] exists for the 134 keV transition except that a 30% increase in the RTP ratio makes the agreement with K=3 slightly worse.

4.4 The K=3 Band at 1662 keV

The 1749 and 1862 keV levels have the correct energy spacing and spin sequence to comprise the 4^+, and 5^+ members of a K=3 rotational band based upon the 1662 keV level. The inertial parameters are A=10.64 keV and B=+26.43 eV. These values are not consistent with those of the ground state band and the K=3 band at 1172 keV, but are in agreement with the values A=10.6 keV and B=+32.2 eV obtained by Prather.[86] The RTP ratios (table 7) for transitions from members of this band to members of the ground state band show overall agreement for $K \geq 2$. The RTP ratios for transitions to members to the K=3 band at 1172 keV show excellent agreement for K=3.

4.5 The K=2 Band at 1466 keV

The 1549, 1657, and 1792 keV levels have the proper energy spacing and spin sequence to constitute the members of a K=2 band based on the level at 1466 keV. The inertial parameters obtained from a fit of the first three levels to equation 1 are A=13.95 keV and B=-15.4 eV. The predicted energy of the 5^+ level using these parameters is 1791.94 keV which is in good agreement with

the observed value of 1792.27 keV. The RTP ratios (table 7) for transitions from members of this band to members of the ground state band uniquely establishes the K=2 assignment.

4.6 The K=2 Band at 1609 keV

The 1700, 1803, and 1926 keV levels appear to comprise the 3^+, 4^+ and 5^+ members of a K=2 band based on the 1609 keV level. The RTP ratios (table 7) from members of this band to levels of the ground state band agree quite well with the K=2 assignment. The RTP ratio from the 1926 keV 5^+ level to the 4^+ and 6^+ members of the ground state band is not meaningful since most of the 1387 keV transition intensity depopulates the 1466 keV level. The value obtained for this ratio (0.086/1) is consistent with this interpretation and indicates that only 5% of the 1387 keV transition intensity depopulates the 1926 keV level. The M1 transitions from the 1700 keV 3^+ member of this band to the K=2 band at 1466 keV and the K=3 band at 1172 keV indicates a K=3 assignment for the 1700 keV level. Additional conflicting information concerning this level arises from the inertial parameter computations. If the 1609, 1700 and 1803 keV levels are used, A=16.03 keV and B=-173 eV; and the 5^+ level is predicted to be at 1894.25 keV which is not at all in agreement with the observed value of 1926.94 keV. However, using only the 1609 keV 2^+ and 1803 keV 4^+ levels to compute A, a more consistent value of A=13.84 keV is

obtained. Assuming the inertial parameters of the 1466 keV K=2 band as applicable, the expected energy of the 3^+ member of the K=2 1609 keV band is 1692.33 keV, 8 keV below the observed value of 1700.57 keV. The K=2 assignment for the band at 1609 keV is supported by Wien[89] and Ottesson and Helmer[88] from studies on the decay of ^{172}Tm. Roche et al.[87] also listed a level at 1608.5 keV from studies on the decay of ^{172}Lu. Prather[86] did not propose the 1609 keV level and assigned the 1700 keV level as the band head for a K=3 band. It appears that the 1609 keV K=2 band is not a very pure band. This is discussed further in the next section.

4.7 The K=4 Band at 2073 keV

The 2073 and 2191 keV levels are proposed to be the 4^+, and 5^+ members of a K=4 band based on the 2073 keV level. The RTP ratio of the transitions from the 2073 keV level to the ground state band are consistent with $K \geq 2$; and the four RTP ratios for transitions from members of the proposed band to members of the K=3 band at 1172 keV agree well with a K=4 assignment. The three remaining RTP ratios do not agree with a K=4 assignment. The inertial parameter obtained from a fit of the energies of the 4^+ and 5^+ levels is A = 11.89 keV. It appears that this band also is not

pure, which in this case is quite reasonable considering the energy at which it occurs.

4.8 The K=3 Band at 2174 keV

The 2285 and 2174 keV levels are proposed to be the 4^+ and 3^+ members of a K=3 band based on the 2174 keV level. The RTP ratio for transitions from the 2174 keV level to the 2^+ and 4^+ members of the ground state band agree with a $K \geq 2$ assignment. The RTP ratios for transitions from members of the proposed band to members of both K=2 bands show general agreement with a K=3 assignment. The RTP ratio of transitions to the K=3 band at 1172 keV shows good agreement with K=3, but the ratio of transitions to the K=3 band at 1662 keV do not. The inertial parameter obtained for this band, A = 13.77 keV, is in good agreement with the other values. This band has been assigned as a K=4 band in ref. 97. In that case A = 11.02 keV, which is actually in good agreement with the inertial parameters of the bands at 2073, 1662, and 1172 keV. However, the RTP ratios favor a K=3 assignment.

4.9 Additional Levels

It was not possible to classify the levels at 1640, 1706, 2181, 2213, and 2343 keV according to K, and for the 1706, 2181, and 2213 keV levels it was not possible to determine unique spin-parity assignments

(see the column at the extreme right of fig. 24).

5. Discussion

In even-even nuclei, the rotational bands based on the ground state and those based on the vibrational states, are of much significance. We have already discussed in Chapter II, the alternative approaches in characterizing these states. The characterization of β and γ vibrations as purely surface vibrations[1,2] is of limited validity and as pointed out in Chapter II, a different approach involving a superposition of quasi-particle states has been proposed.[18,19,68] The extent of the vibrational nature of the excitation depends on the number and nature of the two-quasi-particle states in the superposition and can be explored through the B(E2) ratios which are very sensitive to the extent of the collective component in the levels participating in the decay. Furthermore, two quadrupole excited states (K=2) have been predicted to exist in the 1-2 MeV energy range, though the higher K=2 state has been observed in only a few nuclei.[19] For ^{172}Yb the predicted energies of these quadrupole excited states are 1.4 and 1.7 MeV according to Soloviev[19] and 1.47 and 1.74 MeV according to Bes et al.[31] Soloviev classifies the first state as a two-quasi-particle state and the second one as

predominantly collective. The observed 2^+, K=2 states at 1466.01 and 1609.18 keV correspond remarkably well (energy wise) with the predicted values. As pointed out in the previous paragraph, a comparison of theoretical and experimental B(E2) ratios for transitions from the K=2 bands to the ground state band should indicate the extent of the collective nature of the bands. Such a comparison is presented in table 9. Although the comparison indicates that the band at 1466 keV is more collective than the one at 1609 keV, it must never-the-less be concluded that both bands are appreciably collective. This conclusion is supported by the log ft values (table 6) for electron capture to the states of the bands. However, the rather low log ft for the 1700 keV 3^+ member of the band at 1609 keV indicates, in agreement with the inertial parameter determination (see section 4.6), that the 3^+ member of this band is appreciably mixed.

The coupling of each of the two K=2 bands to the ground state rotational band was computed on the basis of the perturbative band-mixing theory. The values obtained for the mixing parameter z_2 are presented in table 10 along with the theoretical values of Marshalek, Pavlichenkov, and Bes. The z_2 values, 19.6 and 13.8, obtained for the 1609 and 1466 keV bands, respectively, are consistent with the previous

Table 9

Comparison of theoretical and experimental B(E2) ratios for transitions from the K=2 bands to the K=0 ground state band in ^{172}Yb

band	$\frac{I_i \to I_f}{I_i \to I_{f'}}$	$\frac{B(E2; I_i \to I_f)}{B(E2; I_i \to I_{f'})}$	B(E2) ratio (theory)			
			B - M[a]	R - V[b]	A - R[c]	Microscopic[d]
1466 keV K=2	$\frac{2 \to 0}{2 \to 2}$	0.63 ± 0.03	0.698	0.45	0.51	0.68
	$\frac{3 \to 2}{3 \to 4}$	2.04 ± 0.24	2.50	1.07	1.16	2.3
	$\frac{4 \to 2}{4 \to 4}$	0.32 ± 0.05	0.34	0.38	0.11	
1609 keV K=2	$\frac{2 \to 0}{2 \to 2}$	0.59 ± 0.14	0.698	0.45	0.51	0.68
	$\frac{3 \to 2}{3 \to 4}$	1.76 ± 0.12	2.50	1.07	1.16	2.3
	$\frac{4 \to 2}{4 \to 4}$	0.26 ± 0.01	0.34	0.38	0.11	

a) ref. 1 and 2. The Clebsch Gordan coefficients of ref. 102 were utilized

b) ref. 32

c) ref. 32

d) ref. 33

Table 10

Band mixing parameters for the K=2 bands in ^{172}Yb

z_2 experiment

band	$\frac{I_i \to I_f}{I_i \to I_f}$	$\frac{B(E2; I_i \to I_f)}{B(E2; I_i \to I_{f'})}$ [a]	theory [b] (adiabatic)	correction factor	$z_2 \times 10^3$
1466 keV K=2	$\frac{2 \to 0}{2 \to 2}$	0.63 ± 0.03	0.698	$\left(\frac{1 - z_2}{1 + 2z_2}\right)^2$	18.6 ± 8.7
	$\frac{3 \to 2}{3 \to 4}$	2.04 ± 0.24	2.50	$\left(\frac{1 - z_2}{1 + 6z_2}\right)^2$	15.1 ± 8.4
	$\frac{4 \to 2}{4 \to 4}$	0.32 ± 0.05	0.34	$\left(\frac{1 - 5z_2}{1 + 2z_2}\right)^2$	4.74±10.6
				weighted average:	13.8 ± 5.8
1906 keV K=2	$\frac{2 \to 0}{2 \to 2}$	0.59 ± 0.14	0.698	$\left(\frac{1 - z_2}{1 + 2z_2}\right)^2$	29.9 ±35.0
	$\frac{3 \to 2}{3 \to 4}$	1.76 ± 0.12	2.50	$\left(\frac{1 - z_2}{1 + 6z_2}\right)^2$	26.7 ± 5.4
	$\frac{4 \to 2}{4 \to 4}$	0.32 ± 0.05	0.34	$\left(\frac{1 - 5z_2}{1 + 2z_2}\right)^2$	19.1 ± 3.1
				weighted average:	19.6 ± 2.4

z_2 theory (Table 10 continued)

	Marshalek[c]				
	phenomenological	case I	case II	Pavlichenkov[d]	Bes et al.[e]
$z_2 \times 10^3$	38	9.6	8.7	5[f]	10

a) the uncertainty in the efficiency has been reduced to 1% for these computations.
b) calculated from the tabulated Clebsch-Gordan coefficients of Yamazaki, ref. 102.
c) ref. 17.
d) ref. 33.
e) ref. 31.
f) computed by Pavlichenkov from extrapolated values.

statements concerning the K=2 bands. The z_2 value for the band at 1466 keV is in rather good agreement with the microscopic theories.

CHAPTER V

THE DECAY OF ^{172}Hf

1. Introduction

We present in this chapter the results of the study of the electron capture decay of 5 year ^{172}Hf to levels in the 6.7 day odd-odd nucleus ^{172}Lu. In an odd-odd system the last odd nucleons (a neutron and a proton) are not identical and, consequently, they occupy different Nilsson states. The extent of the coupling between the motions of these nucleons is reflected in the level structure of the odd-odd nucleus to such an extent that it is often difficult to deduce the band structure (in contrast to the situation for even-even nuclei). The investigation of the level schemes of odd-odd nuclei is of great importance in regard to the determination of the nature of the residual neutron-proton interaction.

The ^{172}Hf activity was first observed by Wilkinson and Hicks[103] in 1951. Since then, the internal conversion and the gamma spectrum of ^{172}Lu have also been determined.[107-109] The existing level scheme (proposed by Valentin *et al.*[104]) can accomodate only a small number of transitions and as pointed out by the authors, it is not at all unique. Hence, an investigation of the decay of ^{172}Hf, with Ge(Li) and

Si(Li) detectors and sophisticated electronic circuitry is indeed worthwhile. The long half-life of the nucleus made it possible to carry out our systematic study over a period of about 18 months. We have been able to establish definite cascade relationships between the gamma transitions through delayed coincidence measurements. A new level scheme, accomodating most of the sixteen gamma rays observed, has been proposed.

2. Coupling Schemes in Deformed Odd-Odd Nuclei

We discuss first the coupling schemes in odd-odd nuclei as set down in the articles of Gallagher[21] and Gallagher and Moszkowski.[110] Previously, Bohr and Mottelson[2] and Peker[111] had shown that the ground state spins of a large number of deformed odd-odd nuclei could be accounted for by considering the coupling between the last proton and the last neutron. Gallagher and Moszkowski assumed the validity of the (Nilsson) asymptotic quantum number description of particle states and formulated the following general coupling rules:

$$I = \Omega_p + \Omega_n \text{ if } \Omega_p = \Lambda_p \pm \tfrac{1}{2} \text{ and } \Omega_n = \Lambda_n \pm \tfrac{1}{2}$$

$$I = |\Omega_p - \Omega_n| \text{ if } \Omega_p = \Lambda_p \pm \tfrac{1}{2} \text{ and } \Omega_n = \Lambda_n \mp \tfrac{1}{2} \qquad (5.1)$$

For strongly deformed nuclei, Λ and Σ are separately good quantum numbers. The projection (on the symmetry axis) of the total orbital angular momentum is given by $\Lambda_{odd-odd} = \Lambda_p+\Lambda_n$ or $\Lambda_p-\Lambda_n$. But according to these authors, these states would have almost the same energy. Correspondingly, the spin projections Σ_n and Σ_p can couple to a total value of $\Sigma=0$ or $\Sigma=1$. Because of the spin dependence of the neutron proton force, the $\Sigma=1$ state is expected to lie lower than the $\Sigma=0$ state. This has been generally observed to be valid .

The validity of the asymptotic quantum numbers imply the presence of rotational spectra, and there is evidence for this in nuclei such as $^{242}Am^{112}$ and $^{166}Ho.^{113}$ For K=0 ($K_n = K_p \neq \frac{1}{2}$) the experimental energy spectra of the form $E = AI(I+1)+B(-1)^I$ have been observed by these authors. For $K_n = K_p = \frac{1}{2}$, however, bands with K=0 and K=1 are appreciably mixed due to coriolis coupling. This mixing may cause a complete reordering of states. For levels in ^{172}Lu, we think that the coriolis coupling plays a dominant role and that a thorough theoretical investigation is called for.

3. Experimental Procedure and Results

The instrumentation and general experimental methods have been discussed in Chapter III. Here, we discuss only the special methods employed to

study the decay of ^{172}Hf.

3.1 Measurements of γ-ray Energies and Intensities

The energy measurements have been done mainly using the equilibrium sample and Ge(Li) detectors. For the determination of the energies of the weak lines and of those not resolved with the Ge(Li) detectors, spectra were taken with the Si(Li) detector using chemically separated sources. Examples of the γ-spectra obtained in the present investigation are shown in figures 25-28. The comparatively large error in the energy determination of the 24 keV line is due to the lack of a calibration line of close energy. The 44 and 45 keV lines become suppressed by the K_α back-scattered distribution. In order to resolve these lines from this large background, the PDP-8/L was used to normalize a back-scatter spectrum obtained from ^{174}Lu x-rays and perform the corresponding spectrum subtraction. The results are shown in fig. 27.

The intensity computations for the γ-rays of ^{172}Hf as measured with the Si(Li) detector have been done as follows: The source, in liquid form in an HCl solution, was contained in a 5 mm diameter polyethylene vial with a wall-thickness of 1 mm. The mass-absorption co-efficients for water and HCl were obtained from Wapstra et al.[114]

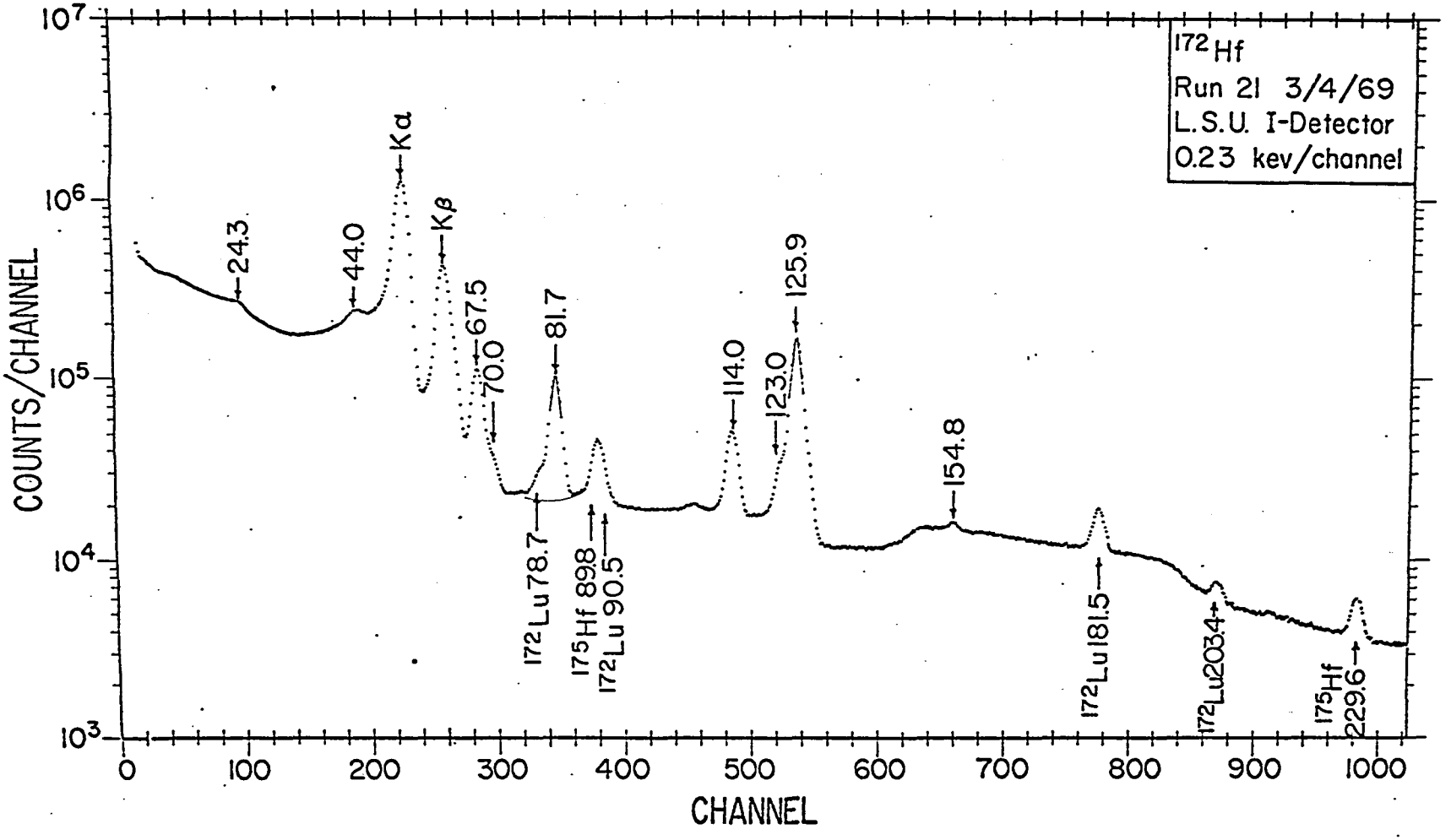

Fig. 25. The ^{172}Hf γ-ray spectrum from 0 → 0.23 MeV.

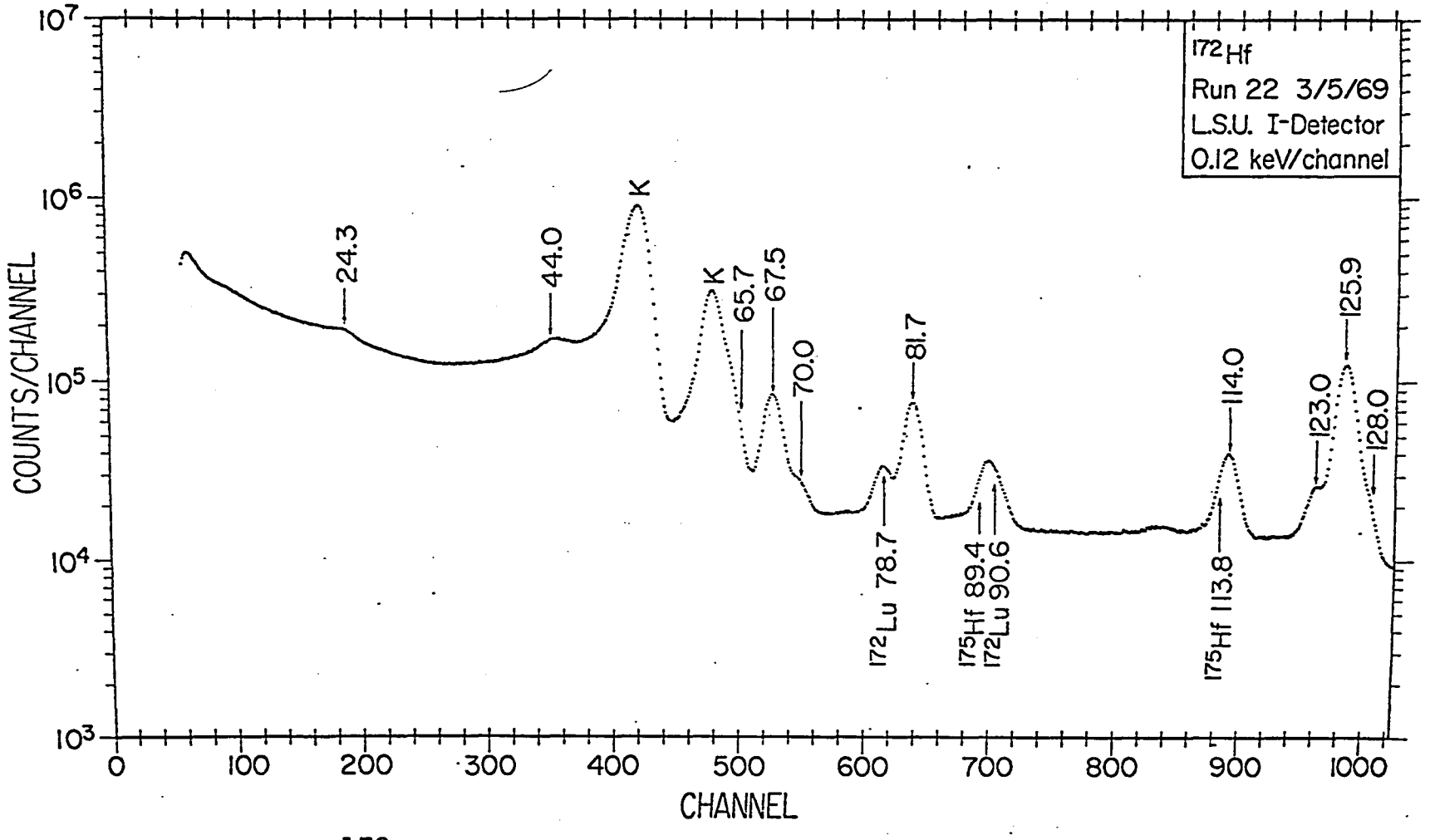

Fig. 26. The ^{172}Hf γ-ray spectrum from 0 → 0.13 MeV.

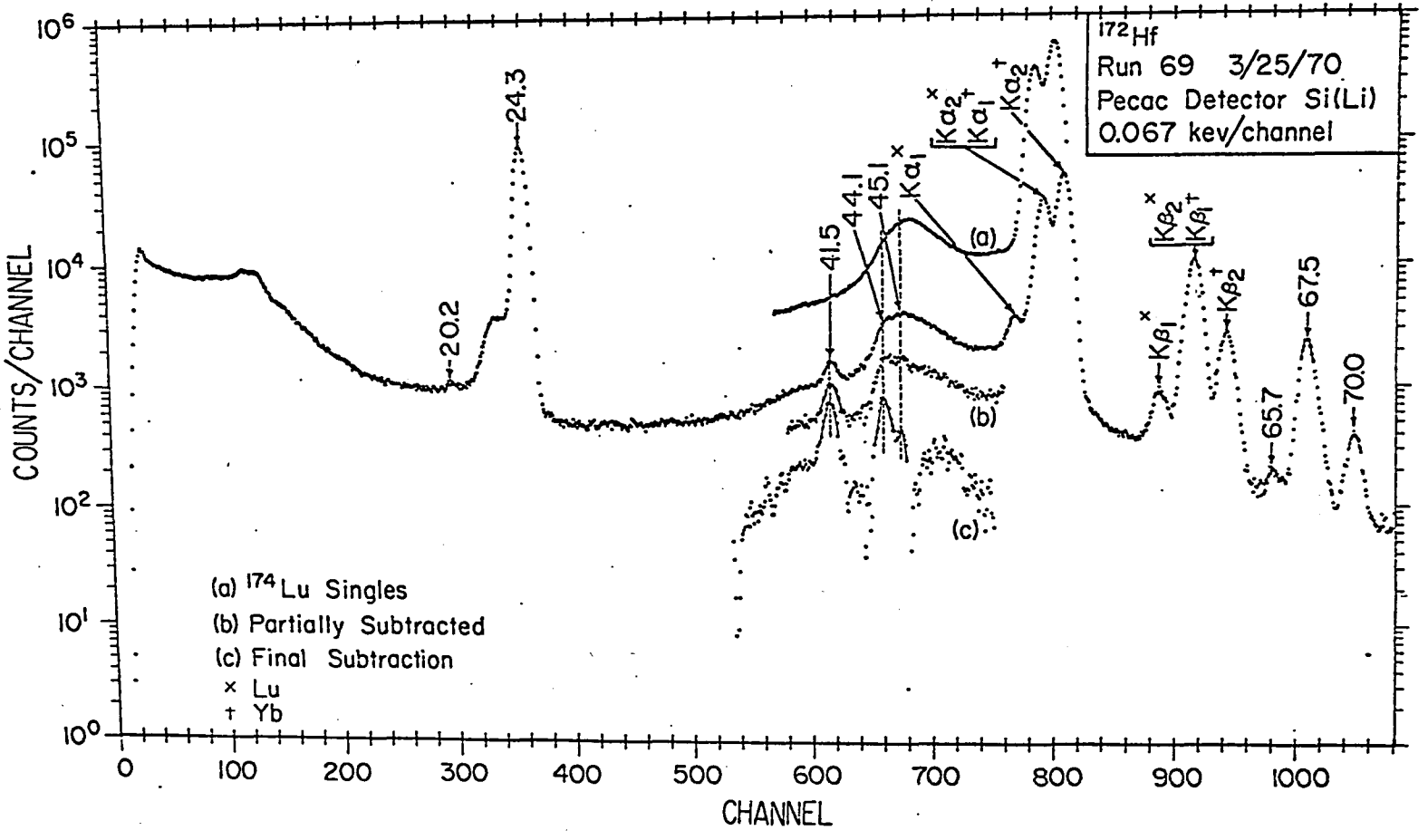

Fig. 27. The ^{172}Hf γ-ray spectrum from 0 → 0.07 MeV.

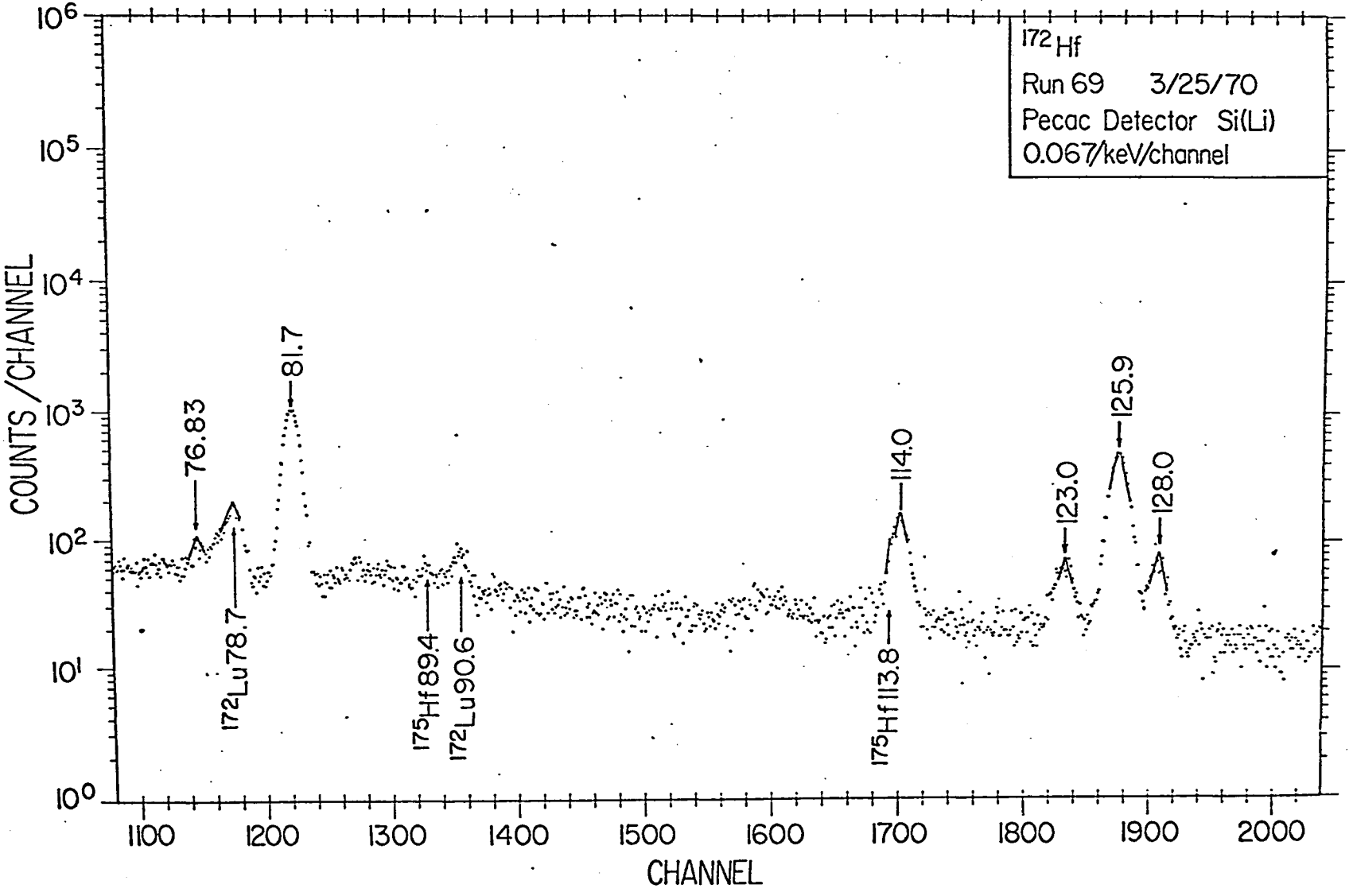

Fig. 28. The ^{172}Hf γ-ray spectrum from 0.07 → 0.13 MeV.

The self-absorption in a thick-source (5 mm) was then computed using the expression

$$\eta_\mu = \left[\frac{e^{-\frac{\mu x}{2n}}(1-e^{-\mu x})}{n(1-e^{-\mu x/n})}\right] \qquad (5.2)$$

where η_μ = self absorption coefficient for energy E_i

x = source thickness

μ = mass absorption coefficient for energy E_i

n = numerical integration factor, $\equiv 10^6$.

A further correction was introduced to take care of the absorption in the polyethylene and that in the 0.01 inch Aluminum detector housing. For each peak the absolute full energy detection efficiency in the Si(Li) detector was obtained from ref. 14. The area under each peak was obtained from the Gaussian analysis computer program.[75] The intensity of a γ-ray relative to that of the 81-keV line in ^{172}Hf was then computed using the expression

$$I_{Rel} = \frac{I_\gamma}{I_{81}} \times 100$$

$$= \left[\frac{A_\gamma}{A_{81}} \times \frac{\varepsilon_{81}}{\varepsilon_\gamma} \times \frac{f_\gamma}{f_{81}}\right] \times 100 \qquad (5.3)$$

where

A = area under the Gaussian

ε = full energy detection efficiency

f = absorption correction factor.

The overall uncertainty in the intensity values was estimated to be about 10%. The correctness of the procedure was verified by comparing the results with those obtained from the Ge(Li) spectra for the 67, 70, 81, 114 and 125 keV lines. The validity of the procedure is further borne out by the consistency in the values for the internal conversion coefficients as will be discussed more fully in section 4.

The energies and intensities of the gamma rays obtained in this investigation are presented in table 11. The uncertainties quoted in bracket refer to the last significant digits mentioned. For example, 1.65(17) means 1.65 ± 0.17 and 42.5(12) means 42.5 ± 1.2. The relative intensities of the sixteen γ-rays reported here remained the same over an 18 month period and hence they have all been assigned to the decay of ^{172}Hf.

3.2 Coincidence Measurements

One of the main problems in establishing a unique level scheme for ^{172}Lu has been the lack of information on the cascade relationship of the γ-transitions.

Table 11

Gamma ray energies, relative intensities and conversion coefficients for transitions in ^{172}Lu

transition	I_γ	I_e [a]					α(Expt)				Assigned σλ
		K	L_I	L_{II}	L_{III}	L	K	L_I	L_{II}	L	
19.87(10)	0.74(13)										
23.96(10)	450(51)		264.7	224.0	381.8	870.5		0.52(5)		1.93(29)	E1
41.02(10)	5.72(24)		35.6					6.20(50)			M1
44.10(20)	~5.7			267.3	310.5	577.8			47(9)	100(10)	E2
45.10(20)	~5										
65.67(3)	3.03(22)										
67.45(3)	109(4)		11.7	≃5.1	<11.2	~28.0		0.11(1)		0.25(3)	E1
70.05(3)	16.74(80)		27.0	<22.9	≃3.1	~53.0		1.61(18)		3.16(35)	M1
76.83(8)	4.62(80)										
77.80(18)	5.3(22)										
81.75(1)	≡100(3)	560.0	101.8	11.7	2.5	116.0	5.6(5)			1.16(12)	M1
114.03(1)	42.5(12)	89.1	12.7				2.1(2)				M1
123.01(2)	23.5(7)	<22.9	≃1.5	5.1	4.3		0.98(10)				M1,E2
125.86(2)	200.7(39)	330.9	50.9	7.1	2.0	60.0	1.65(17)			0.30(3)	M1
127.95(2)	19.4(64)										
154.77(5)	1.92(14)	3.6					1.88(20)				M1

[a] Electron intensities from Harmatz et al. normalized with pure M1 for 81 keV transition and assuming 10% uncertainty.

This has been noted in the work of Valentin et al.[104] Hence, we have done delayed coincidence measurements with a Ge(Li) detector and a thin window NaI(Tℓ) detector. The NaI(Tℓ) detector was used to provide gate pulses resulting from 24 keV gamma rays.

The coincidence arrangement is the same as that shown in figure 15. The coincidence resolving time was 100 ns and a delay of 0.33μ sec was inserted between the NaI gate pulses (24 keV gamma rays) and the signals obtained from the Ge(Li) detector. The coincidence spectrum was taken first at a gain setting of 0.36 keV/channel. Since, it was difficult to discern the coincidence relationship of the 128 and 123 keV lines at 0.36 keV/channel, a second measurement was done using the same set up but a gain setting of 0.12 keV/channel. This second coincidence spectrum was analyzed both by hand and by using the computer program. The results of this analysis are presented in table. 12. The coincidence spectra are shown in figures 29 and 30, along with the corresponding singles spectra. The following relationships have been definitely established: 1) The 70 keV, 81 keV, 114 keV and 125 keV transitions are in direct coincidence with the 24 keV transition. 2) The 67 and 123 keV transitions are definitely not in coincidence with the 24 keV line. We could not

Table 12

Result of coincidence measurements using the 24 keV gate for ^{172}Hf

I_γ / Run	67	70	81	114	123	125
singles	109±4	16±1	≡100	42±1	23±1	200±4
coincidence run 62	≈0	23±8	≡100	43±6	≈0	218.12
coincidence run 63			≡100	38±3	≈0	210±11

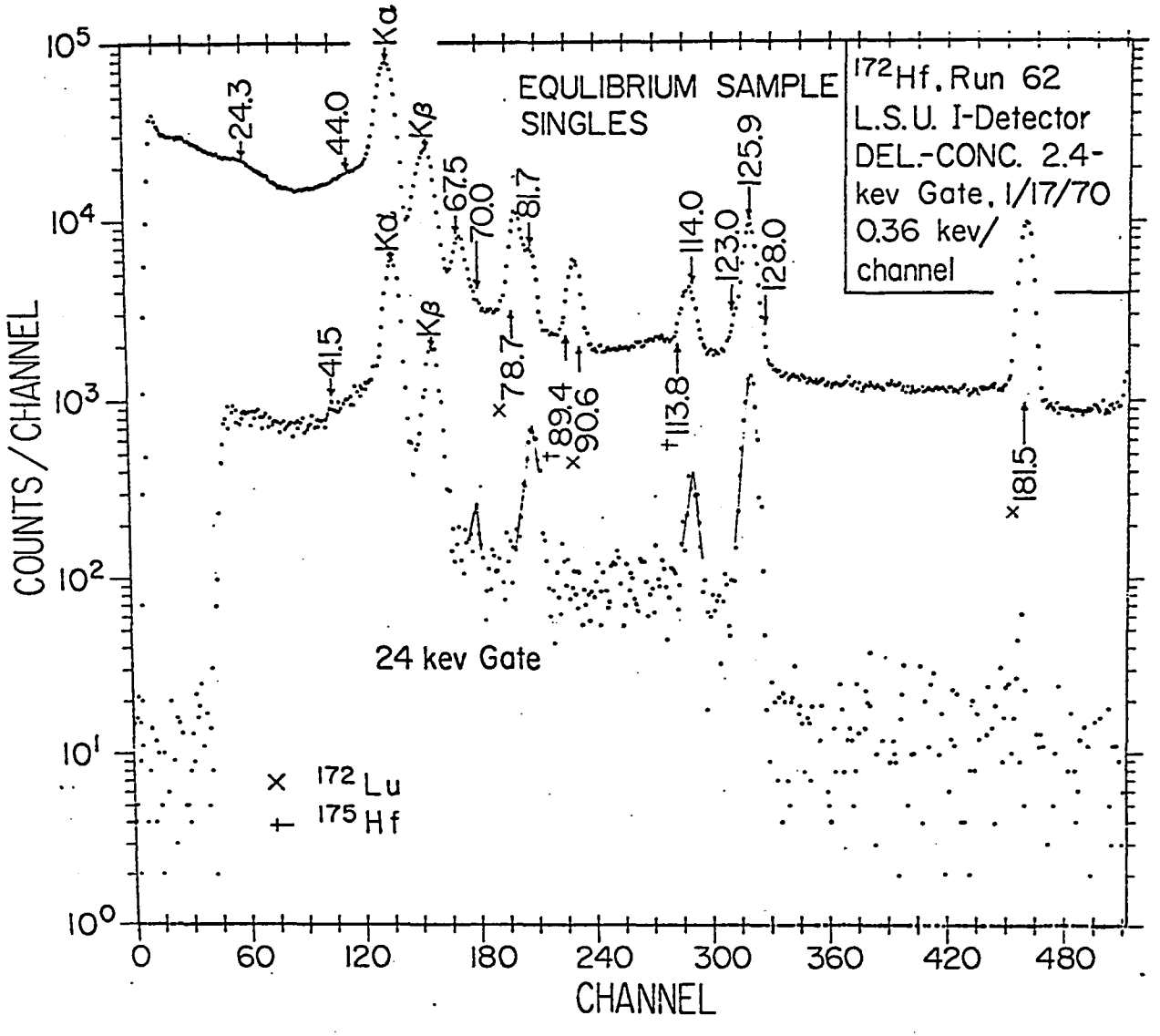

Fig. 29. The delayed coincidence γ-spectrum using the 24 keV gate at 0.36 keV/channel.

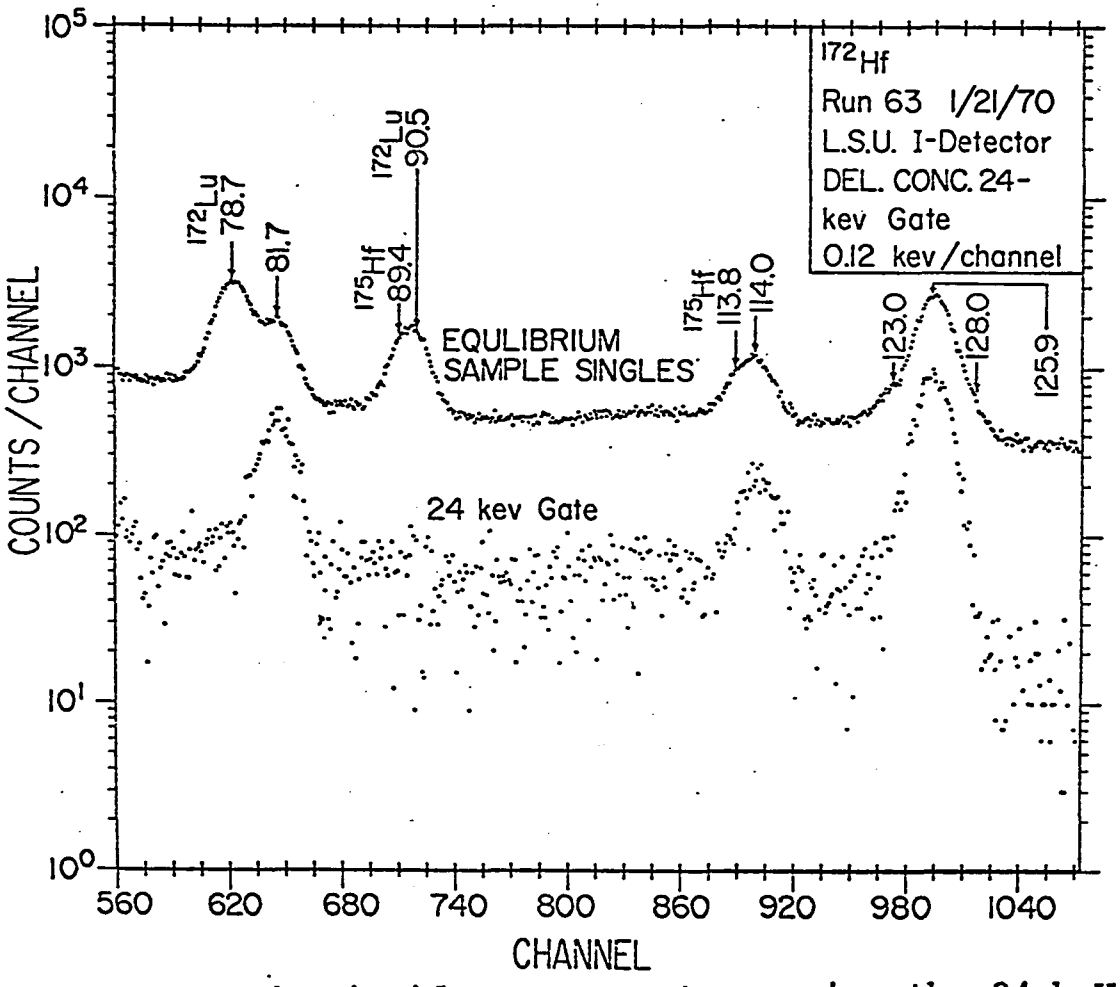

Fig. 30. The delayed coincidence γ-spectrum using the 24 keV gate at 0.12 keV/channel.

reach any definite conclusion regarding the 128 keV transition, although an indirect coincidence with the 24 keV transition is most probable.

3.3 Internal Conversion Coefficients and Transition Multipolarities

The γ-ray intensities obtained from the present investigation were used in conjunction with the electron intensities of ref. 106 to compute the internal conversion coefficients. The 81 keV pure M1 transition was used to normalize the electron intensities. The experimental conversion coefficients obtained are shown in figures 31-33 where a continuous line represents the theoretical conversion coefficients of ref. 99. The consistency of the experimental conversion coefficients point very clearly to the consistency of the measured γ-intensities. For example, the 114 and 125 keV transitions are well known to be pure M1.[103-106] The experimental values obtained in the present investigation are precisely on the theoretical M1 curve. Our measurements are also in very good agreement with the sub-shell ratio measurements of Valentin et al.[104] The internal consistency makes us confident that the conversion coefficients and the assigned multipolarities, presented in table 11, are indeed correct. The total transition intensities obtained using these multipolarity assignments are presented in table 13.

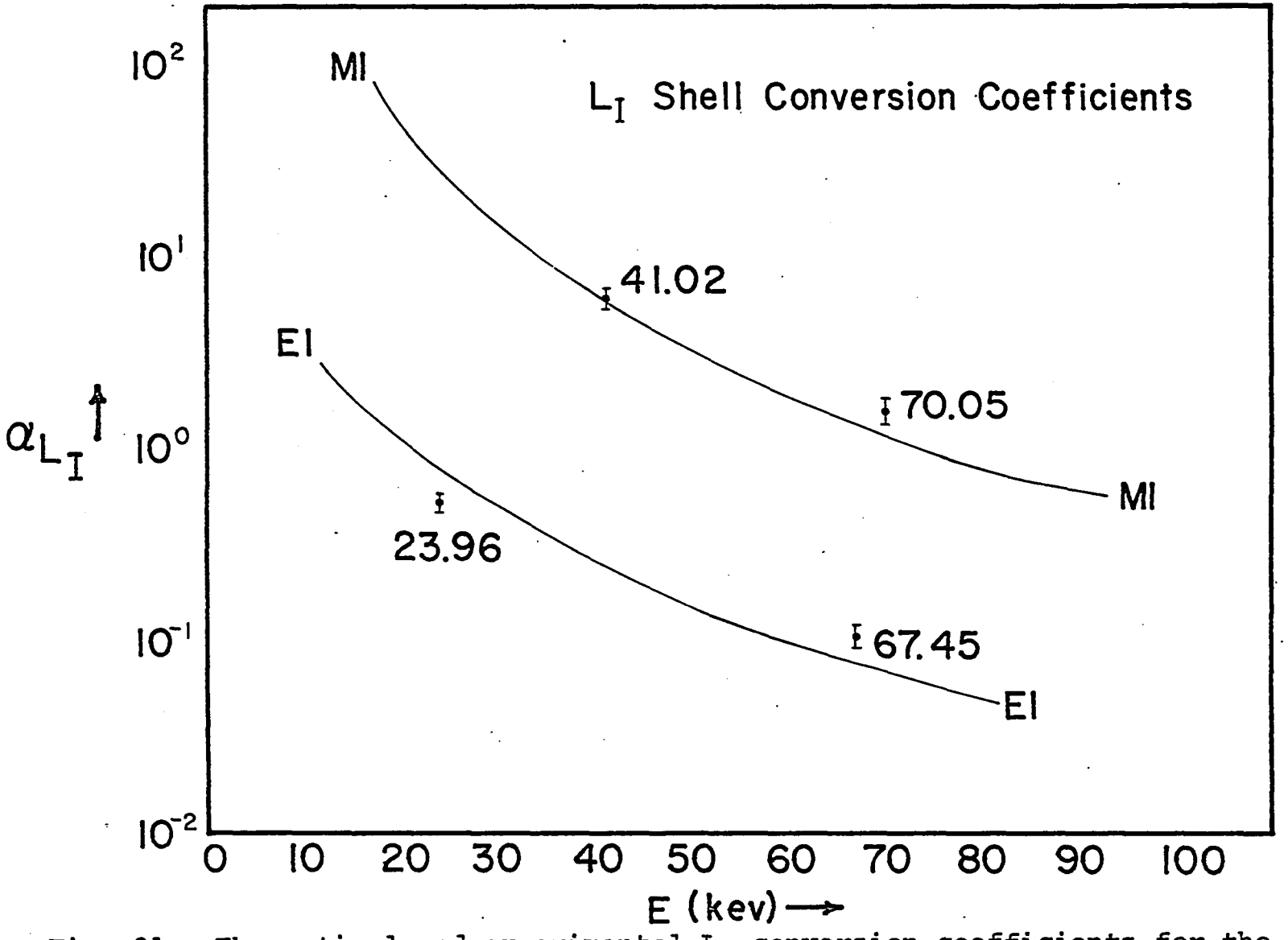

Fig. 31. Theoretical and experimental L_I conversion coefficients for the transitions in the decay of ^{172}Hf.

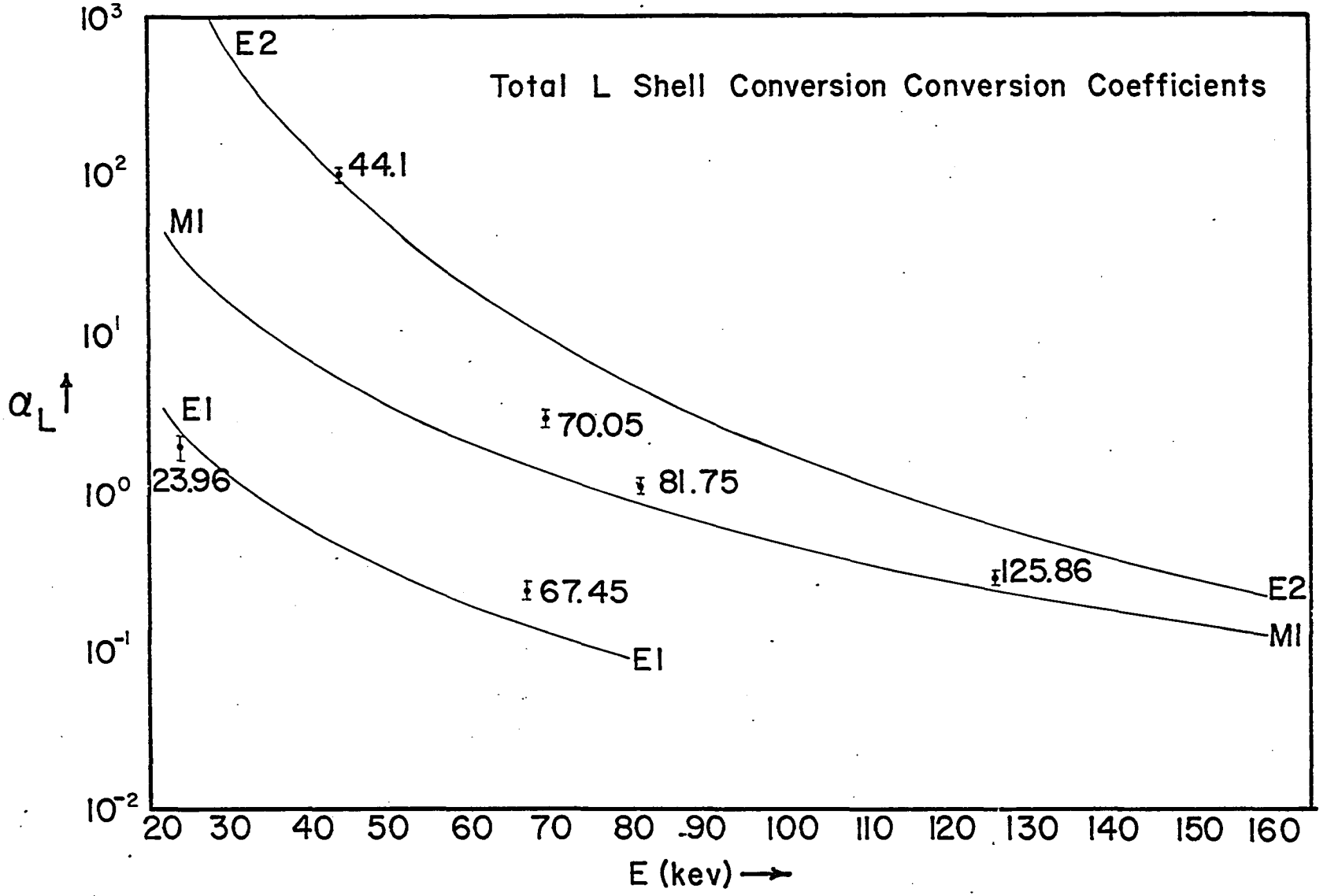

Fig. 32. Theoretical and experimental total L-shell conversion coefficients for the transitions in the decay of ^{172}Hf.

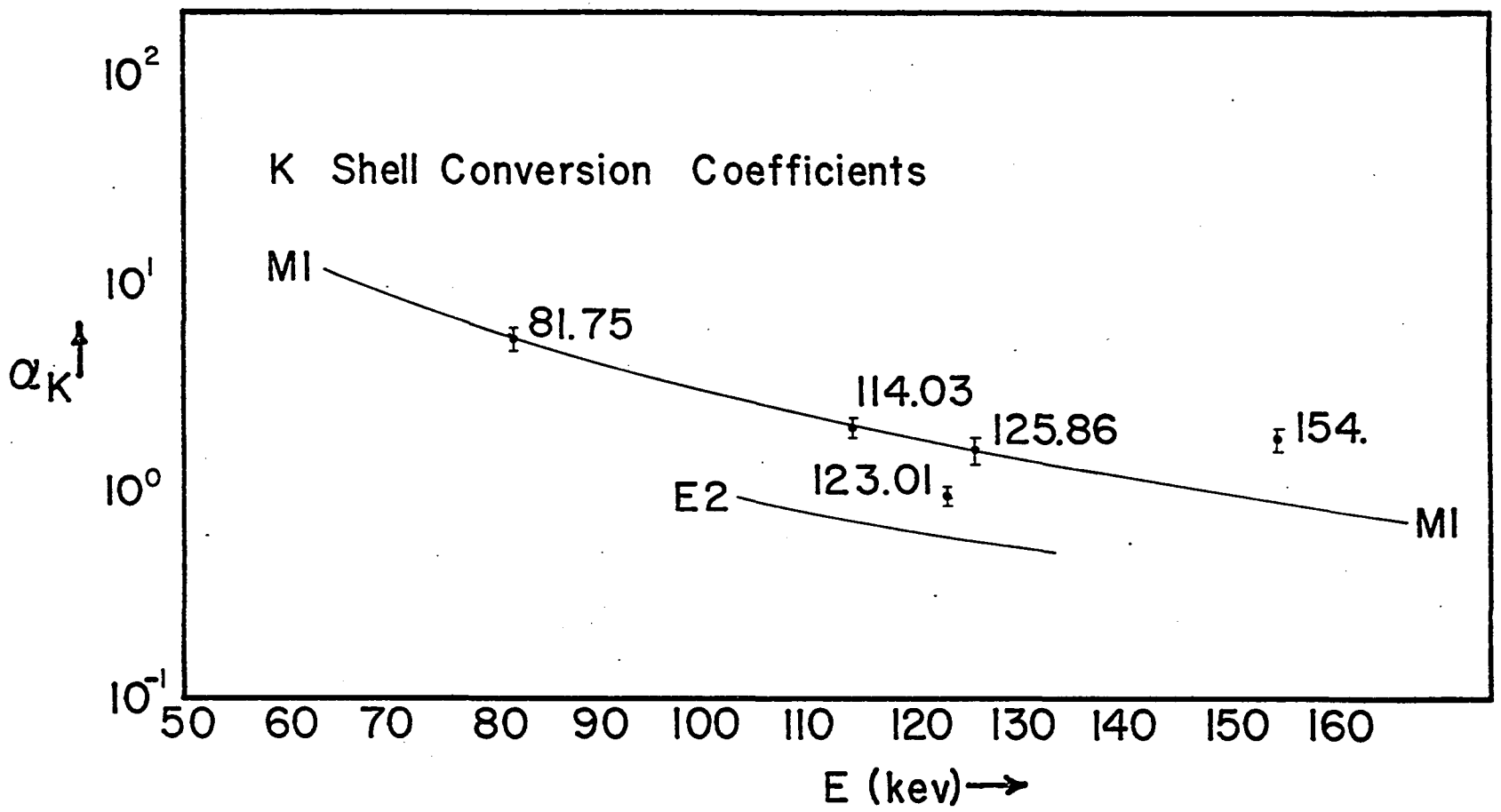

Fig. 33. Theoretical and experimental K-shell conversion coefficients for the transitions in the decay of ^{172}Hf.

Table 13

Total transition intensities for γ rays from ^{172}Hf decay.

γ transition	I_γ	L	α_K	α_L	$\alpha_T = \alpha_K + 1.33\alpha_L$	$(1+\alpha_T)$	total transition intensity
19.87	0.74±0.13						
23.96	450±51.00	E1		2.52	3.35	4.35	1957.5±170.9
41.02	5.72±0.24	M1		6.50	8.65	9.65	55.2± 2.3
41.90		M3					1336.4±133.6
44.10	5.7	E2		95.0	126.4	127.4	726.7± 57
45.10	5.0						
65.67	3.03±0.22						
67.45	109.16±4.0	E1	0.78	0.15	0.98	1.98	216.1± 7.9
70.05	16.74±0.8	M1	8.70	1.4	10.56	11.56	193.5± 9.2
76.83	4.62±0.8						
77.80	5.37±2.2						
81.75	100.00±3.0	M1	5.6	0.86	6.74	7.74	774 ± 23.2
114.02	42.46±1.2	M1	2.18	0.33	2.62	3.62	153.7± 4.3
123.01	23.45±0.75	E2	0.61	0.70	1.54	2.54	59.6± 1.9
125.86	200.74±3.93	M1	1.63	0.24	1.95	2.95	592.2+ 11.6
127.95	19.38±0.64	(M1,E2)	1.55	0.23	1.86	2.86	55.4± 1.8
154.77	1.92±0.14	M1	0.92	0.14	1.11	2.11	4.1± 0.3

4. The ^{172}Lu Level Scheme

We have proposed a level scheme for ^{172}Lu in which twelve of the sixteen γ-transitions observed have been placed. This level scheme, shown in fig. 34, differs significantly from previous schemes proposed by Valentin et al.[104] and by Harmatz and Handley.[106]

The ground state of ^{172}Lu is most probably a 4^- state. This assignment is suggested by the following: First, the electron capture transition to the K=4, I=4 state at 2073 keV in ^{172}Yb has a log ft of 6.44. Second, the Nilsson states for the odd particles in ^{172}Lu are $\frac{7+}{2}[404]$ for Z = 71 and $\frac{1}{2}^-[521]$ for N = 101. These two odd particles can couple (according to the Gallagher and Moszkowski coupling rules) to form the states with spin and parity $4^-(\Sigma=1)$ and $3^-(\Sigma=0)$. As we have discussed in section 2, the Σ=1 state is expected to lie lower in energy.

The 41.9 keV transition is well established[104-106] as an M3 transition deexciting the 41.9 keV isomeric state. The M3 assignment then suggests that the state at 41.9 keV is 1^-. This is in agreement with that predicted by the Nilsson picture (discussed in section 5). This transition, being highly converted ($\alpha_L \tilde{} 7000$), could not be observed in the γ-spectra studied in the present work. We now discuss the placement of the

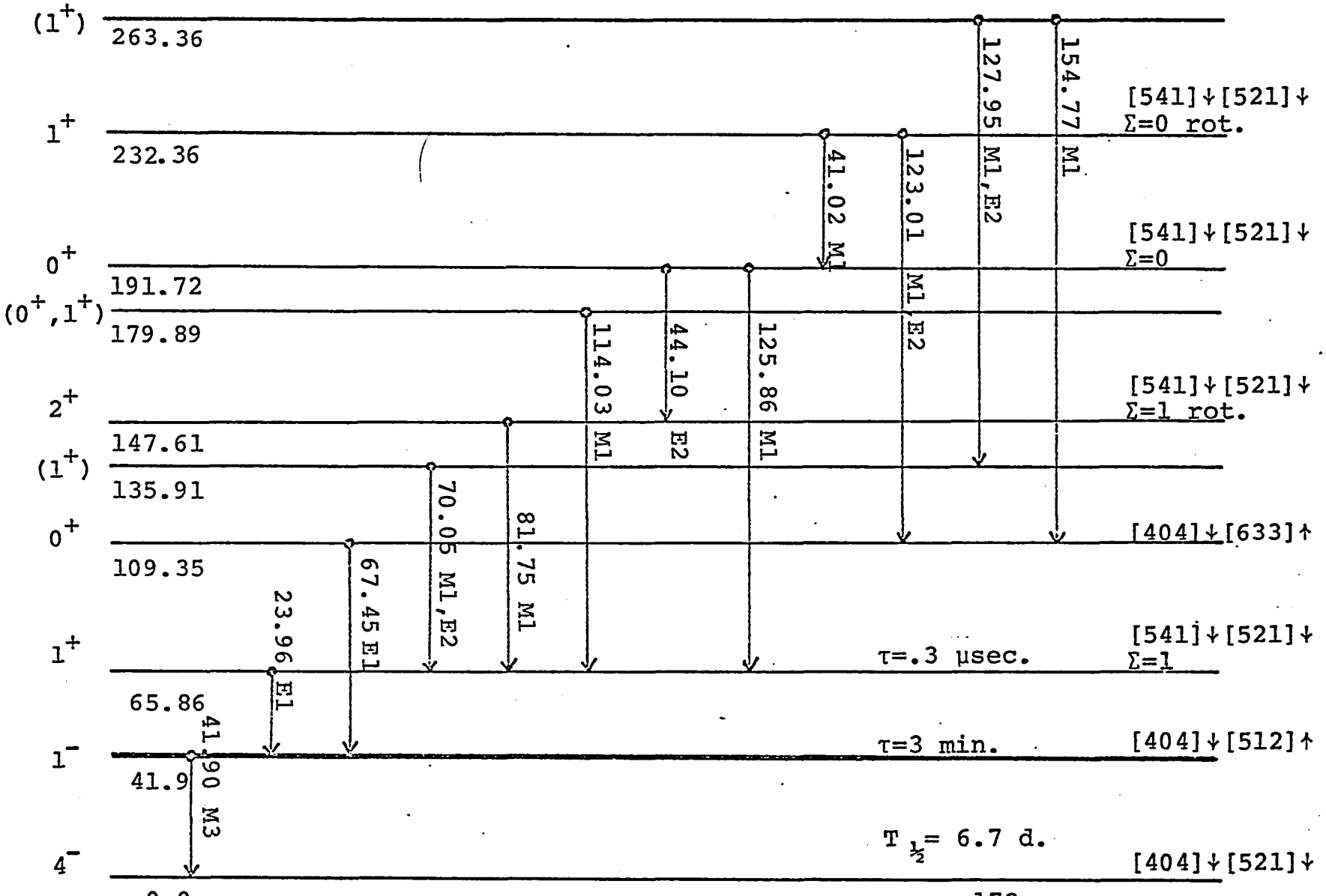

Fig. 34. The level scheme of ^{172}Lu. $^{172}_{71}Lu_{101}$

γ-transitions in the proposed level scheme, by accepting the 4^- and 1^- spin-parity assignments for these states.

The conversion coefficient data definitely establishes the existence of only two E1 transitions, namely those at 24 and 67 keV. The same multipolarity assignment for the 24 keV transition had been given in refs. 104-107. The 67 keV γ-ray was not observed by Valentin et al.[104] However, this strong transition had been assigned an E1 multipolarity in refs. 106 and 107. Furthermore, our delayed coincidence measurements using the 24 keV transition as a gate, definitely show that the 24 keV transition is in direct coincidence with the 70, 81, 114, and 125 keV transitions but is definitely not in coincidence with the 67 keV transition. This means that the 67 keV transition by-passes the 66 keV level. Also, there being no other E1 transitions and no negative parity levels above 41.9 keV, the 67 keV transition must be placed as shown in fig. 34. Harmatz and Handley[106] have wrongly placed this transition as feeding the 66 keV state; and in ref. 107 this strong transition was not even placed in the level scheme. Valentin et al.[104] have placed the 81 keV transition as feeding the level at 109 keV, which is then depopulated by the 44 keV transition.

This is energetically consistent with our scheme, but inconsistent with the fact that one would then have a 67 keV E1 transition (intensity 216) unable to compete with a 44 keV E2 transition (intensity 726). In addition, with the transitions in that order, the 70 keV transition would populate the level at 109 keV. Consequently, its full intensity would not be in coincidence with the 24 keV transition since the 67 keV transition branches past the level at 65 keV. Our coincidence measurements (table 12), on the other hand, show that all of its intensity is in coincidence with the 24 keV γ-ray. Therefore, the 44, 70 and 81 keV transitions must be placed as shown in fig. 34. The 125 keV transition is placed between the 192 and the 66 keV levels. This is in agreement with our coincidence data and also with the placement by Valentin et al.[104]

Our placement of the 125 and 114 keV transitions agree with that of Valentin et al.[104] though the level at 180 keV did not appear well established in their scheme. The coincidence data definitely establishes that the 123 keV transition is not in coincidence with the 24 keV gate. Consequently, it is placed as populating the level at 109 keV. This placement is reinforced by the fact that the 41.02 keV transition fits between the levels at 232 and 192 keV

and is in coincidence with the 24 keV transition (see fig. 29).

Since all transitions except the 24 and 67 keV are M1, E2, or M1 + E2, it can be definitely established that all levels above 41.9 keV have positive parity. Also, since the ground state of ^{172}Hf is 0^+(even-even) there should be no electron capture to levels having I^π values $\geq 2^+$. Obviously, no unique I^π's can be assigned on the basis of transition multipolarities. The spin parities in fig. 34 which are not in parenthesis have been obtained from the Nilsson orbital assignments (see section 5). They are, however, consistent with the multipolarities in every case. The energies of the γ-rays placed in the level scheme are in agreement with the difference between the corresponding level energies.

The percentage of electron capture to different levels have been computed by balancing the total intensity in and out of each level. Since there is no experimental value available for the electron capture decay energy, Q, the log ft values were computed for Q = 1 MeV (estimated from mass formula) and Q = 0.5 MeV (a more reasonable value since states above 263 keV are not observed). There is a definite need for the precise determination of the Q value for the decay of ^{172}Hf. The log ft values and the percentage of electron capture are presented in table 14.

Table 14

Log ft values for electron capture to levels of ^{172}Lu

Level keV	transition intensity in	transition intensity out	% electron capture	log ft	
				Q=500 keV	Q=1000 keV
264	0	59.5± 1.8	2.73±0.2	9.62	10.6
233	0	114.8± 3.5	5.2 ±0.4	9.43	10.3
192	55.2± 2.3	1318.9±57.0	58.2 ±4.8	8.46	9.2
180	0	153.7± 4.3	7.1 ±0.6	9.45	10.3
148	726.7±57.0	774 ±23.2	2.2 ±2.9	9.57	10.8
136	55.4± 1.8	193.5± 9.2	6.3 ±0.7	9.65	10.4
110	63.7± 1.9	216.1± 7.9	7.0 ±0.7	9.60	10.3
66	1713.6±27.0	1957.5± 171	11.2 ±8.0	10.55	11.17

5. Discussion

In regard to the level scheme for ^{172}Lu proposed and discussed in section 4, we have pointed out that unique spin parity assignments are not possible using only transition multipolarities. However, the information on the single particle states in neighboring nuclei may be used along with β-decay selection rules to characterize each level.

In this mass region the value of the deformation parameter ε is ~0.3. A value of ε = 0.29 obtained experimentally in ref. 107, although reasonable, cannot be considered meaningful, since the value was obtained on the basis of the level scheme proposed by Valentin et al. which is not correct. The possible orbitals which may occur at low lying excitations for the 71st proton and 101st neutron may be obtained from the Nilsson level diagrams[45] (see figures 5 and 6). These orbitals and the spin-parity of the resulting states are presented in table 15. In this table we denote the values of $\Sigma = \frac{1}{2}$ and $\Sigma = -\frac{1}{2}$ by the symbols ↑ and ↓ respectively. Some evidence towards this selection of states is provided by the orbital assignments in ^{173}Lu and ^{174}Lu.[104] However, we must keep in mind that in odd-odd nuclei the orbital assignments of neighboring nuclei is not always maintained.[21]

Table 15

Expected Nilsson states in ^{172}Lu

Proton orbital	Neutron orbital	$I\pi$ (p+n)	
		$\Sigma=1$	$\Sigma=0$
[404]↓	[521]↓	4^-	3^-
	[512]↑	1^-	6^-
	[633]↑	0^+	7^+
	[523]↓	6^-	1^-
[541]↓	[521]↓	1^+	0^+
	[512]↑	2^+	3^+
	[633]↑	3–	4^-
	[523]↓	3^+	2^+
[514]↑	[521]↓	4^+	5^+
	[512]↑	7^+	2^+
	[633]↑	8^-	1^-
	[523]↓	2^+	7^+

For the 4^- ground state and the 1^- isomeric 41.9 keV state we have the assignments [404]↓, [521]↓ and [404]↓, [512]↑ respectively. For these two states the same assignments have been made by Valentin et al.[104] They placed the three remaining levels (the 66,110 and 192 keV levels) in their level scheme so as to comprise the 0^+, 2^+ and 1^+ members of a K=0 rotational band based on the [404]↓,[633]↑ configuration. This configuration was selected by them out of four possible level schemes primarily on the basis of Nilsson orbital assignments and beta-decay selection rules. Their explanation of the large percentage of electron capture only to the 192 keV 1^+ state in preference to the 66 keV 0^+ state (having the same configuration) does not appear tenable to us. Furthermore, on the basis of $\varepsilon = 0.3$, it is expected that the [541]↓, [521]↓ configuration would be excited before the [404]↓, [633]↑ configuration. If this is so,we expect to see both members of the [541]↓, [521]↓ doublet ($\Sigma=0$ and $\Sigma=1$) with at least one rotational state with transitions strongly connecting these states. Since such a situation is observed in the decay of ^{172}Hf to the levels of ^{172}Lu, we have assigned the [541]↓, [521]↓ ($\Sigma=1$) configuration to the 66 keV level, with the 147 keV level as its first rotational state. The $\Sigma=0$ member of this configuration is placed at 192 keV

with the 232 keV level as its first rotational state. These states are strongly connected through the 41, 44, 81 and 125 keV transitions.

The inertial parameter, A, for the $\Sigma=0$, 192 keV rotational band and the $\Sigma=1$, 66 keV rotational band are 20.32 and 20.43 keV respectively. In spite of the consistency of the values of A, we think that these two bands should be mixed due to coriolis coupling to such an extent that the inertial parameter may lose its meaning.

From the percentage of electron capture to the different levels (table 14) we observe that more than half the capture occurs to the 192 keV level (58%). Valentin et al. also obtained a similar result, though they did not present any numerical value. With the above assignments we do not have the problem of the large difference in the percentage of electron capture to the ($\Sigma=0$) 192 and the ($\Sigma=1$) 66 keV levels, since their coupled particle configurations are not now identical as was the case in ref. 104. The 147 keV level, being the 2^+ member of the $\Sigma=1$ rotational band, should not have any appreciable electron capture. This is in agreement with the experimental value of 2.2±2.9%. The 109 keV level is most possibly the [404]↓, [633]↑, 0^+ state. This is substantiated by the fact that it is strongly connected to the [404]↓,

[512]↑ 41.9 keV state via the 67 keV transition. No particle configurations can be made at this time for the 136, 180 and 263 keV levels. The spin parity assignments for these levels are solely based on the transition multipolarities, and are, therefore, given in parenthesis in fig. 34.

In concluding this chapter, we would like to emphasize that in order to obtain a more complete picture of the excited states in ^{172}Lu a variety of additional experimentation is required. However, such experiments, described in Chapter VI, could not be included in the present investigations due to a lack of proper equipment.

CHAPTER VI

CONCLUSION

In the previous chapters we have discussed in detail the results of the present investigation. Comparisons of the results of this study with the results of theoretical calculations have been presented on a quantitative basis in Chapters IV and V. Although the conclusions drawn pertain specifically to the collective excitations in ^{172}Yb and ^{172}Lu, some are of a more general nature. We would like to avoid repetition by confining ourselves in this chapter to the more general observations and to a few remarks on prospects for future work.

The collective excitations in even-even nuclei have been well investigated both theoretically and experimentally. However, quantitative agreement has often been lacking. The decay of ^{172}Lu to levels in the even-even nucleus ^{172}Yb provides an excellent case to carry out precise measurements on collective nuclear excitations and their deexciting transitions. A level scheme containing 28 levels has been proposed for ^{172}Yb. Of these, 23 were grouped into 7 rotational bands and a unique K value determined for each band. The unified Model provides a reasonably good account of the general characteristics of the rotational

bands observed in ^{172}Yb. The microscopic theories (though more fundamental) require as many or more adjustable parameters than the Unified Model and even then are often not as successful. However, microscopic calculations designed to take care of departures from adiabaticity seem rather promising. In this regard, we would like to mention especially Pavlichenkov's calculations.

The characterization of the $K=2^+$ states is another interesting point we would like to emphasize. Soloviev has predicted the existence of two quadrupole excited states in all even-even deformed nuclei, though they have been experimentally observed only in a few cases. Our observation of two such quadrupole excited states in ^{172}Yb is rather important. Furthermore, we have shown that both of them show collective behavior to a certain extent. This means that in the quasi-particle approach, these states have to be considered as a superposition of two-quasi-particle states. For a proper appraisal of the nature of such states, it is necessary to carry out measurements involving different physical processes such as nucleon transfer reaction and radiative transitions.

From our investigation of the band-mixing in ^{172}Yb, we conclude that the perturbative approach provides a better account than the microscopic theories.

However, a more precise determination of the z_2 parameter was not possible because of the difficulty involved in determining the intensities of the weak γ-transitions.

In spite of the remarkable results obtained toward a better understanding of the excited states in ^{172}Yb, a few experimental short comings still exist. We would mention in this regard the lack of conversion electron data of desirable precision on the decay of ^{172}Lu, especially for the weak cases such as the very important 1609 keV transition . The large number of γ-transitions (128) observed in the present study suggests that studies with larger Ge(Li) detectors or Compton suppression spectrometers will reveal the presence of many additional γ-rays.

In contrast to the even-even case, the energy spectra of odd-odd nuclei are not as well understood. This is partly due to the fact that the experimental information on odd-odd nuclei is meager. Our investigation of the decay of ^{172}Hf to levels of the odd-odd nucleus ^{172}Lu has been fruitful and interesting in many ways. The coupling schemes in odd-odd nuclei are based on the validity of Nilsson's asymptotic quantum number representation. Although this representation is often not strictly valid, we have nontheless been able to construct a level-scheme

accounting for seven of the 10 levels in ^{172}Lu. Furthermore, the value of the inertial parameter A (~20 keV) obtained for the rotational bands is rather high, which indicates the importance of the coriolis coupling between the Σ=0 and Σ=1 rotational bands in odd-odd nuclei. It appears to be impossible at this time to classify the three remaining levels within the Nilsson-scheme. An understanding of these states is of crucial importance and in that regard it is imperative to further test the validity of the assignments already made and to directly measure the spin of as many levels as is feasible. This can be accomplished, in this particular case, only by means of e^{-}-γ directional correlations.

During the course of the present investigation we have observed the lack of precise Q-values for electron-capture decays. The log ft for each electron capture branch is quite sensitive to the Q-value and consequently, so is the interpretation of energy states based on log ft determinations. This is especially true in the case of ^{172}Lu. A possible way to measure this particular Q-value is by the K-shell to L-shell capture ratio. This is a very difficult measurement but can be done in this case by determining the K-x-ray and L-x-ray intensity which is in prompt coincidence with the 125 keV γ-ray.

At the conclusion of this thesis, it is gratifying to be able to express a marvelous experience of participation (however small) in the "identification of the appropriate concepts and degrees of freedom" suitable for an understanding of the structure and properties of the atomic nucleus. In the absence of a more complete understanding of the interactions involved in the myriad of nucleonic motions we cannot have a theory of nuclear structure in the same sense as we have for the atomic structure. Progress in this direction has been achieved only by a combination of approaches involving clues provided by experimental data and the exploration of the dynamical behavior of simple physical model systems. We must concede that the simple concepts of the Nilsson particle states and the rotational and vibrational excitations in deformed nuclei, however imperfect, still remain as our guidelines for further understanding of the collective nuclear excitations.

REFERENCES

1. A. Bohr, Dan. Mat. Fys. Medd. 26, no. 14 (1952).
2. A. Bohr and B. R. Mottelson, Dan. Mat. Fys. Medd. 27, no. 16 (1953).
3. S. G. Nilsson, Dan. Mat. Fys. Medd. 29, no. 16 (1955).
4. B. R. Mottelson and S. G. Nilsson, Mat. Fys. Skr. Dan. Vid. Selsk. 1, no. 8 (1959).
5. A. Bohr and B. R. Mottelson, Lectures on Nuclear Structure and Energy Spectra (Institute for Theoretical Physics and Nordita, Copenhagen, 1962).
6. J. P. Davidson, Collective Models of the Nucleus, (Academic Press, New York, 1968).
7. O. Nathan and S. G. Nilsson, Alpha-, Beta- and Gamma-Ray Spectroscopy, K. Siegbahn ed. (North Holland, Amsterdam, 1965) chap. X, 601.
8. G. E. Brown, Unified Theory of Nuclear Models and Forces (North Holland, Amsterdam, 1967).
9. A. M. Lane, Nuclear Theory (Benjamin, New York, 1964)
10. D. J. Rowe, Fundamentals in Nuclear Theory, International Center for Theoretical Physics, Trieste (IAEA, Vienna, 1967).
11. G. Dearnaley and D. C. Northrup, Semiconductor Counters for Nuclear Radiations (John Wiley, New York, 1966).

12. G. T. Ewan, Progress in Nuclear Techniques and Instrumentation, Vol. III, F. J. M. Farley ed. (John Wiley, New York, 1966).

13. Semiconductor Nuclear Particle Detectors and Circuits (National Academy of Sciences, Washington D.C., 1969).

14. Semiconductor Detectors, ed. by G. Bertolini and A. Coche (John Wiley, New York, 1968).

15. D. C. Camp, UCRL-50156 (1967).

16. P. O. Lipas, Nucl. Phys. 39 (1962) 468.

17. E. R. Marshalek, Phys. Rev. 158 (1967) 993.

18. C. J. Gallagher and V. G. Soloviev, Mat. Fys. Skr. Dan. Vid. Selsk. 2, no. 2 (1962).

19. V. G. Soloviev, Atomic Energy Rev. 3, no. 2 (1965) 117.

20. M. Baranger, Theory of Finite Nuclei in Cargese Lectures in Theoretical Physics, Maurice Levy ed. (Benjamin, New York, 1963) chapter V.

21. C. J. Gallagher, Selected Topics in Nuclear Spectroscopy, complied by B. J. Verhaar (North Holland, Amsterdam, 1964), Chap. IV, 133.

22. C. Bloch ed. Many Body Description of Nuclear Structure and Reactions (Academic Press, New York, 1966).

23. M. G. Meyer, Phys. Rev. 75 (1949) 1969.

24. O. Haxel, J. H. D. Jensen and H. E. Suess, Phys. Rev. 75 (1949) 1766.

25. V. Weiskopf, Science, 113 (1951) 101.

26. S. A. Moszkowski and B. L. Scott, Ann. of Phys. 11 (1960) 65.

27. J. Rainwater, Phys. Rev. 79 (1950) 432.

28. A. S. Davydov and G. F. Flippov, Nucl. Phys. 8 (1958) 237.

29. A. S. Davydov and V. S. Rostovsky, Nucl. Phys. 12 (1959) 58.

30. A. S. Davydov and A. A. Chaban, Nucl. Phys. 20 (1960) 499.

31. D. R. Bes, P. Federman, E. Maqueda and A. Zucker, Nucl. Phys. 65 (1965) 1.

32. A. Faessler, W. Griener and R. K. Sheline, Nucl. Phys. 70 (1965) 33.

33. I. M. Pavlichenkov, Nucl. Phys. 55 (1964) 225.

34. F. Villars, Ann. Rev. Nuclear Sci. 7 (1957) 185.

35. H. J. Lipkin, The Many Body Problem (Dunod, Paris, 1959) 335.

36. F. Villars and G. Cooper, Ann. of Phys. 56 (1970) 224.

37. B. R. Mottelson, Proceedings of the International School of Physics "Enrico Fermi", Course XV, Nuclear Spectroscopy (Academic Press, New York, 1960) 44.

38. R. Van Lieshout, ibid, Course XL, Nuclear Structure and Nuclear Reactions (Academic Press, New York, 1969) 1.

39. M. Jean, Ibid, Course XXXVI, p. 171.

40. J. P. Elliot, Proc. Roy. Soc. A245 (1958) 128 and 562.

41. G. Racah, Proceedings of the International School of Physics "Enrice Fermi", Course XV (Academic Press, New York, 1960) 1.

42. A. Bohr, B. R. Mottelson and D. Pines, Phys. Rev. 110 (1958) 936.

43. K. Gottfried, Phys. Rev. 103 (1956) 1017.

44. R. H. Lemmer and A. E. S. Green, Phys. Rev. 119 (1960) 1043.

45. I. Lamm, Nucl. Phys. A125 (1969) 504.

46. T. D. Newton, Can. J. Phys. 38 (1960) 750.

47. K. T. Hecht and G. R. Satchler, Nucl. Phys. 32 (1962) 286.

48. P. H. Stelson and L. Grodzins, Nuclear Data IA (1965) 21.

49. K. T. Hecht, Selected Topics in Nuclear Spectroscopy complied by B. J. Verhaar (North Holland, Amsterdam, 1964) Chap. II, 51.

50. E. R. Marshalek, UCRL-10046 (1962) Thesis, University of California.

51. G. Alaga, Proceedings of the International School of Physics "Enrico Fermi", Course XL, M. Jean ed. Nuclear Structure and Nuclear Reactions (Academic Press, New York, 1969 28.

52. M. A. J. Mariscotti, G. S. Goldhaber and B. Buck, Phys. Rev. 178 (1969) 1864.

53. J. J. Griffin and M. Rich, Phys. Rev. 118 (1960) 850.

54. S. G. Nilsson and O. Prior, Dan. Mat. Fys. Medd. 32, no. 16 (1961).

55. S. A. Moszkowski, in Alpha-, Beta- and Gamma-Ray Spectroscopy, K. Siegbahn ed. (North Holland, Amsterdam, 1965) Chap. XV, 863.

56. G. Alaga, K. Alder, A. Bohr and B. R. Mottelson, Dan. Mat. Fys. Medd. 29, no. 9 (1955).

57. A. Bohr and B. R. Mottelson, Atomnaya Energiya 14, no. 1 (1963) 41.

58. M. E. Rose in Alpha-, Beta and Gamma-Ray Spectroscopy, K. Siegbahn ed. (North Holland, Amsterdam, 1965) Chap. SVI, 887.

59. L. A. Sliv and I. M. Band, ibid, Appendix 5, 1639.

60. R. S. Hager and E. C. Seltzer, Nucl. Data, 4A, (1968) 1.

61. K. Kumar and M. Baranger, Nucl. Phys. A92 (1967) 608.

62. G. G. Dussel and D. R. Bes, Nucl. Phys. A143 (1970) 623.

63. S. M. Abecasis, H. E. Bosch and C. A. Heras, Nuovo Cim. 51B (1967) 310.

64. S. M. Abecasis and H. E. Bosch, Nuovo Cim. 53B (1968) 147.

65. S. M. Abecasis and H. E. Bosch, Nucl. Phys. A129 (1969) 434.

66. N. N. Bogoliubov, JETP 7 (1958) 41; Nuovo Cim. 7 (1958) 794.

67. J. G. Valatin, Nuovo Cim. 7 (1958) 843.

68. S. T. Belyaev, Collective Excitations in Nuclei (Gordon and Breach, New York, 1968).

69. A. B. Migdal, Nuclear Theory: The Quasiparticle Method (Benjamin,New York, 1969).

70. V. G. Soloviev, Dan. Mat. Fys. Skr. 1, no. 11 (1961).

71. A. F. Miranda and M. A. Preston, Nucl. Phys. 44 (1963) 443.

72. K. Sawada, Phys. Rev. 119 (1960) 2090.

73. J. M. Araujo, Nucl. Phys. 13 (1959) 360.

74. B. R. Mottelson and J. G. Valatin, Phys. Rev. Lett. 5 (1960) 520.

75. G. E. Keller, Ph.D. thesis, Louisiana State University, Baton Rouge (1969).

76. R. G. Helmer, R. L. Heath, M. Putnam and D. H. Gipson, Nucl. Instr. 57 (1967) 46.

77. C. M. Lederer, J. M. Hollander and I. Perlman, Table of Isotopes (John Wiley and Sons, Inc., New York, 1967).

78. Nuclear Data Sheets of the National Academy of Sciences, National Research Council, Vols. 1-6.

79. B. Harmatz, T. H. Handley and J. W. Michelich, Phys. Rev. 114 (1959) 1082, and 123 (1961) 1758.

80. R. G. Wilson and M. L. Pool, Phys. Rev. 118 (1960) 1067.

81. G. Kaye and R. L. Graham, AECL Report No. A3027B (1963).

82. B. S. Dzelepov et al., Nucl. Phys. 56 (1964). 283.

83. Ya. Vrzal et al., preprint, JINR, P2651 (1966).

84. M. M. Stautberg, E. B. Shera and K. J. Casper, Phys. Rev. 130 (1963) 1901.

85. H. Blumberg et al., Nucl. Phys. A90 (1967) 65.

86. J. G. Prather, Ph.D. thesis, Utah State University, Logan, Utah (1967).

87. M. F. Roche et al., Bull. Am. Phys. Soc. 14 (1969) 586.

88. O. H. Ottesson and R. G. Helmer, Phys. Rev. 164, (1967) 1485.

89. K. Wien, Z. Phys. 216 (1968) 1.

90. D. G. Burke and B. Elbek, Mat. Fys. Medd. Dan.

Vid. Selsk., 36, no. 6 (1968).

91. J. De Boer, G. Goldring and H. Winkler, Phys. Rev. 134B (1964) 1032.

92. Y. Yoshizawa et al., Nucl. Phys. 73 (1965) 273.

93. R. Sayer, Ph.D. thesis, University of Tennessee, Knoxville, Tennessee (1968).

94. P. Kleinheinz et al. Nucl. Phys. A91 (1967) 329.

95. G. Kaye, Nucl. Phys. A108 (1968) 625.

96. R. Vukanovic et al., UUIP, 577 (Uppsala, 1968).

97. R. A. Belt et al., Nucl. Phys. A134 (1969) 225.

98. M. Forker and H. E. Wagner, Nucl. Phys. A138 (1969) 13.

99. R. S. Hager and E. C. Seltzer, Nucl. Data, 4A (1968) 1.

100. L. A. Sliv and I. M. Band, Alpha-, Beta- and Gamma-Ray Spectroscopy, K. Siegbahn ed., North Holland Publishing Co., Amsterdam, 1965) Appendix 5.

101. O. Dragoun, Z. Plahner and F. Schmutzler, MPIH V5 (1969) Heidelberg.

102. T. Yamazaki, Nucl. Data A1 (1966) 453.

103. G. Wilkinson and H. J. Hicks, Phys. Rev. 81 (1951) 540.

104. J. Valentin, D. J. Horen and J. M. Hollander, Nucl. Phys. 31 (1962) 373.

105. V. Brabec and J. Jursik, Czech. J. Phys. B15 (1965) 317.

106. B. Harmatz and T. H. Handley, Nucl.Phys. 81 (1966) 481.

107. J. Jastrzebski, M. Moszynski, Z. Preibsz, K. Stryczmewicz, P. Paris and J. Treherne, Nucl. Phys. A104 (1967) 459.

108. M. H. Abou-Leila, C. R. Acad. Sc. Paris, t259 (1964) 3003.

109. M. H. Abou-Leila, R. Ceuleneer and J. Vanhorenbeeck, Nucl. Phys. A115 (1968) 635.

110. C. J. Gallagher and S. A. Moszkowski, Phys. Rev. 111 (1958) 1282.

111. L. K. Peker, Izvest. Akad. Nank. S.S.S.R. Ser. Fiz. 31 (1957) 1029.

112. F. Asaro, I. Perlman, J. O. Rasmussen and S. G. Thompson, Phys. Rev. 120 (1960) 934.

113. R. G. Helmer and S. B. Burson, Phys. Rev. 119 (1960) 788.

114. A. H. Wapstra, G. J. Nijgh and R. Van Lieshout, Nuclear Spectroscopy Tables (North Holland, Amsterdam, 1959).

VITA

Dilip Sen was born January 1, 1934 to Dr. Hiran Kumar Sen and Mrs. Nirupama Sen at Calcutta, India. After being educated at the school system affiliated to Calcutta University he matriculated in 1948. After two years of intermediate science education at Asutosh College (Calcutta), he entered the Presidency College (Calcutta) in 1950. He received both the Bachelor of Science (Honours) in 1952 and Master of Science (Class I) in 1955 from Presidency College (Calcutta University). He then received training as a post M.Sc.student at Saha Institute of Nuclear Physics during September 1955 - September 1956. From September 1956, he spent three years working as a research scholar in the Department of Applied Mathematics (Calcutta University). Before joining the Louisiana State University as a graduate student in Fall 1965, he had been working as a lecturer at Jadavpur University (Calcutta), since November 1959. In November 1963 he was married to Swati Ghosh. They have a five year old daughter. At this time he is a candidate for the Doctor of Philosophy degree in the Department of Physics and Astronomy (Louisiana State University).

EXAMINATION AND THESIS REPORT

Candidate: Dilip Sen

Major Field: Physics

Title of Thesis: The Collective Excitation in ^{172}Yb and ^{172}Lu

Approved:

Edward Zganjar
Major Professor and Chairman

Max Goodrich
Dean of the Graduate School

EXAMINING COMMITTEE:

Ralph

Paul Vanderbilt

John J. Matese

J. Olsen

Date of Examination:

July 22, 1970